CHEMICAL
RESEARCH,
DEVELOPMENT &
ENGINEERING
CENTER

CRDEC-CR-053

INVESTIGATIONS OF POLARIZED LIGHT SCATTERING FROM ROUGH SURFACES

William S. Bickel

UNIVERSITY OF ARIZONA
Tucson, AZ 85721

November 1989

U.S. ARMY
ARMAMENT
MUNITIONS
CHEMICAL COMMAND

Aberdeen Proving Ground, Maryland 21010-5423

Disclaimer

The findings in this report are not to be construed as an official Department of the Army position unless so designated by other authorizing documents.

Distribution Statement

Approved for public release; distribution is unlimited.

UNCLASSIFIED
SECURITY CLASSIFICATION OF THIS PAGE

REPORT DOCUMENTATION PAGE

Form Approved OMB No. 0704-0188

1a. REPORT SECURITY CLASSIFICATION UNCLASSIFIED	1b. RESTRICTIVE MARKINGS
2a. SECURITY CLASSIFICATION AUTHORITY	3. DISTRIBUTION/AVAILABILITY OF REPORT Approved for public release; distribution is unlimited.
2b. DECLASSIFICATION/DOWNGRADING SCHEDULE	
4. PERFORMING ORGANIZATION REPORT NUMBER(S) CRDEC-CR-053	5. MONITORING ORGANIZATION REPORT NUMBER(S)
6a. NAME OF PERFORMING ORGANIZATION University of Arizona 6b. OFFICE SYMBOL (If applicable)	7a. NAME OF MONITORING ORGANIZATION
6c. ADDRESS (City, State, and ZIP Code) Tucson, AZ 85721	7b. ADDRESS (City, State, and ZIP Code)
8a. NAME OF FUNDING/SPONSORING ORGANIZATION See Reverse 8b. OFFICE SYMBOL (If applicable)	9. PROCUREMENT INSTRUMENT IDENTIFICATION NUMBER DAAL03-86-D-0001
8c. ADDRESS (City, State, and ZIP Code)	10. SOURCE OF FUNDING NUMBERS PROGRAM ELEMENT NO. / PROJECT NO. / TASK NO. / WORK UNIT ACCESSION NO.

11. TITLE (Include Security Classification)

Investigations of Polarized Light Scattering From Rough Surfaces

12. PERSONAL AUTHOR(S)
Bickel, William S.

13a. TYPE OF REPORT	13b. TIME COVERED	14. DATE OF REPORT (Year, Month, Day)	15. PAGE COUNT
Contractor	FROM 87 Feb TO 88 Dec	1989 November	129

16. SUPPLEMENTARY NOTATION

COR: Arthur H. Carrieri, SMCCR-DDT, (301) 671-2437

17. COSATI CODES			18. SUBJECT TERMS (Continue on reverse if necessary and identify by block number)
FIELD	GROUP	SUB-GROUP	Polarized light scattering, Mueller matrix, Nephelometer, Perfect and perturbed optical surfaces
20	06		

19. ABSTRACT (Continue on reverse if necessary and identify by block number)

Polarized light scattering at two visible wavelengths from natural and fabricated surfaces is investigated before and after contamination by liquids of different optical properties. Measurements of the Mueller matrix elements were performed from such surfaces, demonstrating a time dependence of scattering as the liquid diffuses into the surface. The matrix elements found most sensitive to the liquid's presence were also isolated for more detailed analysis.

20. DISTRIBUTION/AVAILABILITY OF ABSTRACT ☒ UNCLASSIFIED/UNLIMITED ☐ SAME AS RPT. ☐ DTIC USERS	21. ABSTRACT SECURITY CLASSIFICATION UNCLASSIFIED
22a. NAME OF RESPONSIBLE INDIVIDUAL SANDRA J. JOHNSON	22b. TELEPHONE (Include Area Code) (301) 671-2914 22c. OFFICE SYMBOL SMCCR-SPS-T

DD Form 1473, JUN 86 *Previous editions are obsolete.* SECURITY CLASSIFICATION OF THIS PAGE

UNCLASSIFIED

8a. Names and Addresses of Funding/Sponsoring Organizations (Continued)

Cdr, CRDEC, ATTN: SMCCR-DDT, Aberdeen Proving Ground, MD 21010-5423
BATTELLE, Research Triangle Park, NC 27709-2297

PREFACE

The work described in this report was authorized under Contract No. DAAL03-86-D-0001. This work was started in February 1987 and completed in December 1988.

The use of trade names or manufacturers' names in this report does not constitute an official endorsement of any commercial products. This report may not be cited for purposes of advertisement.

This report has been approved for release to the public.

Acknowledgments

The following people have contributed to the research reported in this report, and I extend my sincere appreciation for the work they have done. They are David Abromson, Padma Bandu, Shu Chung Chiao, Vince Iafelice, Eric Simms, John Pattison, Karen Halstead, Jodi Barnhill, Joe Boyer, and Tom Wentzel.

I want to give special thanks to June Yann Shu, who has assumed great responsibility for the project during the past few years. He has become an expert in sample preparations and has made virtually all of the experimental measurements. His very careful work, skill, patience, and dedication to the project are a great credit to him and one of which I am proud. He is well on his way to becoming a first-class, small-particle spectroscopist. Some of the work he did on this project will be included in his M.S. Thesis in physics.

Blank

CONTENTS

INVESTIGATIONS OF POLARIZED LIGHT SCATTERING FROM ROUGH SURFACES

1. INTRODUCTION

The object of this research is to experimentally investigate the polarized light scattered from natural and fabricated surfaces that have been contaminated with trace amounts of two liquids of different optical properties. The main questions are: 1) to what sensitivity can we detect the liquids' presence? 2) What is the time dependence of the scattering light as the liquid diffuses into the surface? and 3) What matrix elements are most sensitive to the liquids' presence?

Our approach was to start with perfect (ideal) systems for which light-scattering data can be predicted by existing theories. These systems include the perfect sphere, fiber, surface, double fibers and fibers on a surface. We examined in detail polarized light scattering from perfect smooth surfaces, perturbed (slightly rough) surfaces, and very rough surfaces. These led to the complex systems, i.e., scratched, sand blasted, and corroded surfaces, and then to surfaces covered with sand, salt, soil, clay, and biological material.

A major amount of time was spent on surface preparation. We developed techniques that produce families of reproducible surfaces, i.e., surfaces fabricated by progressively increasing the perturbation on a perfect surface until the light scattering no longer responds to the perturbation.

Techniques were devised to coat surfaces with liquids of specific optical properties. Our goal is to control the quantity and rate of liquid deposition to the surface and make measurements as a function of time after deposition.

All surfaces were examined with our nephelometer device, which measures the 16 Mueller matrix elements. Some of the 16 elements are redundant, and some are insensitive to surface structure. We concentrated on those elements which exhibited a significant change with angle.

Over 600 surfaces belonging to ten different substrate classes were examined. Analysis of 6 matrix elements per surface required over 3600 measurements. We report here our final conclusions and show some representative matrix element curves which led to these conclusions.

2. LIGHT SCATTERING FROM PERFECT MIRROR SURFACES AS A FUNCTION OF ILLUMINATING ANGLE

Our first experiments with perfect surfaces were performed by Vince Iafelice, University of Arizona, reporting rather complete results in his thesis, "The Polarized Light Scattering Matrix Elements for Select Perfect and Perturbed Optical Surfaces."[1] Figure 1 shows the S_{11} for a "nearly perfect aluminum surface" as a function of illuminating angle α. These data are representative of a number of near-perfect surfaces of various materials -- namely brass, gold, stainless steel, copper, glass, and plastic. Perfect surfaces yield specular reflection with no scatter. The amount of radiation scattered out of the specular peak is therefore a measure of the quality of the surface. If the S_{ij} are a signature or probe of surface quality, the S_{ij} must respond to these changes. As the surfaces degrade in time, or are perturbed by adding defects or contaminations, the S_{ij} must respond to these changes. Controlled experiments must use perfect surfaces as the starting point for further studies of surface modification.

Figure 1 shows the following:

1. The sharp specular peak at $\theta = 20°$ shows a high-quality reflecting surface.

2. The amount of scatter at angles other than $\theta = 20°$ is decreased by nearly three orders of magnitude.

3. The scattered intensity, even though much lower than the specular peak, varies by several orders of magnitude (see thick solid curve for $\theta = 11°$).

Data taken from more perfect surfaces show that scattered intensities can be as much as five orders of magnitude lower than the specular peak. We have removed all sources of noise and spurious reflections of specular peaks from our scattering nephelometer.

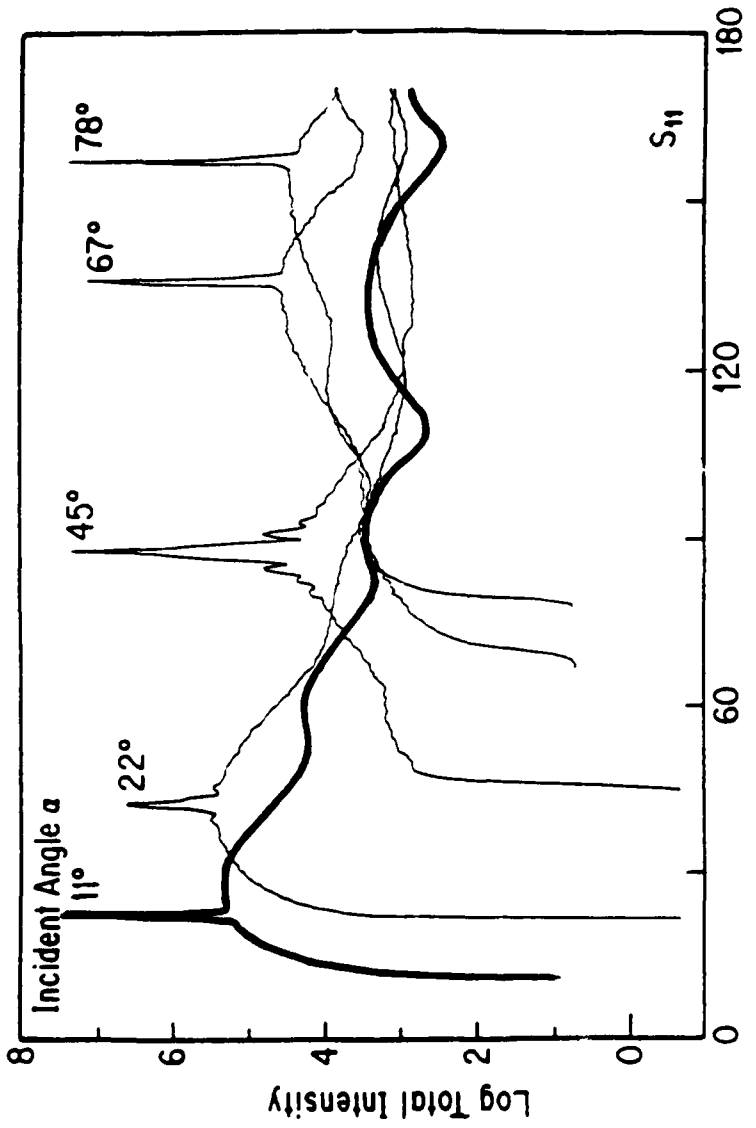

FIGURE 1. Light scattering from a nearly perfect aluminum surface as a function of incident illumination angle α.

3. LIGHT SCATTERING FROM A FIBER ON A MIRROR

Figure 2 shows the 16 Mueller matrix elements for a nearly perfect (surface roughness = 45 Å) flat aluminum mirror illuminated at incident angle $\theta = 11°$ The specular peak in the total intensity curves (column 1) has been truncated. The scattered intensity, I_s, which varies throughout θ, is less than 10^{-5} I_o, where I_o is the intensity of the specular peak. Even where the scattered intensity is low, its polarization can be as large as ±100% (see S_{33} and S_{34}).

Figure 3 is a plot of all 16 Mueller matrix elements for a 0.6 micron quartz fiber in contact with the aiuminum mirror from Figure 2, and for the 0.6 micron fiber alone. The S_{ij} for fiber-on-the-mirror case has higher phase frequency than for the fiber in air. The fiber-on-the-mirror polarizations are dramatically different than for the single fiber; furthermore, the single fiber theory does not accurately predict the size of the fiber on the plane. A single photoelectric modulator is used to measure these matrix elements. Therefore, the lower left and upper right quadrants of the matrix are not the same, since the S_{ij} are mixtures of certain matrix elements. For example, $S_{34} \equiv (S_{14} + S_{34})/(S_{11} + S_{31})$ which is equal to the normalized $S_{34} = S_{34}/S_{11}$, since $S_{14} = S_{31} = 0$; $S_{33} \equiv (S_{13} + S_{33})/(S_{11} + S_{31})$, which is equal to the normalized S_{33}/S_{11}, since $S_{13} = S_{31} = 0$; and $S_{12} = S_{12}/S_{11}$, while $S_{21} = S_{11} + S_{21}$. S_{11}, S_{32} and $S_{42} = S_{12}$. These signals are discussed in detail in references by Bell et al.[2]

This system represents an "exactly known defect" on a perfect surface. Controlling the parameters of both the surface and "defect" make the data amenable to theoretical treatment and gives insight into how geometrical surface defects can affect the far field scatter from surfaces.

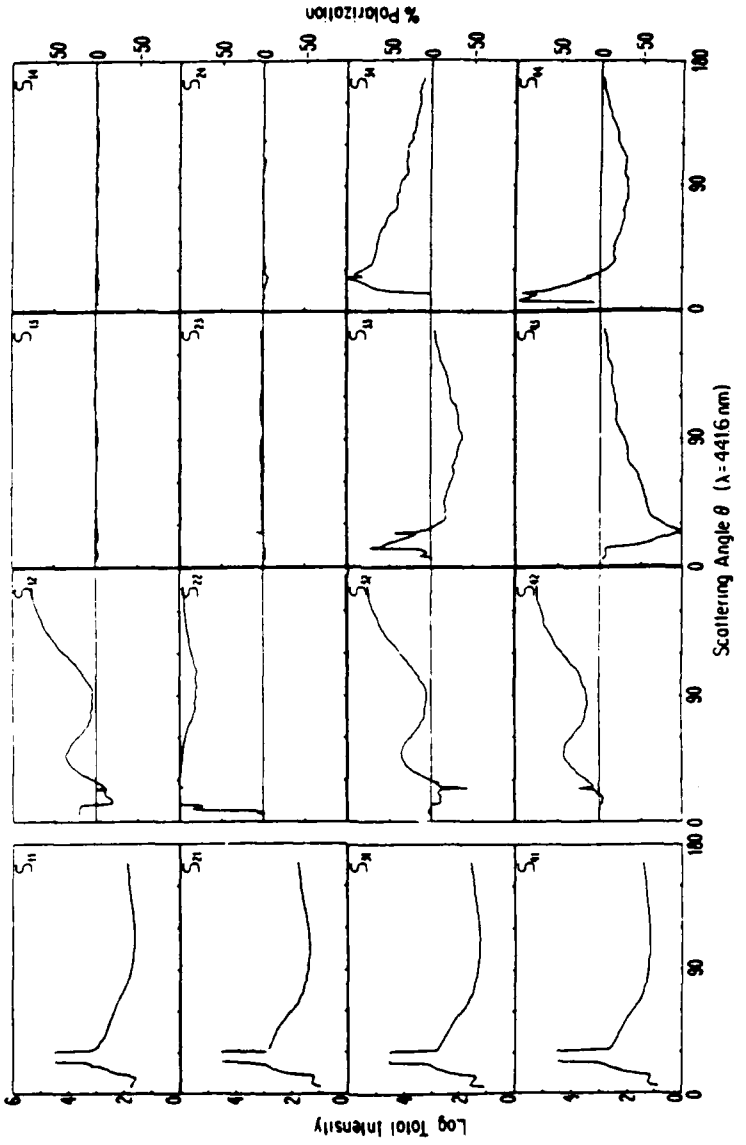

FIGURE 2. The matrix elements for a nearly perfect aluminum surface illuminated at an incident angle of $\alpha = 10^{o}$.

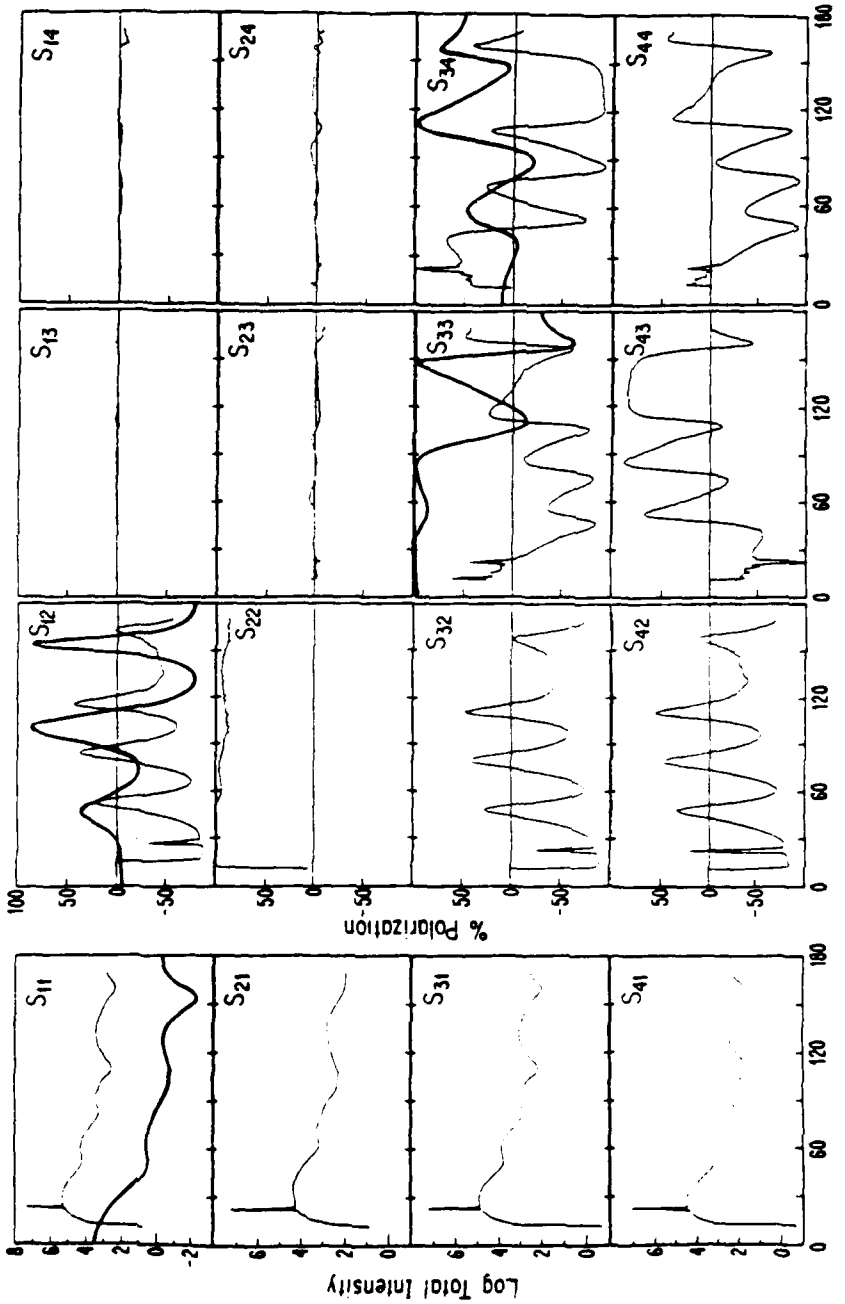

FIGURE 3. The matrix elements for a 0.6 micron quartz fiber (thick line) and for the 0.6 *micron fiber on a nearly perfect aluminum mirror illuminated at an incident angle of* $\alpha = 10^{o}$.

4. LIGHT SCATTERING FROM LIQUID COATED SURFACES AS A FUNCTION OF TIME-DEPENDENT THICKNESS

Perfect surfaces coated with pure liquids with index n and thickness t constitute a completely characterized optical system that can be described exactly by the Fresnel equations for reflection. As the thickness varies, either spatially across the sample or temporally at a fixed sample position, the phase changes at the interfaces will affect all matrix elements. We investigated two time-dependent phenomenona: changes in liquid surface thickness with time due to evaporation, and changes in surface structure due to liquid diffusion into the porous surface. We discuss here the response of S_{ij}'s to changing surface thickness due to evaporation. At t = 0, a liquid is ejected onto a surface, and it spreads out to make a uniform thickness that decreases to zero as the liquid evaporates. The two curves of Figure 4 show how the reflected intensity S_{11} changes as alcohol evaporates from a smooth glass surface. The difference in the two curves represents different (uncontrolled) evaporation rates. Time increases from left to right. At time indicated by **A** on Figure 4, approximately 5 ml of alcohol is ejected onto the glass surface coincident with the incident laser beam. As the surface coats, S_{11} decreases rapidly and then increases as the liquid develops into a uniform film. As evaporation continues, "thin film" interference effects cause oscillations in the reflected intensity. As the last layers evaporate, the oscillation rate decreases, yielding minima, before returning to the S_{11} for an uncoated surface at point **B** of Figure 4. Although equal amounts of liquid are ejected onto the surface each time, the evaporation rate is not controlled in these experiments. All four curves are similar in that all features reproduced during evaporation.

Figures 5, 6, and 7 show the response of the polarization matrix elements S_{12}, S_{33}, and S_{34}. S_{34} and S_{33} are especially interesting, both showing ~5% oscillations in the polarization. The vertical scales for these matrix elements is ±100%. These variable-thickness coated scattering systems (smooth liquid surfaces on a mirror surface) form the quantitative starting point for scattering from coated rough surfaces.

These highly structured oscillatory matrix element curves will not occur for the liquid coated rough surfaces to be studied later. These curves were obtained in reflection and the flat parallel surfaces that bound the liquid coating create the interference effects. Rough surfaces generally show no reflected peak or a preferred scattering direction. The far field intensity distribution appears more like a speckle pattern where each point in the far field is illuminated by many points on the surface. The random interference causing scatter is little affected by the addition of a thin liquid film onto the rough surface. In this case the surface structure dominates the far field scatter and overwhelms the subtle differences caused by thin liquid layers.

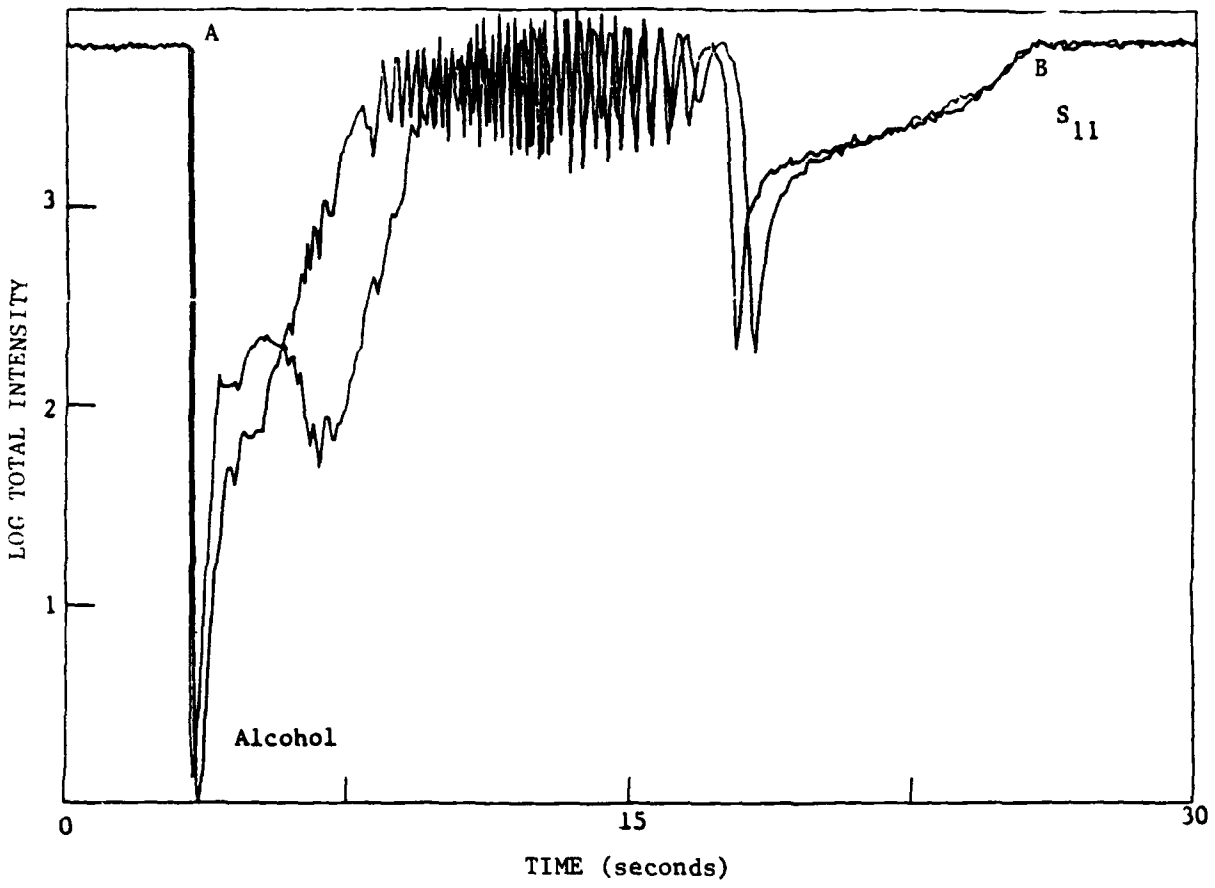

FIGURE 4. Matrix element S_{11} in reflection as a function of alcohol thickness (time) as alcohol evaporates from an aluminum mirror.

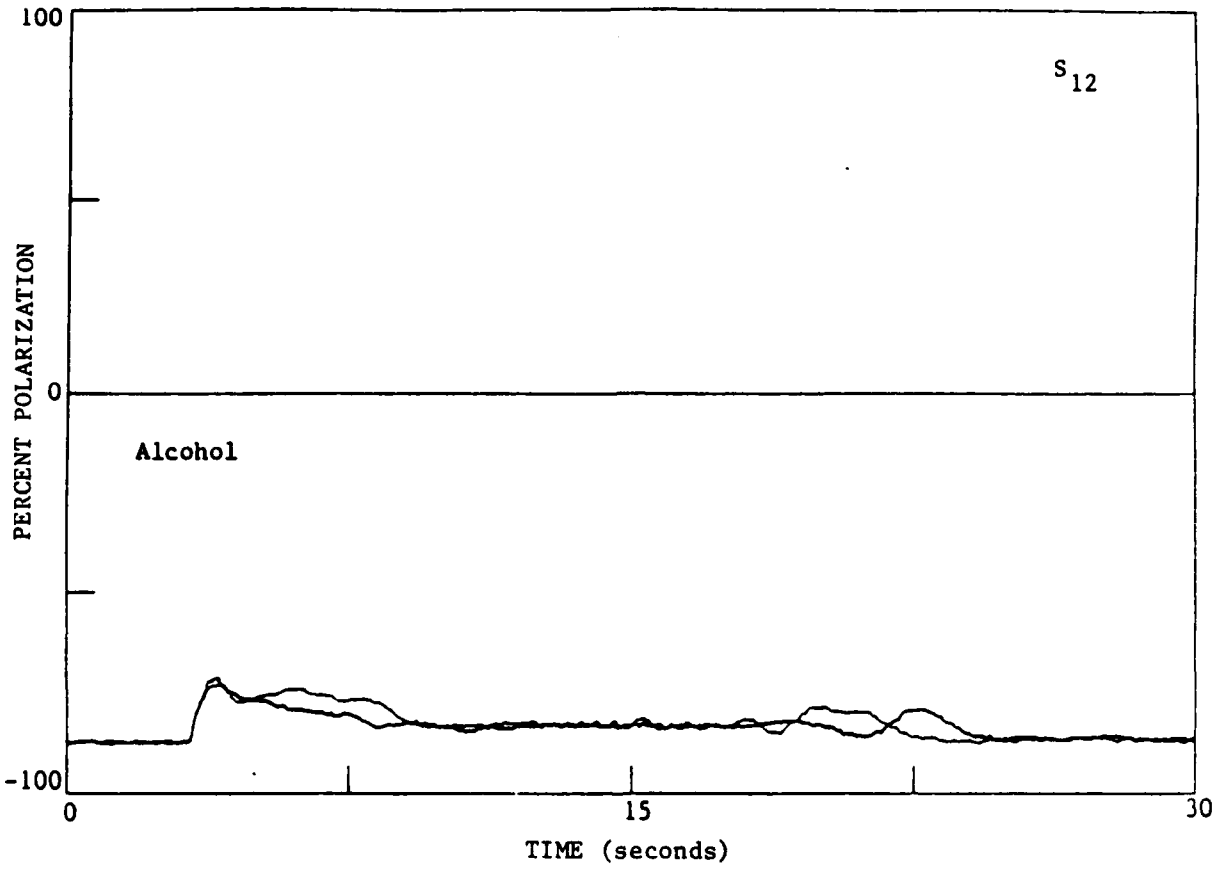

FIGURE 5. Matrix element S_{12} in reflection as a function of alcohol thickness (time) as alcohol evaporates from an aluminum mirror.

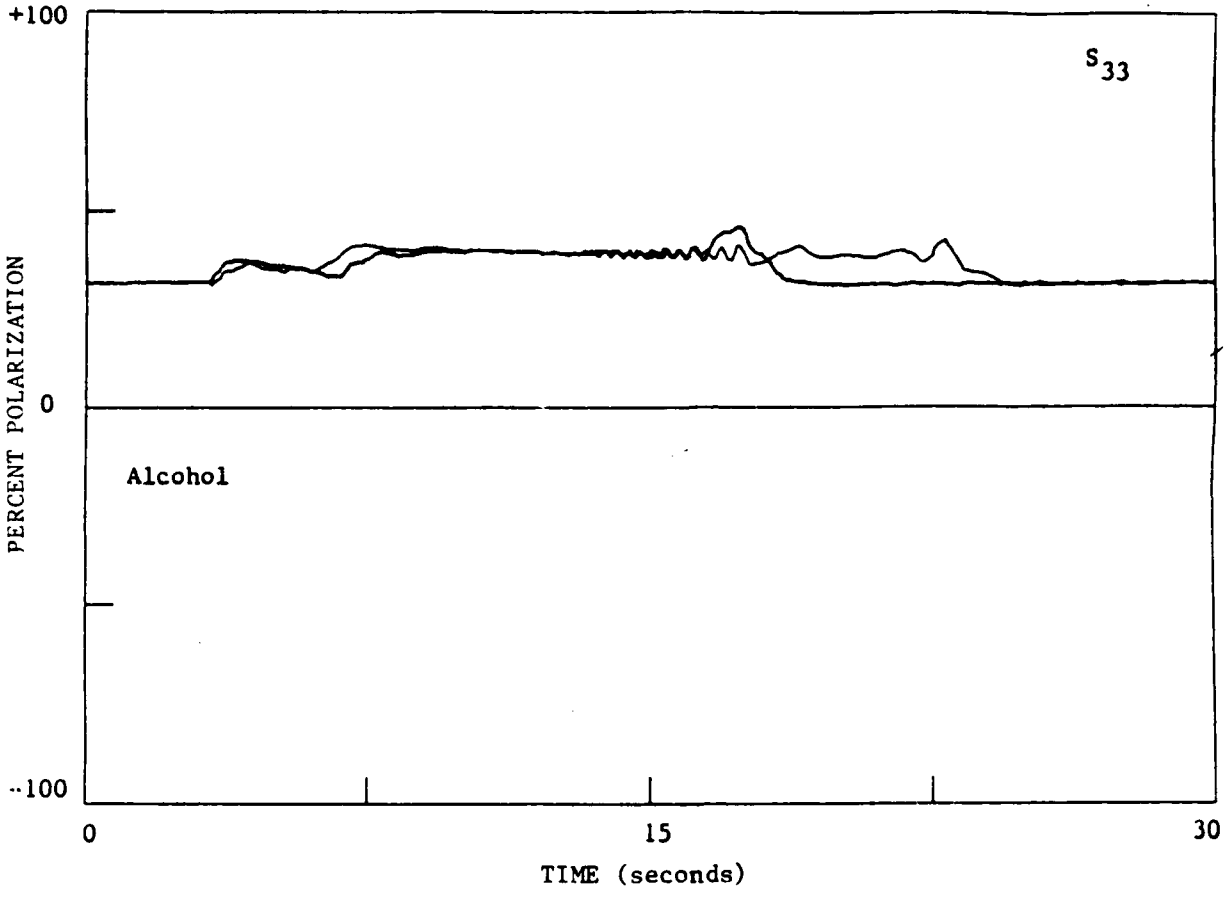

FIGURE 6. Matrix element S_{33} in reflection as a function of alcohol thickness (time) as alcohol evaporates from an aluminum mirror.

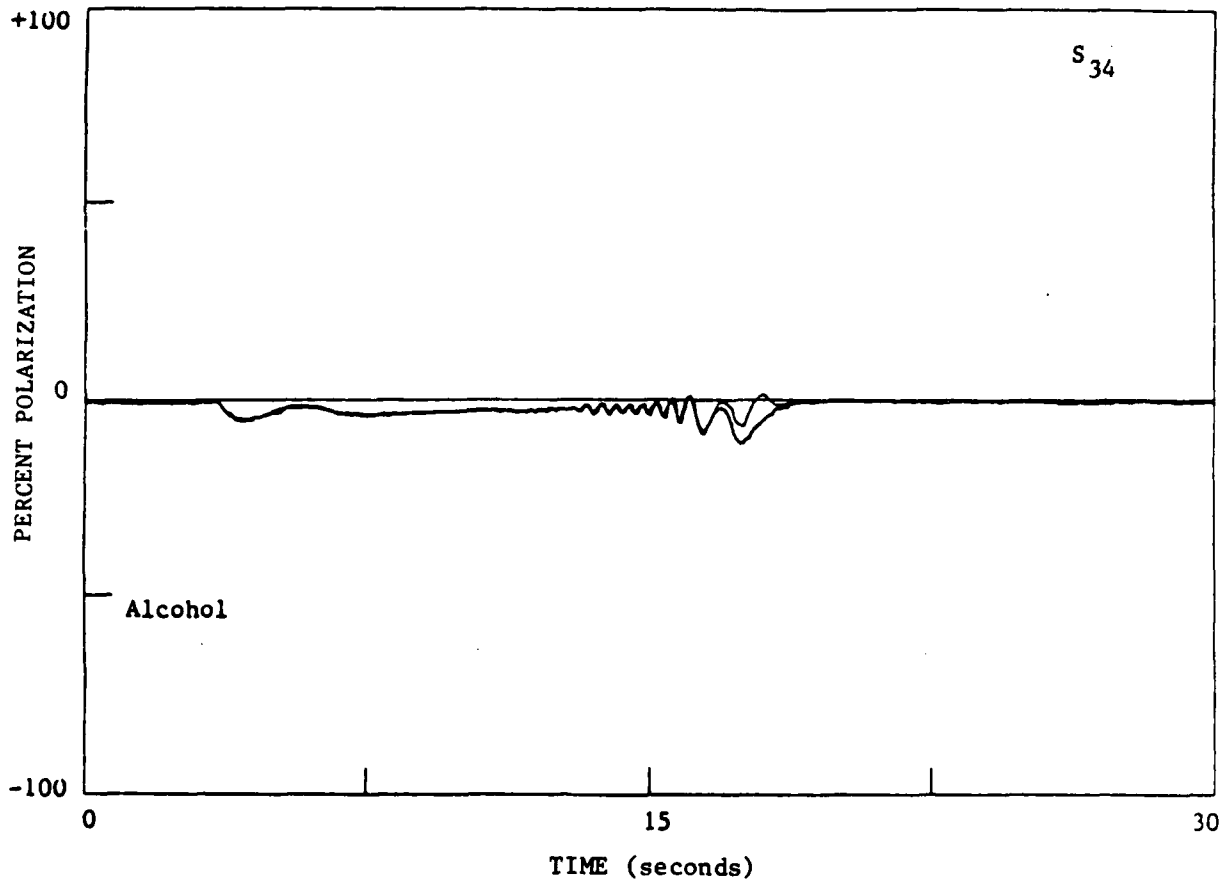

FIGURE 7. Matrix element S_{34} in reflection as a function of alcohol thickness (time) as alcohol evaporates from an aluminum mirror.

5. THEORETICAL INVESTIGATION OF SCATTERING FROM LIQUID COATED SURFACES

Liquid coated smooth surfaces form the logical theoretical starting point for studies of liquid coated, rough, porous, surfaces. Using the Fresnel equations, we can generate the theoretical Mueller scattering matrix elements for specular reflection from ideal surfaces and thinly coated surfaces.

We start with the Fresnel equations for an interface between two media, and transform them into the Mueller matrix element representation for reflection and transmission. With this approach, we can use theoretical models of scattering from surfaces and compare them to experimental measurements.

The relationships between the Fresnel equations and four of the Mueller scattering matrix elements are given by:[3]

$$S_{11} = (|S_1|^2 + |S_2|^2)/2 \qquad S_{12} = (|S_2|^2 - |S_1|^2)/2$$

$$S_{33} = \text{Real}\,(S_1\,S_2^*) \qquad S_{34} = \text{Imaginary}\,(S_2\,S_1^*) \quad ,$$

where S_1 is the Fresnel equation for the perpendicular electric field and S_2 is for the parallel electric field,

$$S_{1,R} = \frac{n_i \cos\theta_i - n_t \cos\theta_t}{n_i \cos\theta_i + n_t \cos\theta_t} \qquad S_{1,T} = \frac{2n_i \cos\theta_i}{n_i \cos\theta_i + n_t \cos\theta_t}$$

$$S_{2,R} = \frac{n_t \cos\theta_i - n_i \cos\theta_t}{n_t \cos\theta_i + n_i \cos\theta_t} \qquad S_{2,T} = \frac{2n_i \cos\theta_i}{n_t \cos\theta_i + n_i \cos\theta_t} \quad ,$$

where i is the incident medium, and t is the transmission medium. There will be one set of matrix elements for reflection (R) and one for transmission (T).

The Fresnel equations for the parallel and perpendicular electric field components for reflection and transmission at a single interface are shown in Figure 8 (top and bottom). These curves are the standard textbook electric field amplitudes for a pair of nonabsorbing media.[4] In the Mueller matrix representation, the curves for the same interface are shown in Figure 9. The total intensity matrix element, S_{11}, is the average of the intensity of the two electric field components. The other elements show ratios of the various polarizations. Note that for nonabsorbing media, S_{34} is always zero.

We now can consider a thin layer of an optically transparent material between two regions of air. This will give a series of different curves as a function of the layer thickness as shown in Figure 10 (top and bottom) for reflection and transmission, respectively. For a very thin layer (two boundaries), less than a wavelength of the incident light, the effect is similar to that of a surface (one boundary). At larger thicknesses, interference effects start to occur that cause the reflectance to approach and in some cases equal zero. For thick layers, more than a few wavelengths, this can occur at several different incidence angles. There is also a loss of symmetry between the reflection and transmission curves for the polarization matrix elements (S_{12}, S_{33}, and S_{34}).

Any matrix element, examined as a function of layer thickness at a particular incidence angle, shows oscillations in the curves from these interference effects. Zeroes in the polarization curves are due to interference between multiple internal reflections. One interesting effect is an inflection point that occurs in the S_{34} matrix element as a function of

thicknesses shown in Figure 11. This point occurs at the third zero and every fourth one after that point. It remains there even when the polarization reverses as the refractive index increases from $n_1 = 1.4$ to 1.6 and then 1.8.

Experimentally measured "Fresnel curves" for slightly rough surfaces at angles slightly larger and smaller than the reflection angle show how scattering affects the Fresnel curves. The simulations are an excellent starting point for studying the scatter from rough surfaces.

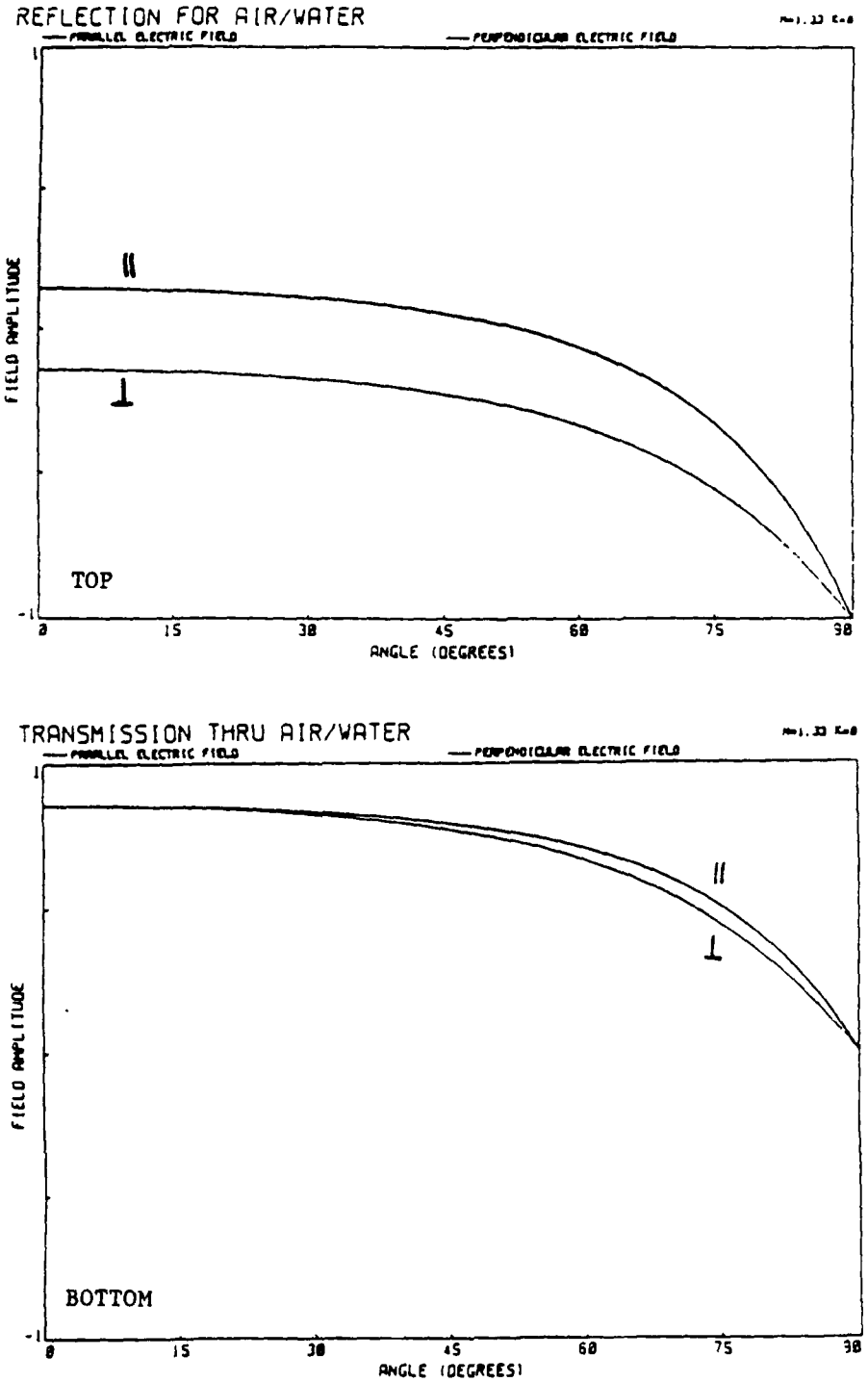

FIGURE 8. Polarized field amplitudes for reflections from an air-water interface (TOP). Polarized field amplitudes for transmission through an air-water interface (BOTTOM).

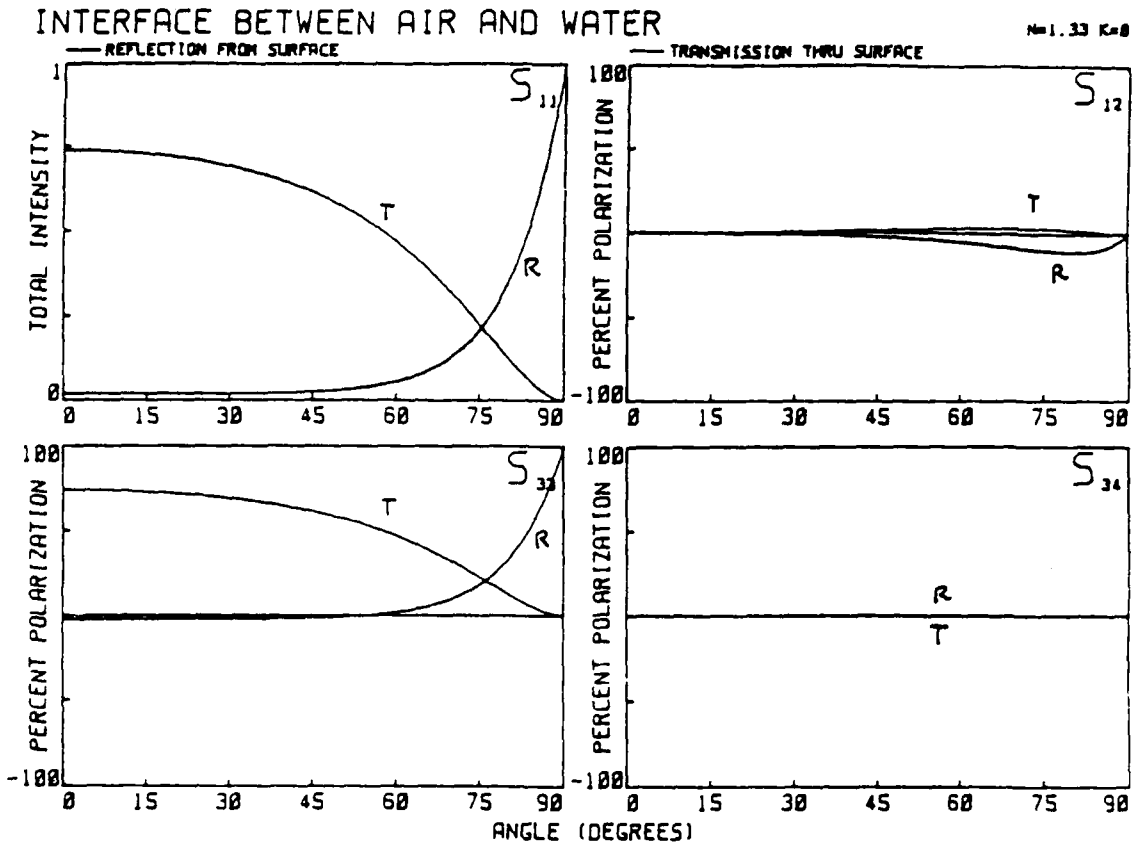

FIGURE 9. The matrix elements for reflection and transmission at an air-water interface.

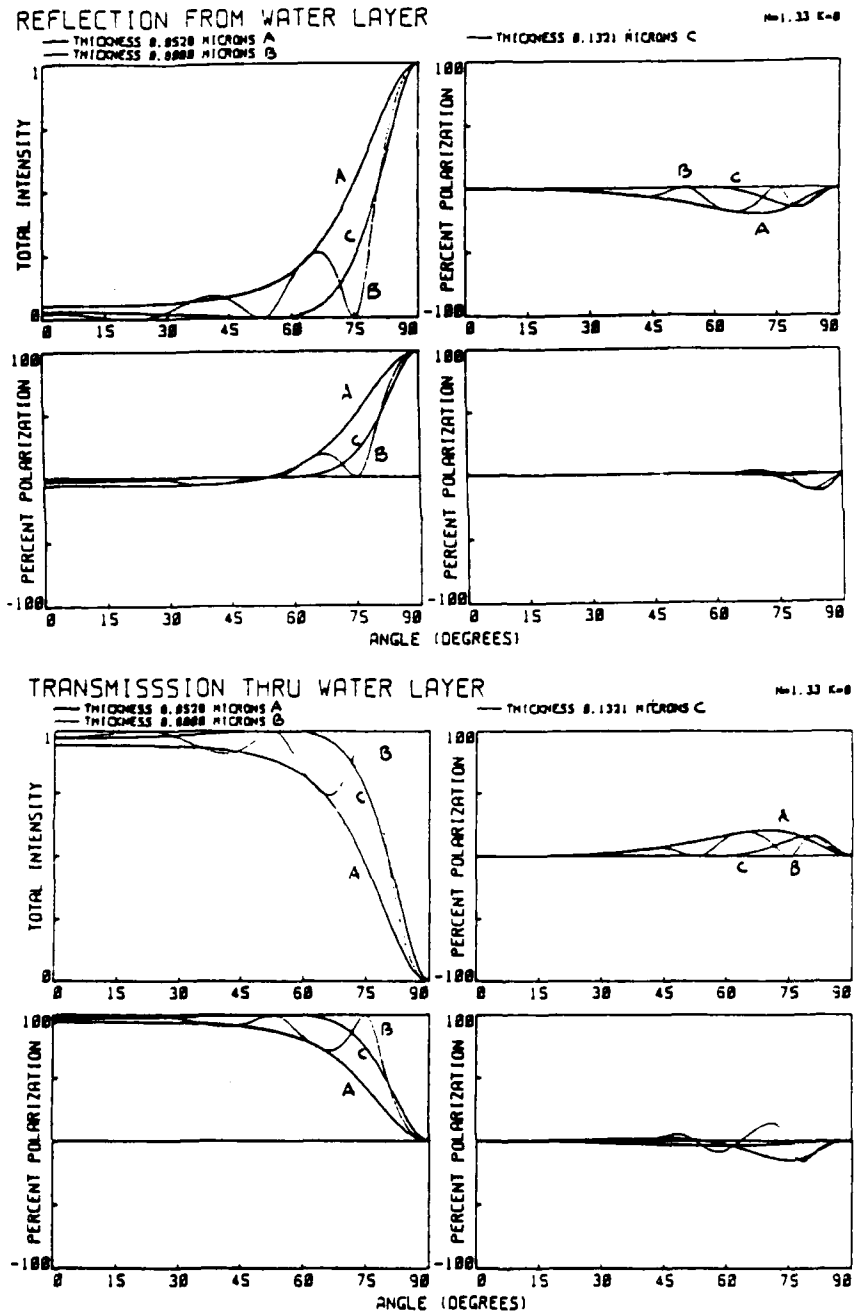

FIGURE 10. The matrix elements for reflection from a water layer as a function of thickness (TOP). The matrix elements for transmission through a water layer as a function of thickness (BOTTOM).

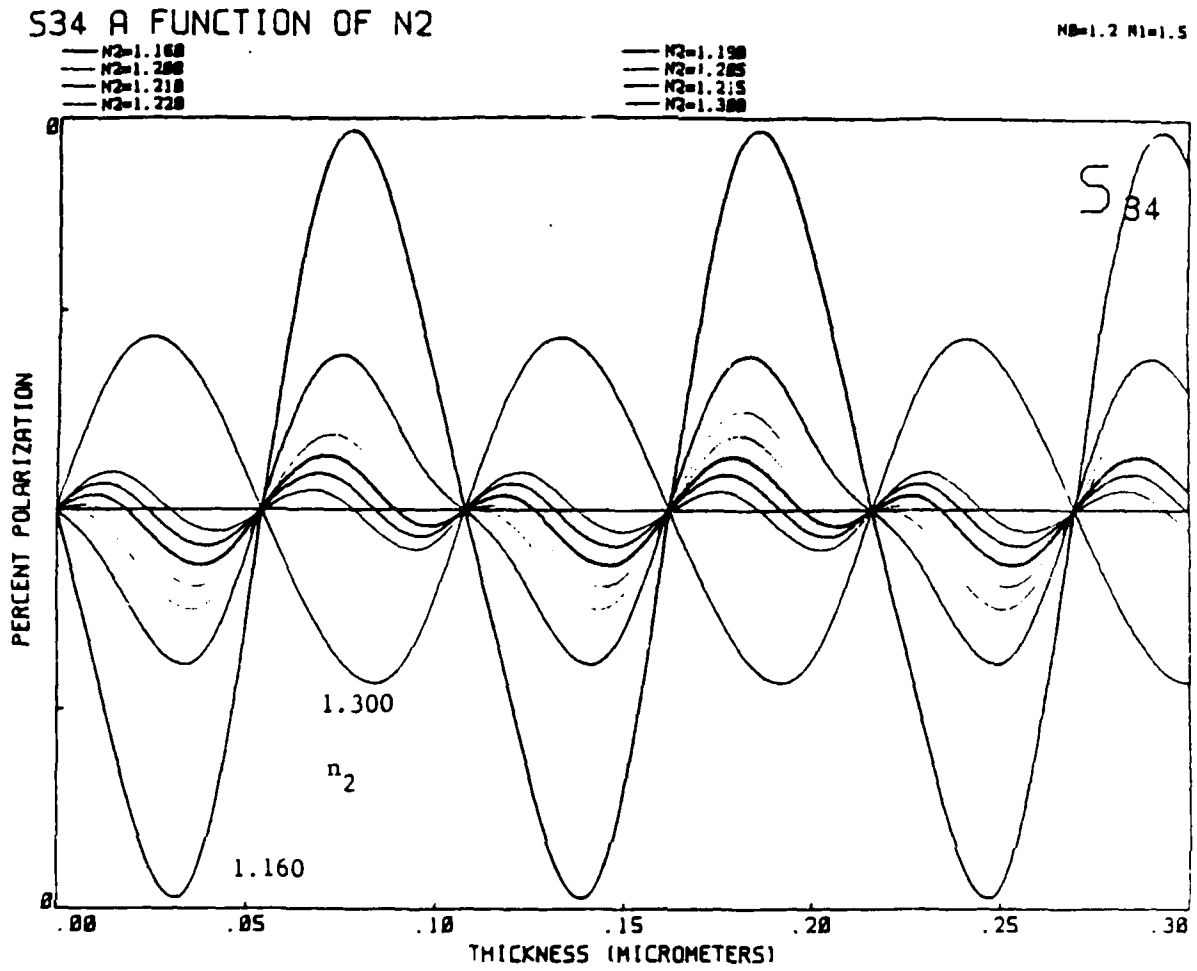

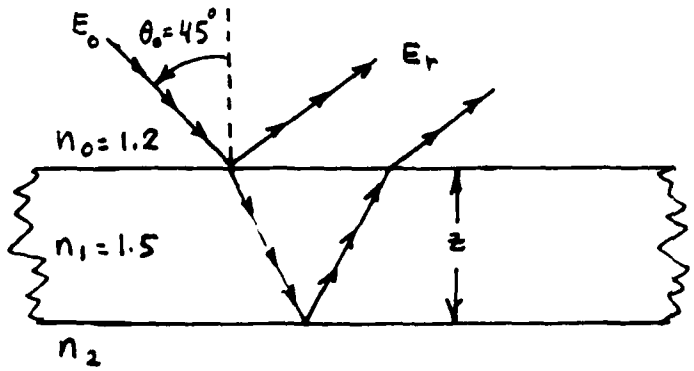

FIGURE 11. Matrix element S_{34} for reflection from a water layer on a substrate as a function of substrate index n_2 and water layer thickness.

6. LIGHT SCATTERING FROM ROUGH TEXTURED, POROUS SURFACES (SAND AND SALT)

Rough-textured porous surfaces are the most complex surfaces we have studied. They represent terrain, man-made painted metals, etc., and are of importance to the remote-sensing community. Our approach to these surfaces is the same as for the simpler systems: We start with a prepared system and then change its character. The two systems discussed here are for salt and sand, which we compact to different degrees and mount on microscope slides. Compacting the granules increases surface smoothness and decreases particle spacing -- decreasing the volume of liquid that can soak in. We also distinguish between two kinds of porous surfaces: those that are made from non-permeable particles, so that spreading occurs on the particle surface, such as sand and salt, and those that are permeable where the particles themselves absorb the liquid.

Salt crystals, while pure NaCl with exactly known optical properties, are polydispersed in size, shape (rounded curves, broken cubes) and in orientation. The salt crystal layer was thick enough to completely mask the underlying glass supporting surface so that all S_{ij} signals are of the salt surface only.

Sand quartz crystals are polydispersed in all geometrical and optical properties. We found that the matrix elements respond more readily to changes in salt surfaces than to sand.

Figures 12, 13, 14, and 15 show the backscatter signals for the four matrix elements S_{11}, S_{12}, S_{33} and S_{34} for sand. These matrix elements have been measured in the backscattering (θ = 165°) direction while the sample surface was rotated from α = 0 to 90° with the geometry shown by the insert in Figure 12.

Our backscatter studies of many rough porous surfaces, including soil, sand, concrete, leaves, etc., have yielded similiar results:

1) Matrix elements S_{11} and S_{33} are more sensitive to surface changes than are S_{12} and S_{34}.

2) The largest signal differences occur in the "reflected" peak.

3) The S_{ij} are quite sensitive to surface smoothness (compaction). The three curves shown for the matrix elements S_{11}, S_{12}, S_{33}, and S_{34} of Figures 12, 13, 14, and 15 represent three different surface roughnesses. Curve A is for loosely packed salt, curve B is for medium compacted while, curve C is for very compact salt.

Figures 16, 17, 18, and 19 show the four backscatter matrix elements for salt. We call attention to several important observations.

1) S_{11} and S_{33} show great sensitivity to compaction. The specular peak-to-backscatter intensity ratio decreases by over four orders of magnitude as compaction increases.

2) Significant differences in S_{11} occur over the entire θ-range with minimal sensitivy to change occuring at $\alpha \doteq 18°$.

3) Matrix element S_{12} shows a very slight sensitivity near α = 33° and near the specular peak (in contrast to sand).

We also studied surfaces of clay, soil, ground quartz, Arizona road dust, and glass spheres in various degrees of compaction (surface roughness) in preparation for the "liquid coating" studies. These experiments set the stage for our final efforts with four soil surfaces which were studied in a dry (uncoated) and wet (coated) condition. Two oily liquids were used: one that was relatively absorbing at the laser probe wavelength and one that was relatively transparent. We have also done extensive coating experiments with water, alcohol, and acetone to observe the effects of evaporation rate and viscosity. The results of these final experiments and conclusions drawn are given in the following sections. We first discuss the techniques used to prepare the four soil surfaces, the oils used for coating the surfaces, and surface-coating techniques.

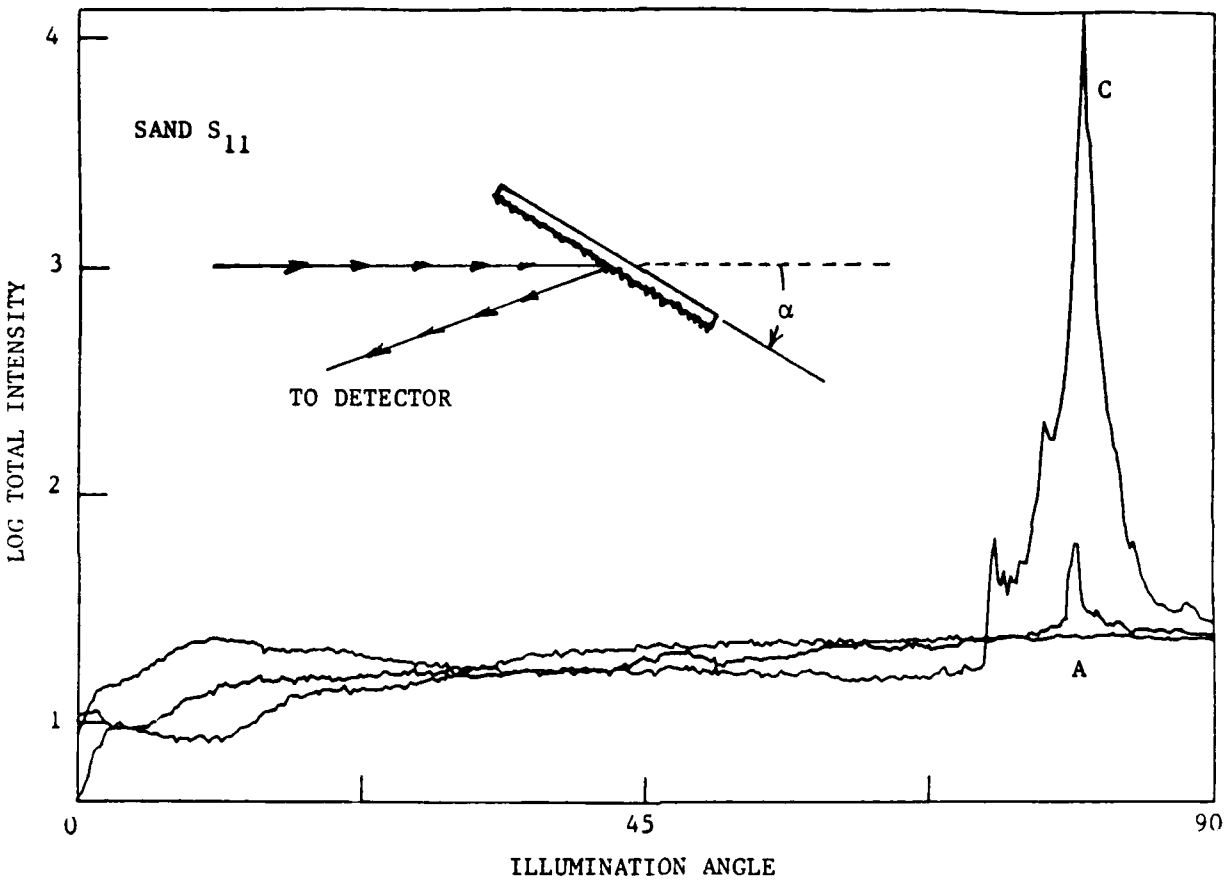

FIGURE 12. Matrix element S_{11} for three sand surfaces measured in the backscatter as a function of surface compaction and illumination angle α.

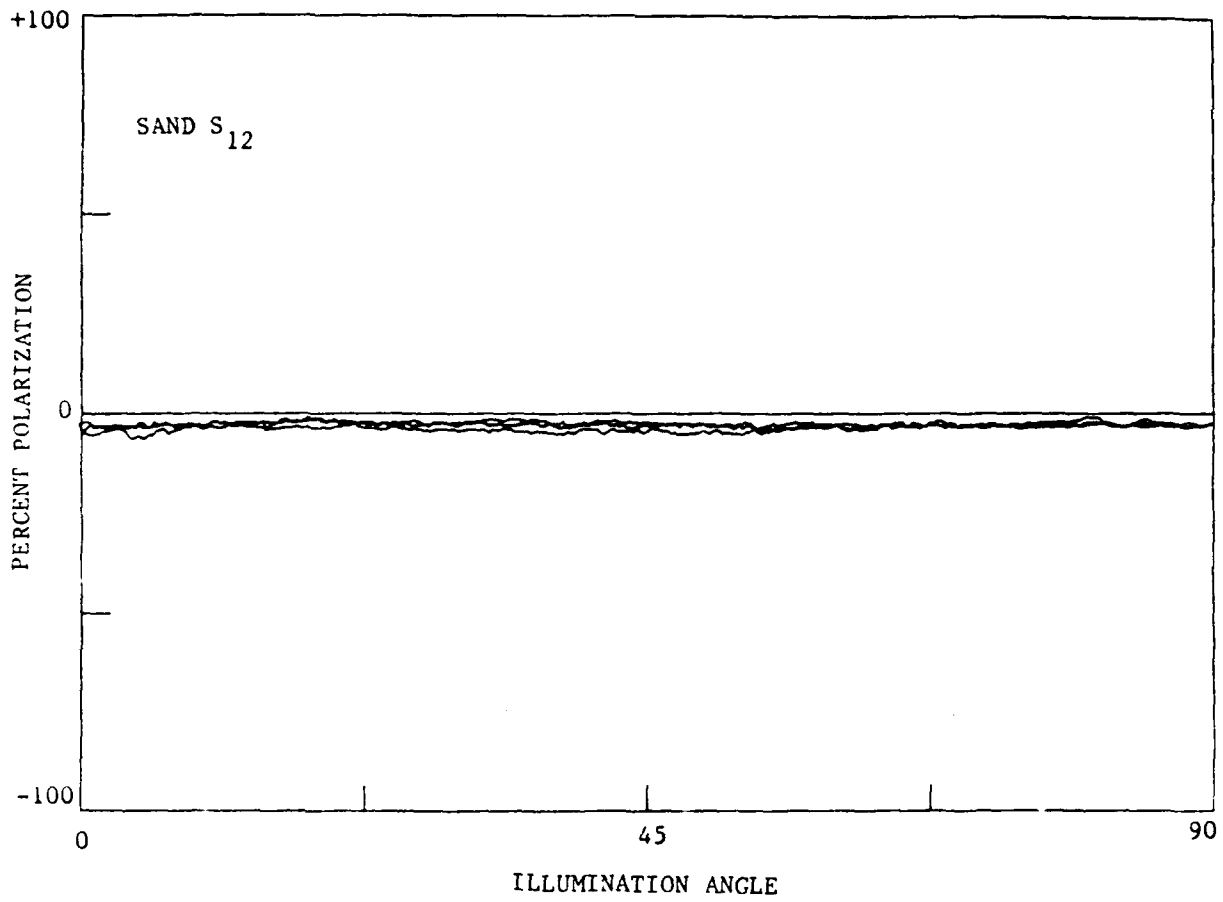

FIGURE 13. Matrix element S_{12} for three sand surfaces measured in the backscatter as a function of surface compaction and illumination angle α.

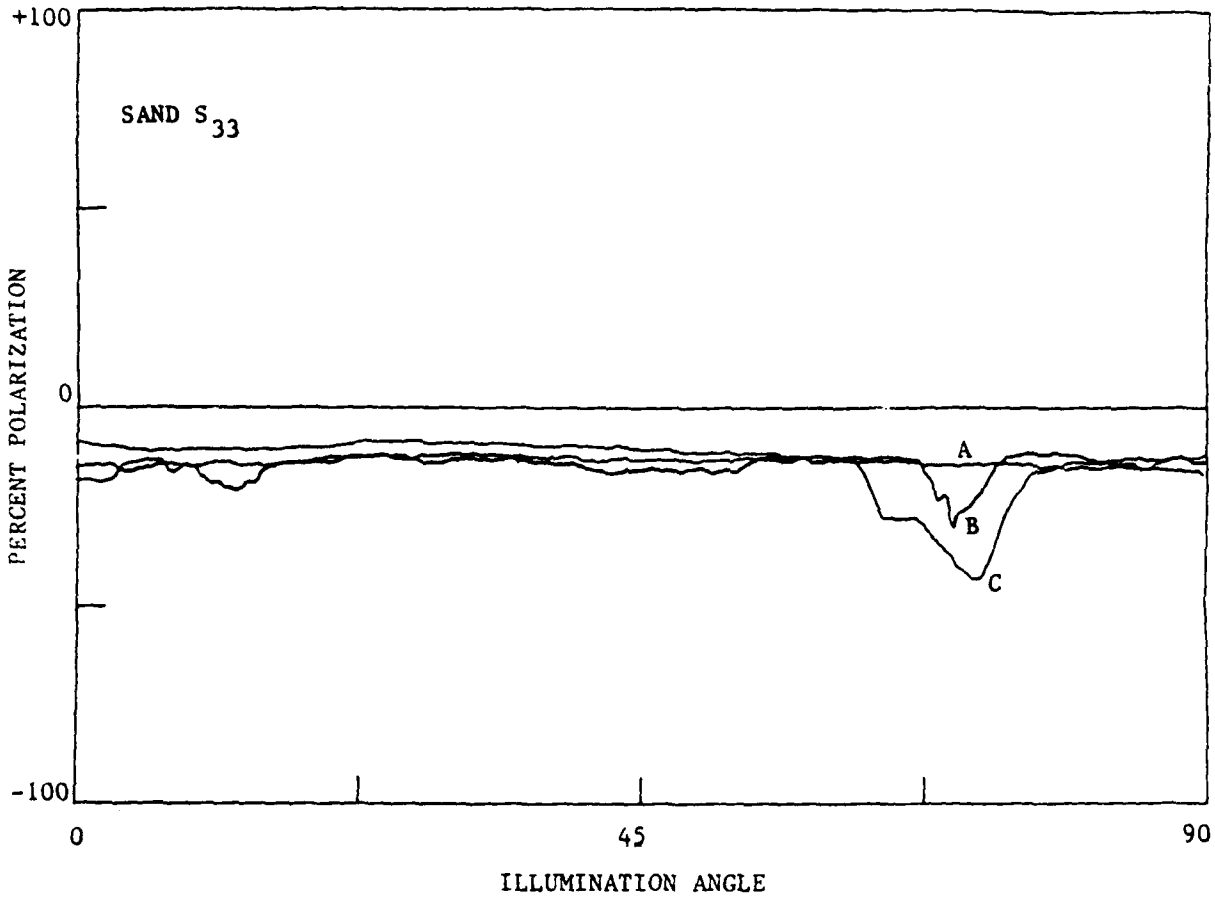

FIGURE 14. Matrix element S_{33} for three sand surfaces measured in the backscatter as a function of surface compaction and illumination angle α.

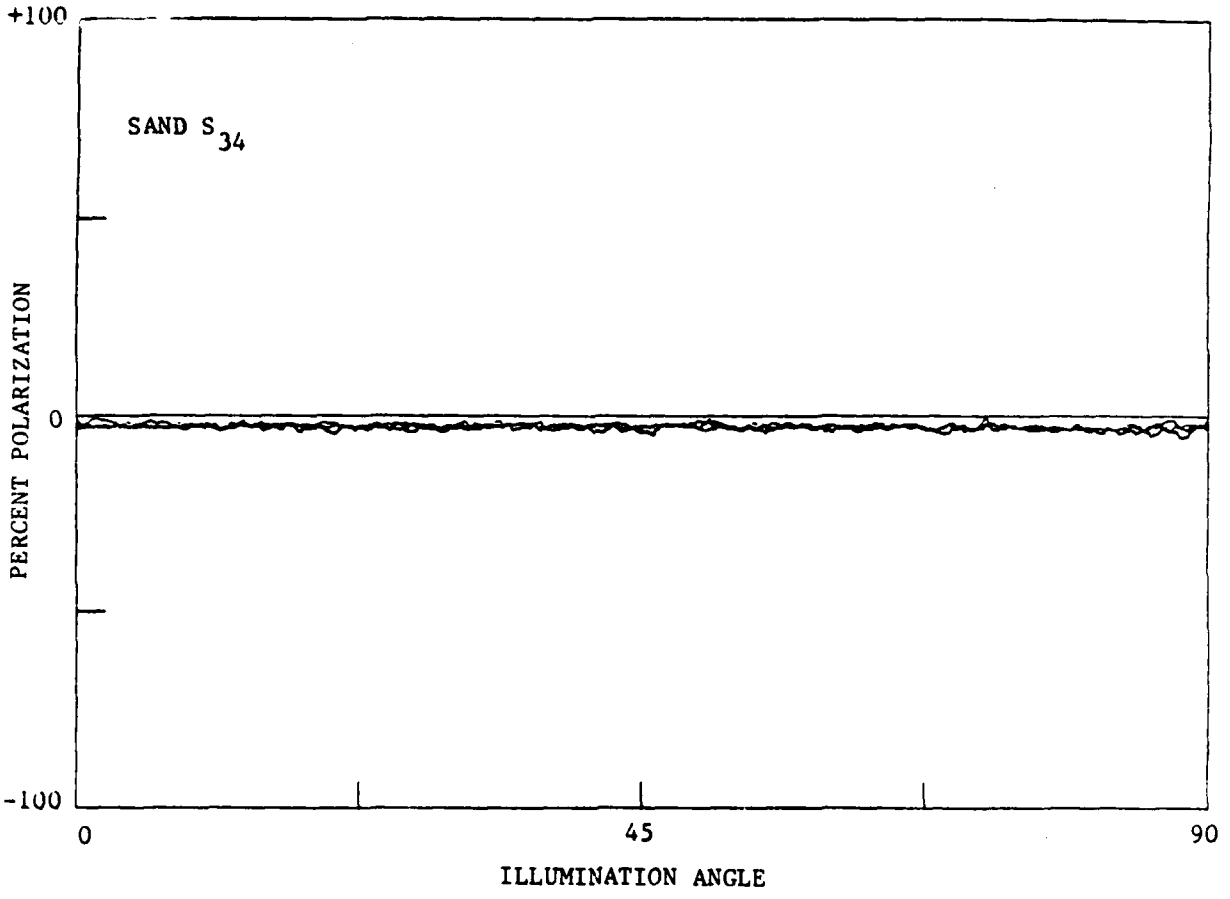

FIGURE 15. Matrix element S_{34} for three sand surfaces measured in the backscatter as a function of surface compaction and illumination angle α.

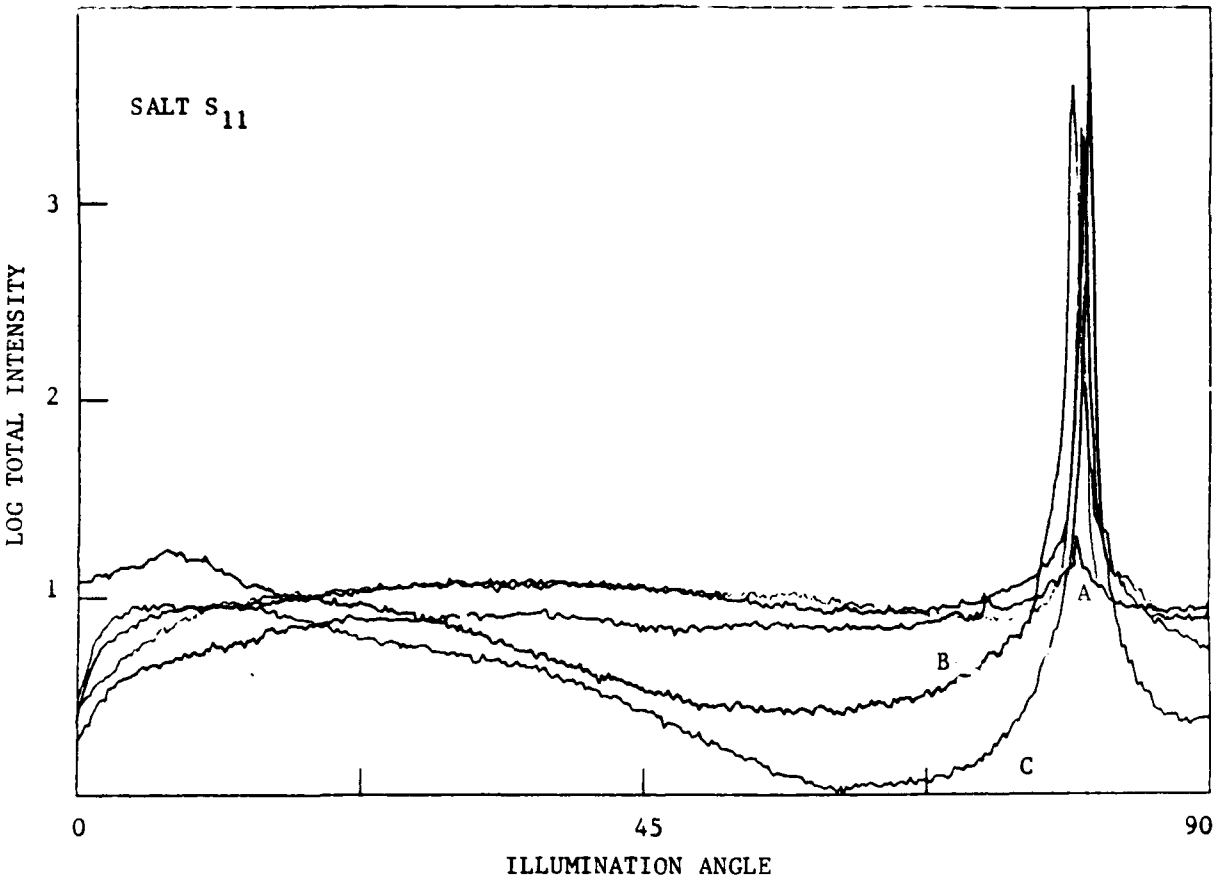

FIGURE 16. Matrix element S_{11} for salt surfaces measured in the backscatter as a function of surface compaction and illumination angle α.

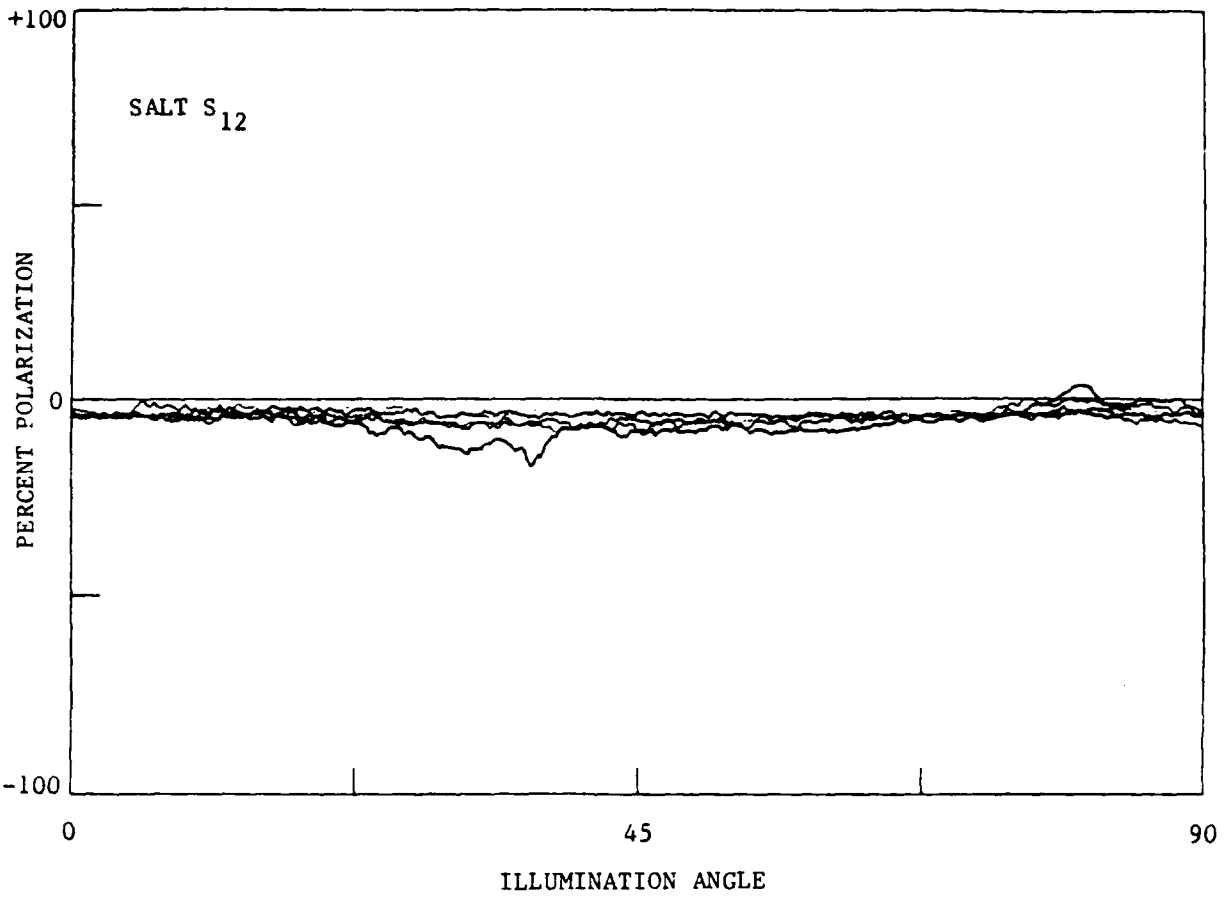

FIGURE 17. Matrix element S_{12} for salt surfaces measured in the backscatter as a function of surface compaction and illumination angle α.

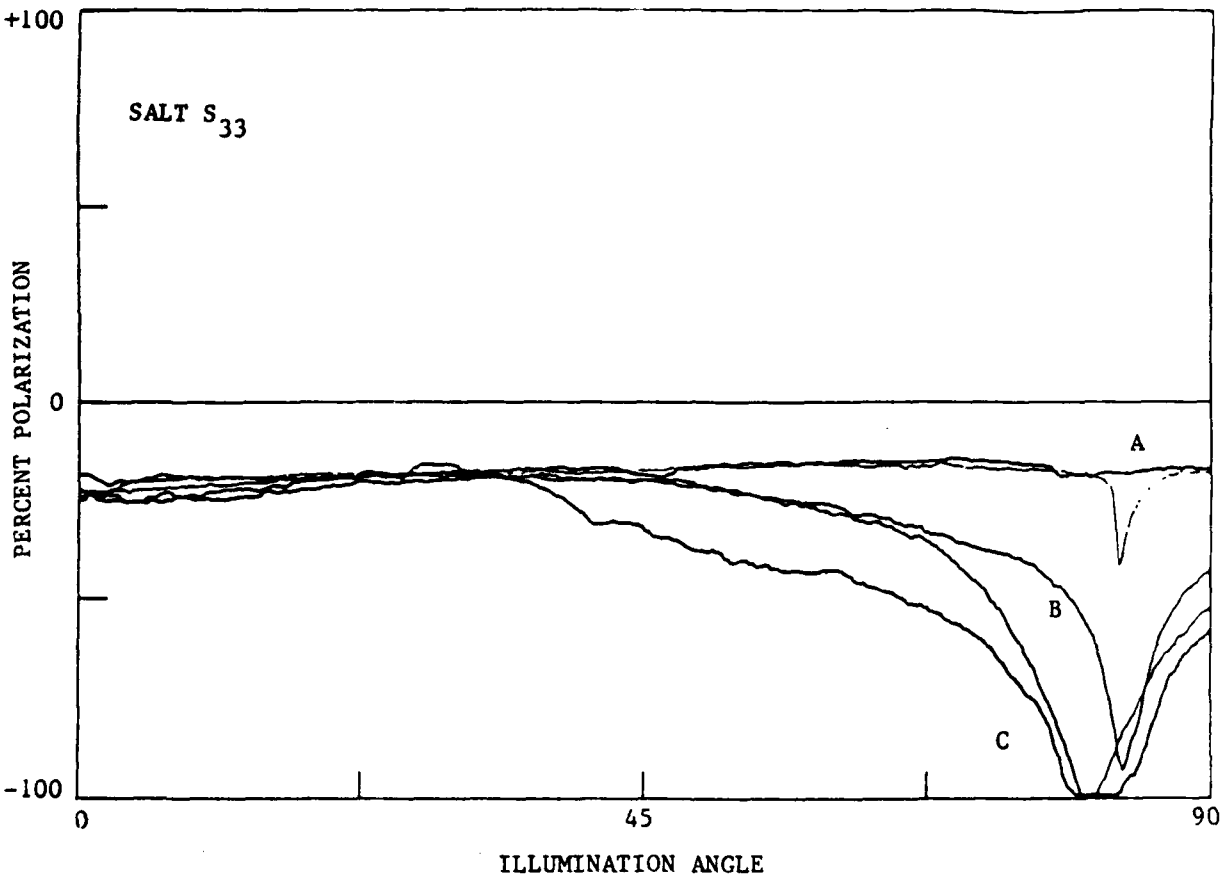

FIGURE 18. Matrix element S_{33} for salt surfaces measured in the backscatter as a function of surface compaction and illumination angle α_2.

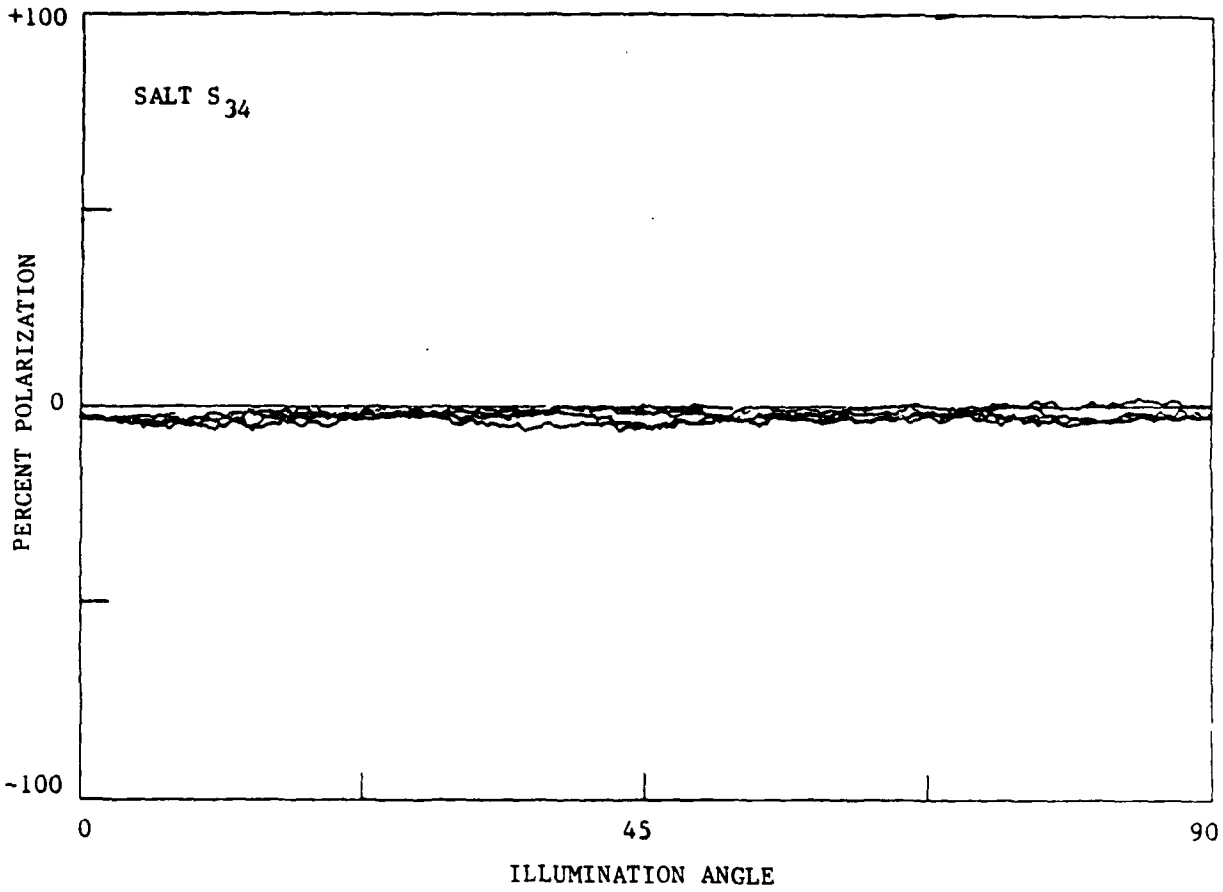

FIGURE 19. Matrix element S_{34} for salt surfaces measured in the backscatter as a function of surface compaction and illumination angle α.

7. PREPARATION OF FOUR SOIL SURFACES FOR LIGHT SCATTERING

Four standard soil samples were given to us by Dr. Donald F. Post of the UA Agriculture Department. These soils are generic in that they have been created as "standards" for various experiments where characterized and reproducible soils are needed.

The ingredients, soil characteristics, and particle sizes are given in Table I below:

TABLE I
INGREDIENT AND SIZE RANGE OF PARTICLES IN FOUR SOILS

SAMPLE	CLAY <0.002 mm	SILT 0.002-0.05 mm	SAND 0.05-2 mm
SAND (S) Superstition (Yuma) sand Yuma, Az	2.0%	1.7%	96.3%
SANDY-SOIL (SS) Aqua	12.3%	29.0%	58.7%
CLAY-SOIL (CS) White house clay soil from semi-arid regions	33.0%	18.0%	49.0%
LOAMY-SOIL (LS) Cloversprings loamy soil from semi-arid regions	20.7%	39.7%	39.6%

The procedure for collecting these soils and their preparations for experiments and display is given in Ref. 4.

We used the "vinyline resin method" to mount the four soil samples on 25 x 75 mm glass microscope slides. A 10% vinyl plastic solution in a keytone is used as a fixative. The vinyl plastic fixative can be purchased as a powder from the Union Carbide Corporation, Chemical and Plastic Division, 120 South Riverside Plaza, Chicago, Illinois, 60606. The methyl ethyl ketone ($CH_3COCH_2CH_3$) is not only a satisfactory solvent, but it also works well on all soils. The surfaces for the four soils described above were prepared using the following procedure:

First, three drops of plastic fixative (approximately 0.15 ml) were applied evenly on a 2.5 x 2.5 square-centimenter area of a microscope slide. After twenty seconds, the soil was

carefully sprinkled onto the surface to cover the plastic fixative area. After three minutes, the excess loose soil was gently blown from the surface of the sample using dry compressed air.

Second, the soil surface was coated with six drops (0.3 ml) of the plastic fixative and the soil was again sprinkled on to cover the area. After three minutes, the loose soil was again gently blown off. Three minutes later, the process was repeated.

The final result was a 2.5 × 2.5 square-centimeter soil surface about 0.2 cm thick on a glass microscope slide. After about one-half hour, the sample was dry and ready to use for light scattering studies. This is a very good way to produce many reproducible soil surfaces for light scattering studies. For these experiments, 15 samples of each soil were prepared and checked for uniformity.

8. THE θ-DEPENDENT MATRIX ELEMENTS S_{11}, S_{12}, S_{33}, AND S_{34} FOR THE FOUR SOILS

Our previous experiments with rough surfaces have established the fact that the matrix elements S_{11}, S_{12}, S_{33}, and S_{34} are the most likely candidates useful to characterize rough surfaces and detect changes in their structure. During our preliminary studies these four matrix elements were measured for as many as ten separate but identically prepared samples of each soil surface. These measurements resulted in (4 matrix elements) x (4 soils) x (10 measurements/soil) or about 160 matrix element curves. These data showed us the best way to prepare reproducible surfaces of each soil. We then studied matrix element reproducibility for all four (identically prepared) soils buy making three different sets of measurements:

1. We measured the entire matrix element $S_{ij}(\theta)$ for fixed a for three different positions on the same soil surface. These are shown in Figures 20, 21, 22 and 23.

2. We measured the entire matrix element $S_{ij}(\theta)$ for fixed a for three different samples of the same soil. These are shown in Figures 24, 25, 26 and 27.

3. We also measured a particular matrix element (for fixed θ and two different α) as a function of position on the same soil surface.

In this section we discuss the results of measurements 1 and 2. The results of measurement 3 are discussed in the next section.

Figures 20, 21, 22 and 23 show three curves for each of the four matrix elements for the four soils illuminated at $\alpha = 10°$. All three curves of a particular matrix element should coincide if the surfaces are identical at the three different illumination points.

Figure 20 for sand shows that except for S_{33} around $\theta = 30°$ the surfaces are essentially uniform.

Figure 21 for sandy soil shows a slight difference in the total scattered intensity S_{11} for one of the three samples and a deviation on S_{33} around 30° as was the case for sand.

Figure 22 for clay soil shows slight differences in the total scattered intensity S_{11} for all three samples and deviations in the forward scatter of S_{12}. Matrix elements S_{33} and S_{34} show negligable differences between the three samples.

Figure 23 for loamy soil shows only slight differences in the forward scatter of S_{11} and S_{33}.

These measurements, and the results of similar measurements on the other identically prepared samples, indicate the reproducibility of the S_{ij} from sample to sample of the same soil.

We summarize the results in Table II.

TABLE II
MAXIMUM MATRIX ELEMENT FLUCTUTATION (PERCENT)
FOR THREE DIFFERENT POSITIONS ON THE SAME SOIL SAMPLE

S_{ij}	Sand	Sandy soil	Clay soil	Loamy soil
S_{11}	40	50	60	60
S_{12}	6	8	18	14
S_{33}	20	25	18	15
S_{34}	12	13	15	14

As expected, the unnormalized intensity S_{11} shows the largest variations. The matrix element S_{34} is essentially zero at all θ for all four soils. In addition it shows very little sensitivity to changes in soil structure. The fact that the matrix element is zero is not as significant as the fact it is a poor indicator of change. This was first realized in the studies of salt and sand (Figures 15 and 19) where it was totally insensitive to composition. We conclude that the S_{34} matrix element is a poor signature for rough surfaces (soils) and a poor indicator of change. This conclusion is strengthened by the data shown in the next four figures. These data in these two sets of figures are essentially similar. In the just discussed case (Figures 20, 21, 22 and 23) we measured S_{ij} for 3 different positions on the same sample whereas in the second case (Figures 24, 25, 26 and 27) we measure the S_{ij} for 3 different but identically prepared samples.

In the second case the Figures 24, 25, 26 and 27 show the three curves for each of the four matrix elements illuminated at $\alpha = 10$ degrees. All curves of a particular matrix element should coincide if the three different but identically prepared surfaces are identical at their illumination points.

The results of these two sets of measurements show that variations in S_{ij} from point to point on the same surface are about the same as the variations from different but identically prepared surfaces. Table III shows the average fluctuations of each S_{ij} for the three different (but identically prepared) soil samples and gives the average values, in brackets, obtained from both sets of these measurements.

This table shows that the fluctuations are greatest for S_{11} and least for S_{34}.

TABLE III
MAXIMUM MATRIX ELEMENT FLUCTUATION (PERCENT)
FOR THREE DIFFERENT (BUT IDENTICALLY PREPARED) SOIL SAMPLES

S_{ij}	Sand	Sandy Soil	Clay Soil	Loamy Soil
S_{11}	65 (53)	80 (65)	60 (60)	50 (55)
S_{12}	22 (14)	9 (8)	17 (17)	18 (16)
S_{33}	10 (15)	27 (26)	18 (18)	22 (19)
S_{34}	12 (12)	14 (14)	16 (15)	15 (14)

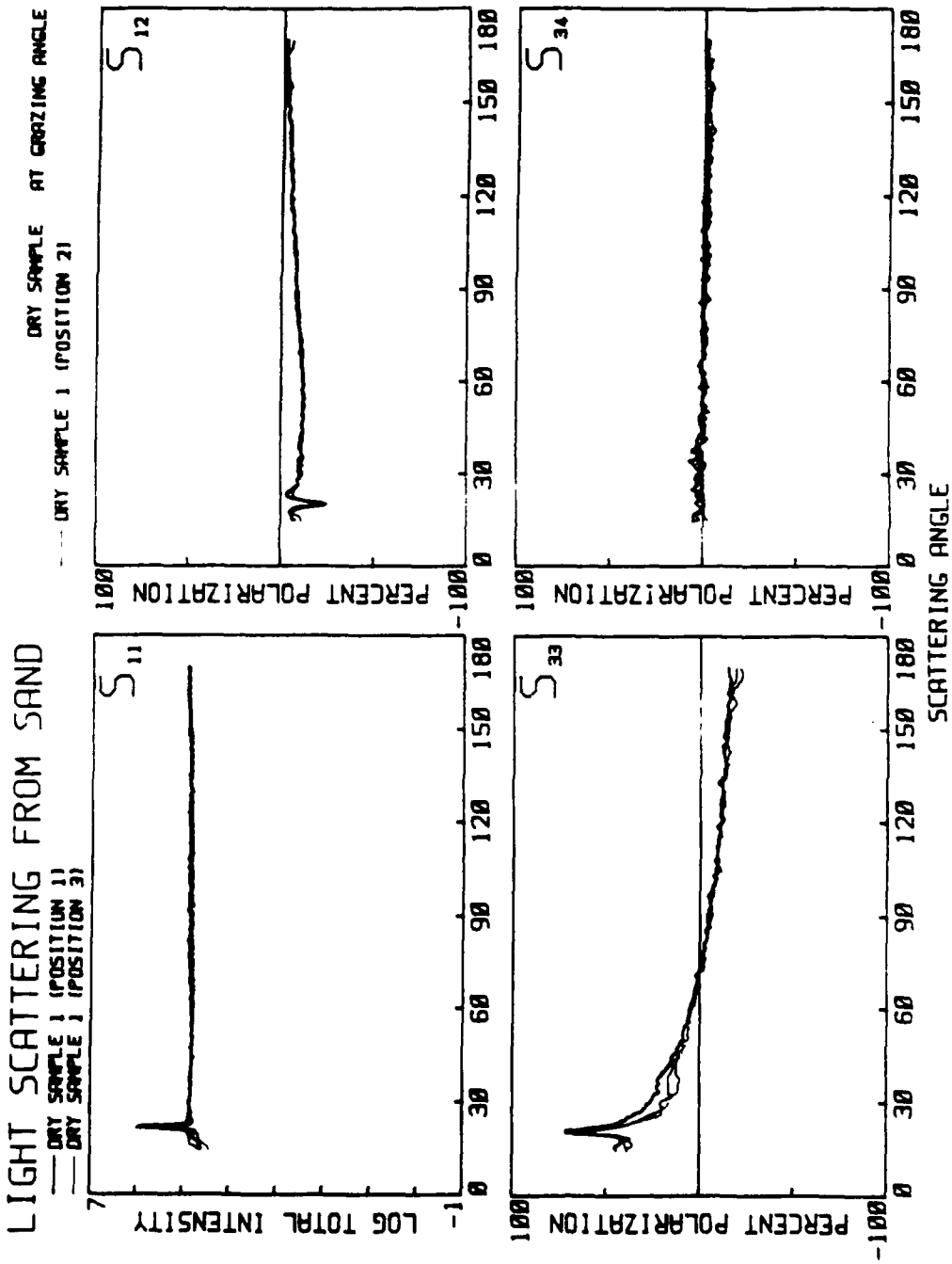

FIGURE 20. The matrix elements for sand measured at three different positions on the surface. Illumination is at near grazing incidence.

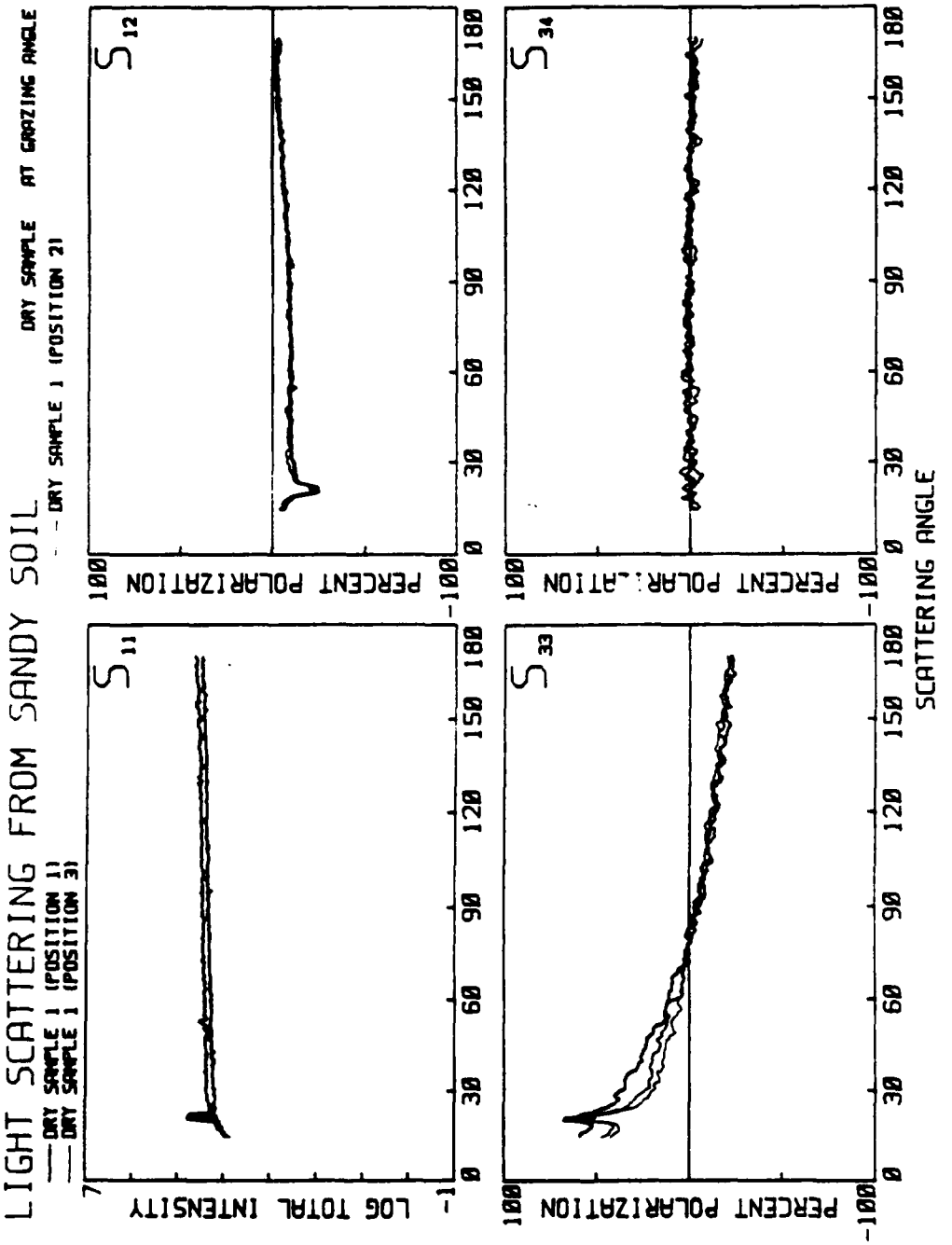

FIGURE 21. The matrix elements for sandy soil measured at three different positions on the surface. Illumination is at near grazing incidence.

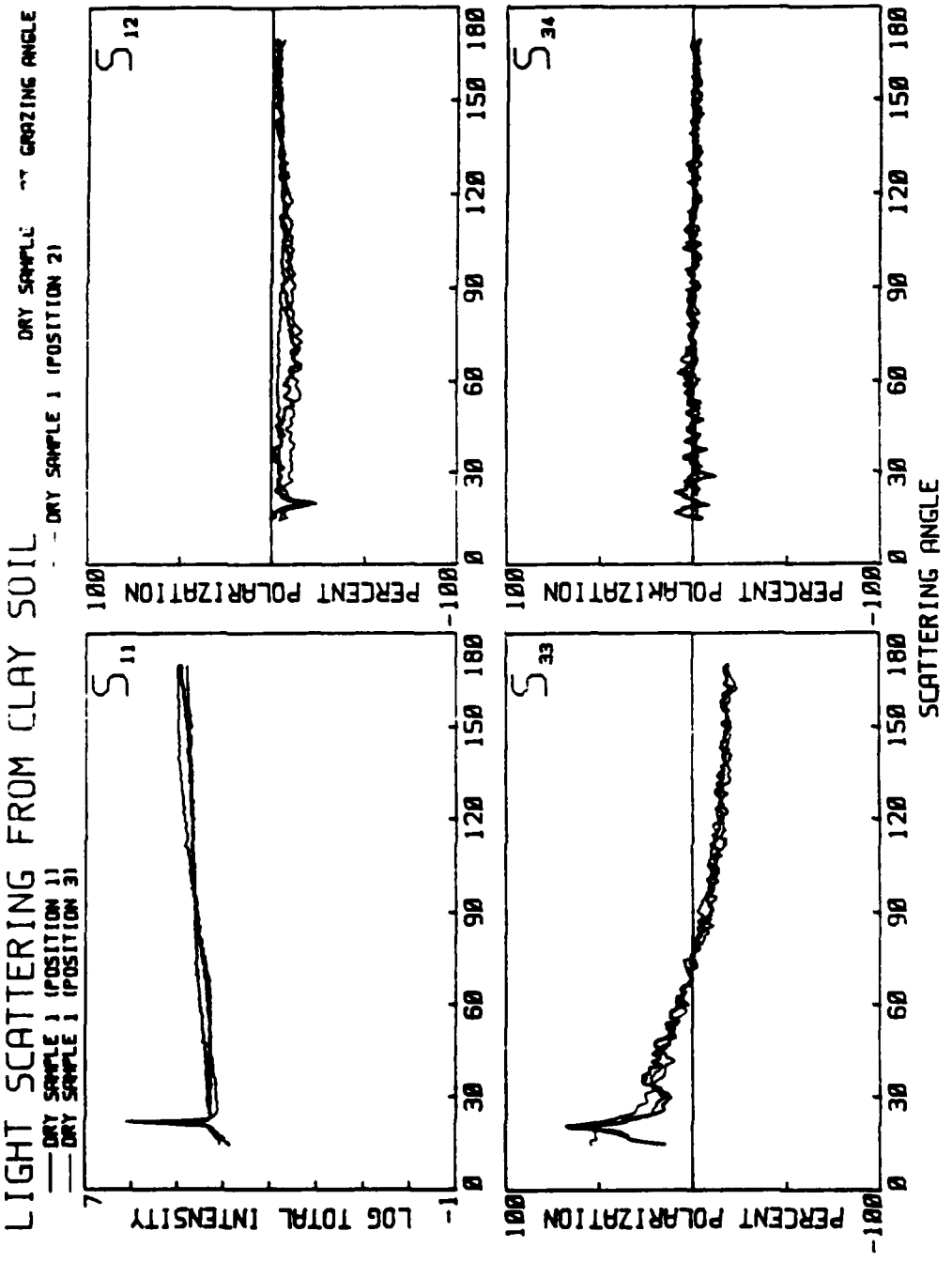

FIGURE 22. The matrix elements for clay soil measured at three different positions on the surface. *Illumination is at near grazing incidence.*

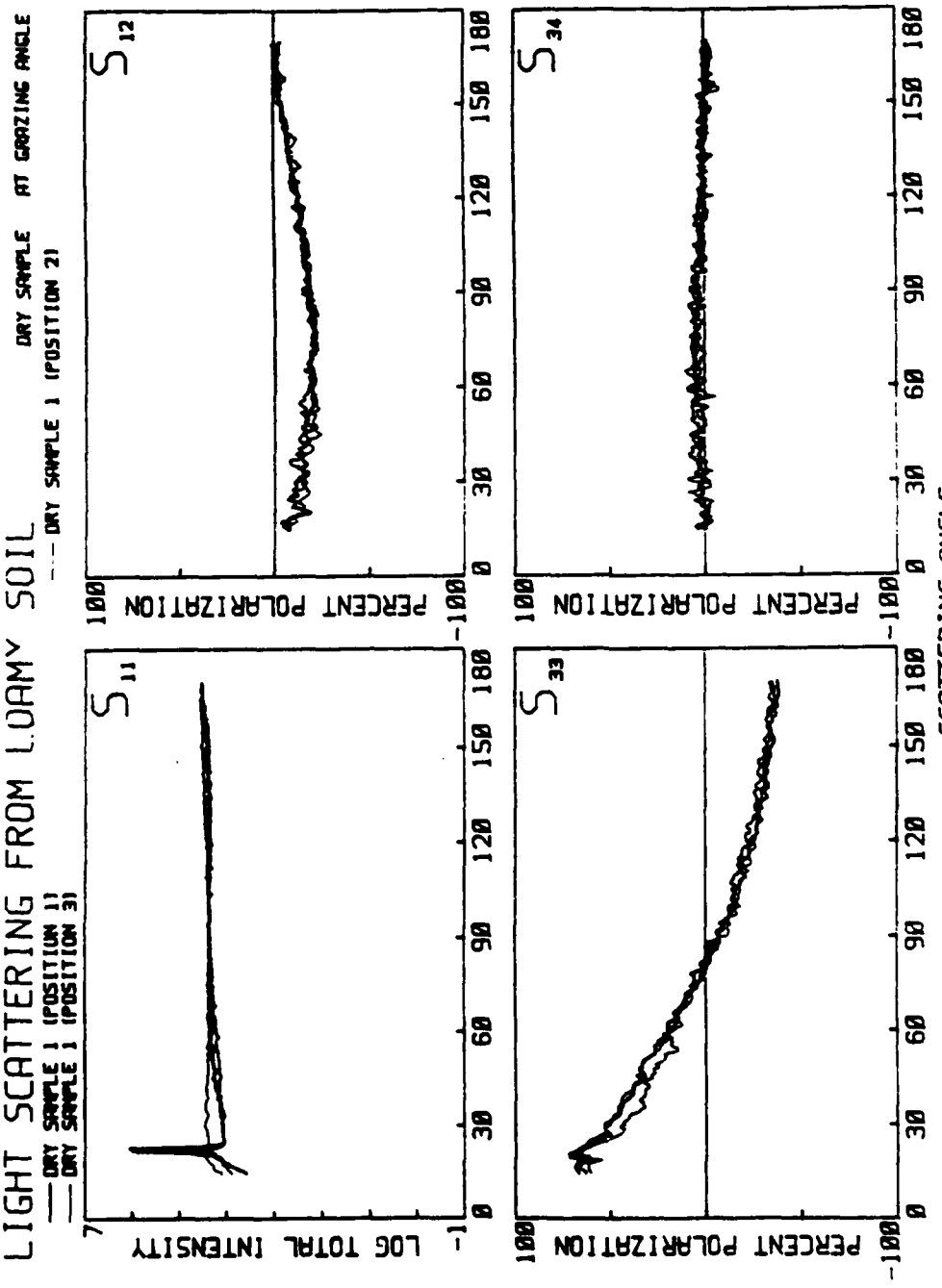

FIGURE 23. The matrix elements for loamy soil measured at three different positions on the surface. Illumination is at near grazing incidence.

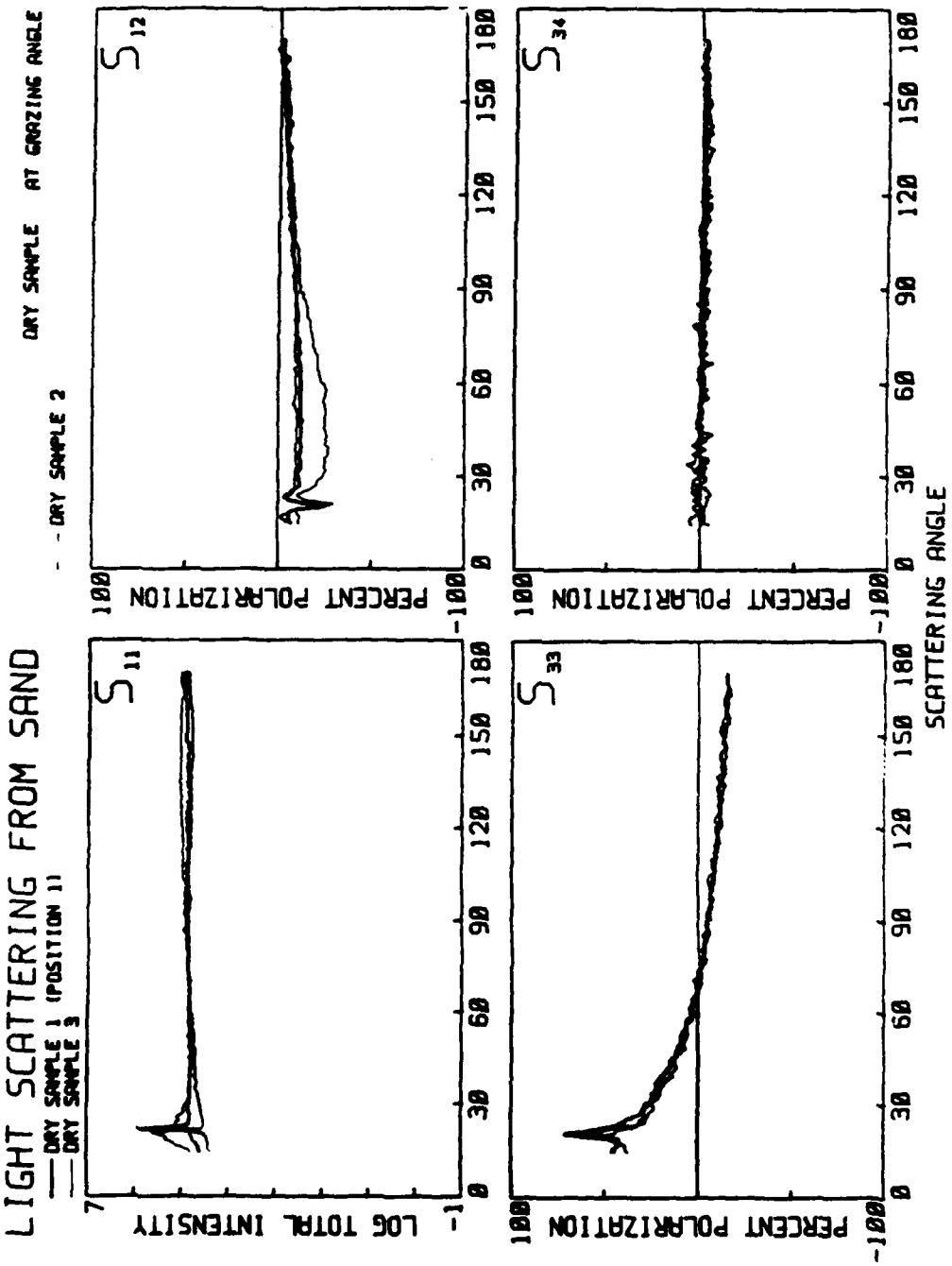

FIGURE 24. The matrix elements for three different sand surfaces. Illumination is at grazing incidence.

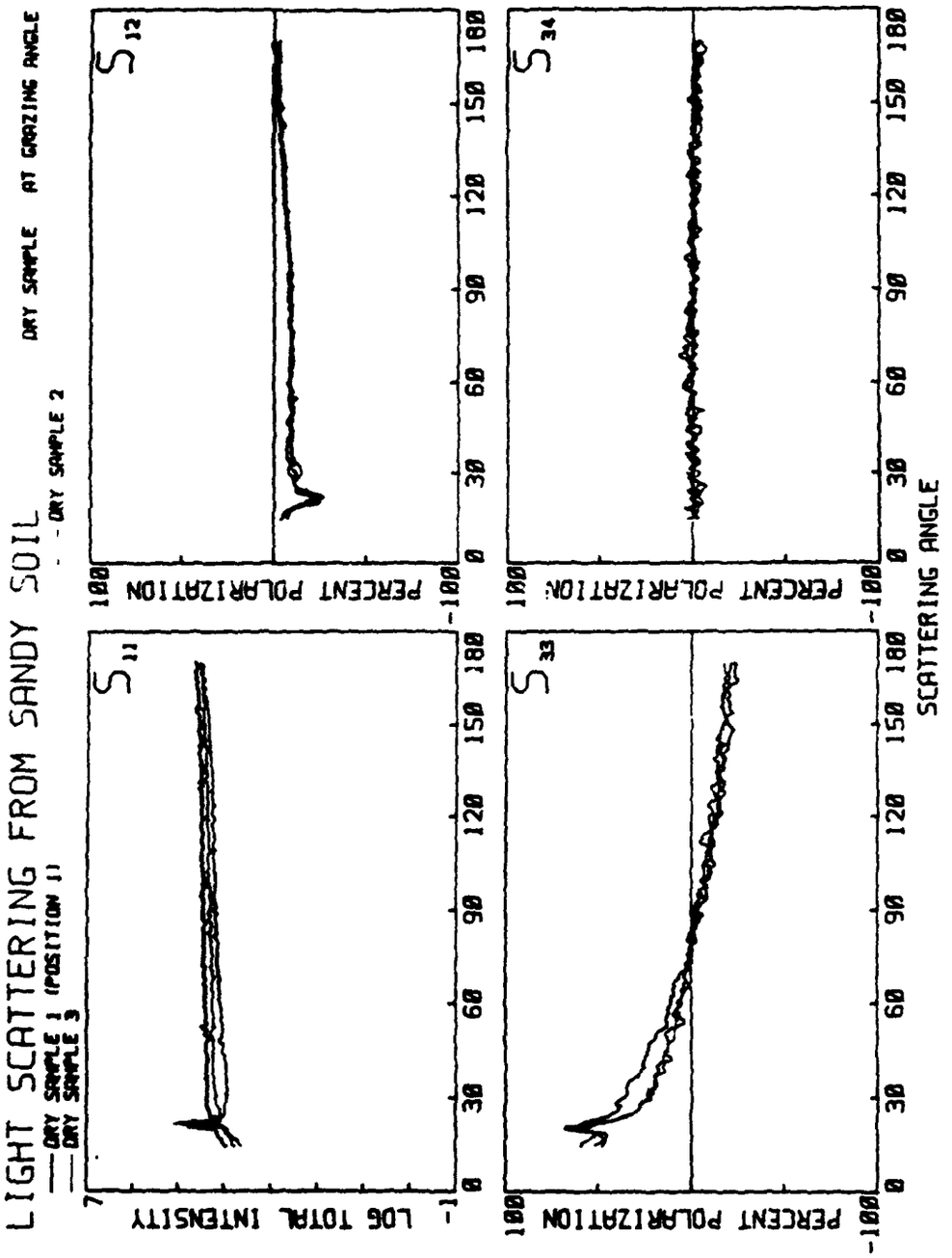

FIGURE 25. The matrix elements for three different sandy soil surfaces. Illumination is at grazing incidence.

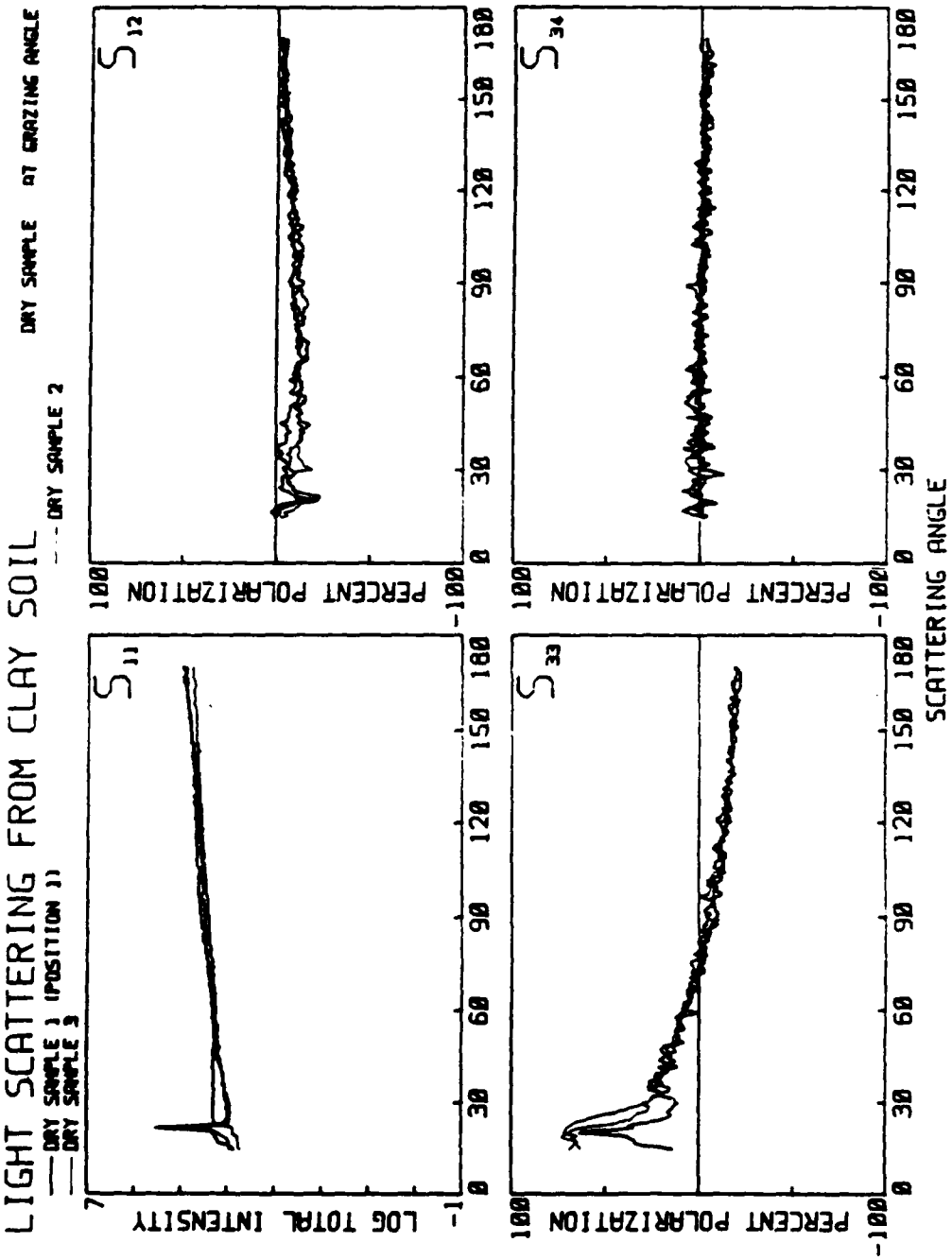

FIGURE 26. The matrix elements for three different clay soil surfaces. Illumination is at grazing incidence.

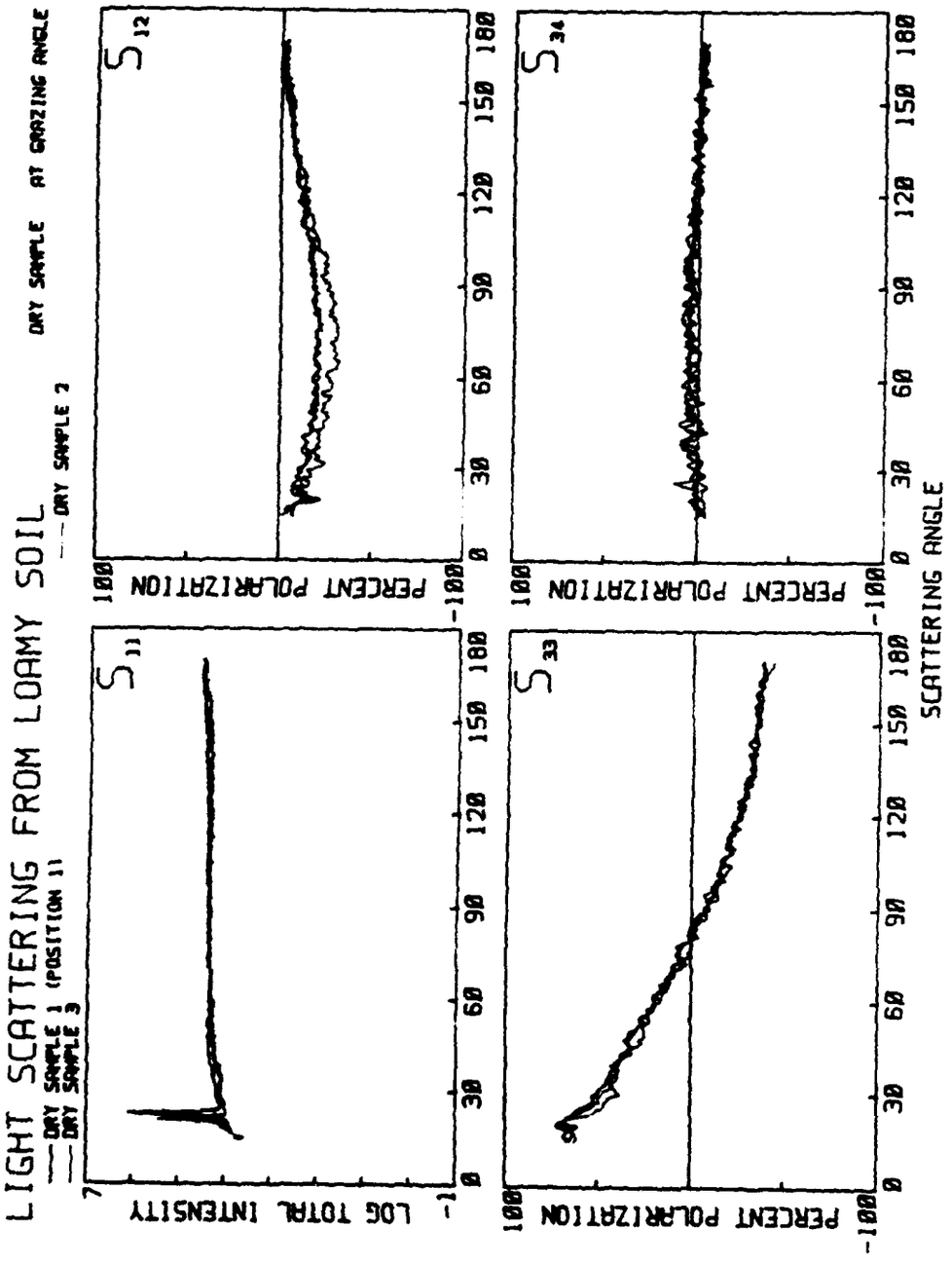

FIGURE 27. The matrix elements for three different loamy soil surfaces. Illumination is at grazing incidence.

9. SIGNAL VARIATIONS AS A FUNCTION OF SOIL SAMPLE, MATRIX ELEMENT AND ILLUMINATION ANGLE

In this section, we discuss the reproducibility of the matrix element signals S_{11}, S_{12}, S_{33} and S_{34} for the four soil samples as a function of two illumination angles α.

The soil samples studied were sand, sandy soil, clay soil and loamy soil. The experimental procedure was as follows:

1) A microscope slide containing the soil sample was placed in the nephelometer and illuminated with HeNe λ6328 Å radiation. The detector arm was set at θ = 165° (backscatter). The sample was set at illumination angle α = 45°. The electronics were adjusted to measure a particular matrix element S_{ij}.

2) The matrix element signal was measured as the 2.5cm square soil sample was slowly scanned from the bottom (B) to top (T) to bottom (B). This was done by moving the sample holder up and down in the z-direction as indicated in Figure 28.

This measurement created an S_{ij} signal symmetric about the Top (T) position which varied as the beam passed over different positions of the sample. After the signal for α = 45° was obtained, the sample was then set at illumination angle α = 90° and measured again.

The measurements were repeated for all four soil samples. The results are shown in Figures 29, 30, 31 and 32. We first discuss some general observations for the four matrix elements.

Fluctuations of S_{11}

Figure 29 shows the variation of S_{11} for the four soils at the two illumination angles α = 45° and α = 90°.

The horizontal axis consists of two parts: to the left of center is the scan from B to T to B with α = 45°; to the right of center is the same scan with α = 90°. The symmetry axis occurs at T. The first curve at the top is for sand, followed by sandy soil, clay soil, and loamy soil.

The vertical axis is the relative intensity S_{11} signal plotted on a log scale. The absolute intensity assigned to each soil curve on the log scale is arbitrary; however, the fluctuations in each curve can be read as a percentage of the total signal. The signal fluctuations of all S_{11} matrix elements are "of the order of" a factor of 2. The loamy soil gives the smallest fluctuations at both angles, while the clay soil gives the largest. There is an insignificant difference between the fluctuation at α = 45° as compared to α = 90° for all surfaces.

Fluctuations of S_{12}

Figure 30 shows the variation of S_{12} for the four soil samples at the two illumination angles α = 45° and α = 90°.

The horizontal axis is the same as that for S_{11}. The vertical axis is the percent polarization signal S_{12} plotted on a linear scale. The fluctuatuions of each signal occur

about a zero polarization reference line. We see that the fluctuations increase as one goes down the column for the $\alpha = 45^\circ$ curves, going from 10% for the sand to 20% for the loamy soil. Also, the fluctuations for the illumination angle $\alpha = 45^\circ$ are 2 to 5% larger than the ones at $\alpha = 90^\circ$ except for the loamy soil, where they are equal. The sand gives the smallest fluctuations at both angles; the loamy soil gives the largest.

Fluctuations of S_{33}

Figure 31 shows the variation of S_{33} for the four soil samples at the two illumination angles $\alpha = 45^\circ$ and $\alpha = 90^\circ$.

The horizontal and vertical axis are the same as those for S_{12}. For sand, the fluctuations at $\alpha = 90^\circ$ are larger than they are at $\alpha = 45^\circ$. However, for the other three soils, the fluctuations are larger at 45°.

Fluctuations of S_{34}

Figure 32 shows the variations of S_{34} for the four soil samples at the two illuminating angles $\alpha = 45^\circ$ and $\alpha = 90^\circ$. The horizontal and vertical axis are the same as for S_{12} and S_{33}. The fluctuations on S_{34} are larger than on the other polarization matrix elements S_{12} and S_{33}. Sand gives the smallest fluctuations and sandy soil the largest.

These are general observations made from the raw data. A more quantitative comparison of the fluctuations is given in Table IV.

Table IV shows the quantitative results of the reproducibility studies of the four matrix elements for the four soils as a function of illumination position and illumination angle α. The percent fluctuations for each matrix element are listed in separate columns to distinguish between the $\alpha = 45^\circ$ and $\alpha = 90^\circ$ illuminations. The percent fluctuations for each soil are listed in separate rows. The numbers represent the maximum percent fluctuations observed in a given matrix element signal. For example:

a) For the sandy soil illuminated at $\alpha = 90^\circ$, S_{11} is 58%. Since this is an unnormalized total intensity measurement, this percentage fluctuation is independent of the incident intensity.

b) For the clay soil illuminated at $\alpha = 45^\circ$, the fluctuation in S_{11} is 150%.

c) For the loamy soil illuminated at $\alpha = 45^\circ$, the fluctuation in the polarization signal S_{33} is 27.5%. Since these are normalized polarization signals, the maximum fluctuation obtainable can be ±100% (or 200%) if the signal would vary from +100% to -100%.

d) For the sand illuminated at $\alpha = 45^\circ$ the fluctuations in the matrix element S_{34} are 30%.

TABLE IV
PRESENT FLUCTUATIONS IN THE MATRIX ELEMENTS
FOR THE VARIOUS SOILS AS A FUNCTION OF ILLUMINATION ANGLE α

	Matrix element									
α / Soil	S_{11}		S_{12}		S_{33}		S_{34}		AVERAGE	
	45°	90°	45°	90°	45°	90°	45°	90°	I	POL
Sand	77	11	10	12.5	22.5	32.5	30	27.5	94	23
Sandy soil	88	58	12.5	17.5	45	30	42.5	42.5	73	33
Clay Soil	150	170	17.5	20	30	25	32.5	40	160	23
Loamy Soil	58	67	20	20	27.5	25	35	37.5	63	28
average for α	93	101	15	17.5	31.3	20.5	35	36.7		
average for S_{ij}	97		16		26		36			

These fluctuations represent the maximum deviation of a particular matrix element signal. For example, suppose for a particular situation the backscatter from a clay soil surface illuminated at α = 90° gives an S_{33} signal equal to -14%. The 25% value for the fluctuation of this signal read from the table says that this -14% value could increase to -14 + 25 = 11% or decrease to -14 -25 = -39% or if the measured -14% value happened to be the average for that soil, the -14% value could fluctuate by ±12.5%, i.e., vary between 26.5% and 1.5%. When a surface is initially illuminated in remote sensing, it is not known whether the detected signal is at the average, at the extreme, or at some intermediate value of its fluctuation. The percents given in Table IV can be converted to the usual ± percent fluctuation by dividing by two. Then, for example, a 30% maximum fluctuation would indicate a ±15% fluctuation in the signal.

At the bottom of the table, a row of numbers are listed for "average for α." This number is the average fluctuation for a particular matrix element at that α. Also listed is a row of numbers for "average for S_{ij}." This number is the average fluctuation for that particular matrix element averaged over both α.

In Table IV, a column of numbers on the right, under "average I" and "average Pol" indicates the average fluctuation for the total intensity signal S_{11} for both angles and the average fluctuation for the three polarization signals S_{12}, S_{33} and S_{34} for both angles. For example, average I for sand is 94% (this is the average of 77% and 111%). The average Pol for sand is 23% (this is the average of all polarization signals at both angles).

We can draw some important conclusions from Table IV.

1) The "average for α" fluctuations in S_{11} are 93% and 101% for $\alpha = 45°$ and $\alpha = 90°$, respectively. This indicates that there is not much difference in fluctuation of S_{11} signals taken at $\alpha = 45°$ and $90°$. The same observation holds for matrix elements S_{12} and S_{34} where the fluctuations are essentially independent of α. S_{33}, however, shows strong α dependence, giving fluctuations at $\alpha = 90°$ 30% smaller than those at $\alpha = 45°$.

2) The "average for S_{ij}" fluctuations are largest for S_{11} (97%). Note these are from three to six times larger than the fluctuations on the polarization matrix elements S_{12} (16%), S_{33} (26%) and S_{34} (36%).

3) The matrix element S_{12} gives the smallest fluctuation of the polarizations signals (16%) while S_{34} gives the largest (36%).

4) For all soils, at both angles α, the fluctuations in the total intensities S_{11} are larger than for the polarization signals. The size of the S_{11} fluctuations are soil dependent -- the largest occurring for clay soil (160%), the smallest for loamy soil (63%). The size of the polarization fluctuations are not as dependent on soil. Their values lie between 23-33%.

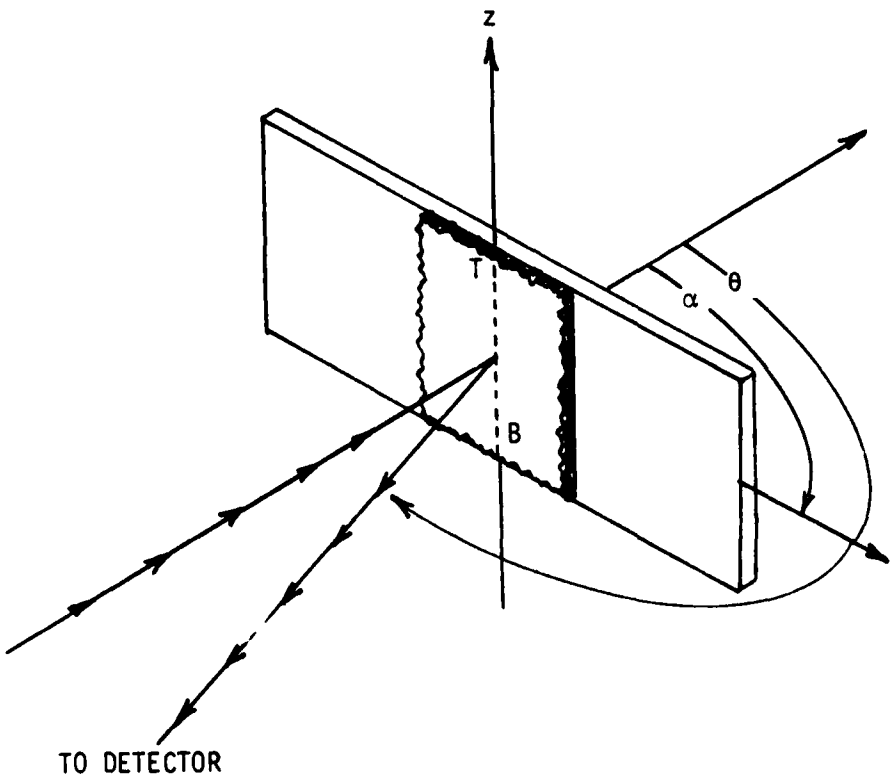

FIGURE 28. The geometry used to scan a soil surface from top (T) to bottom (B) as a function of illumination angle α and scattering angle θ.

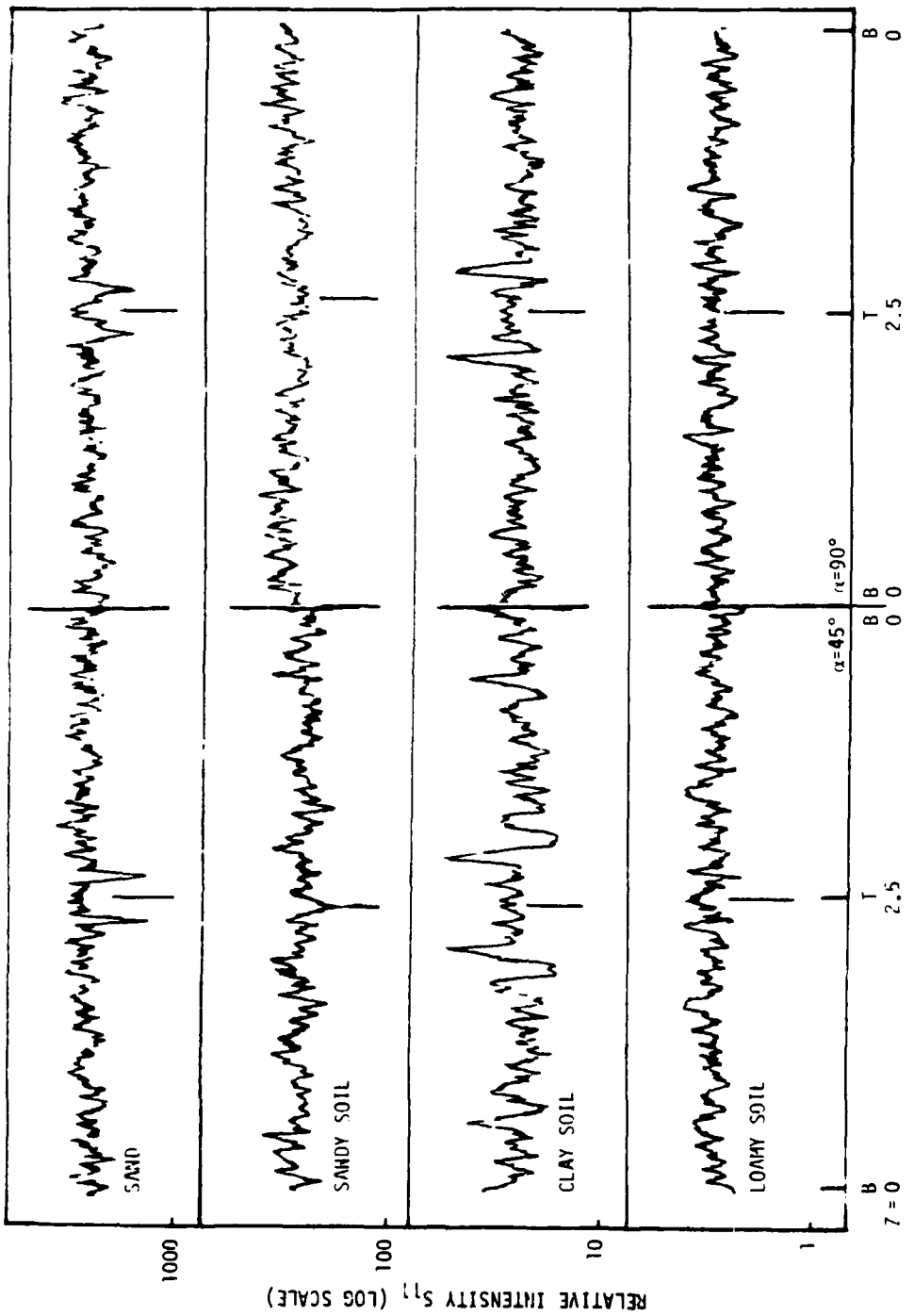

FIGURE 29. Fluctuations in S_{11} as a function of illumination position and illumination angle α for the four soils.

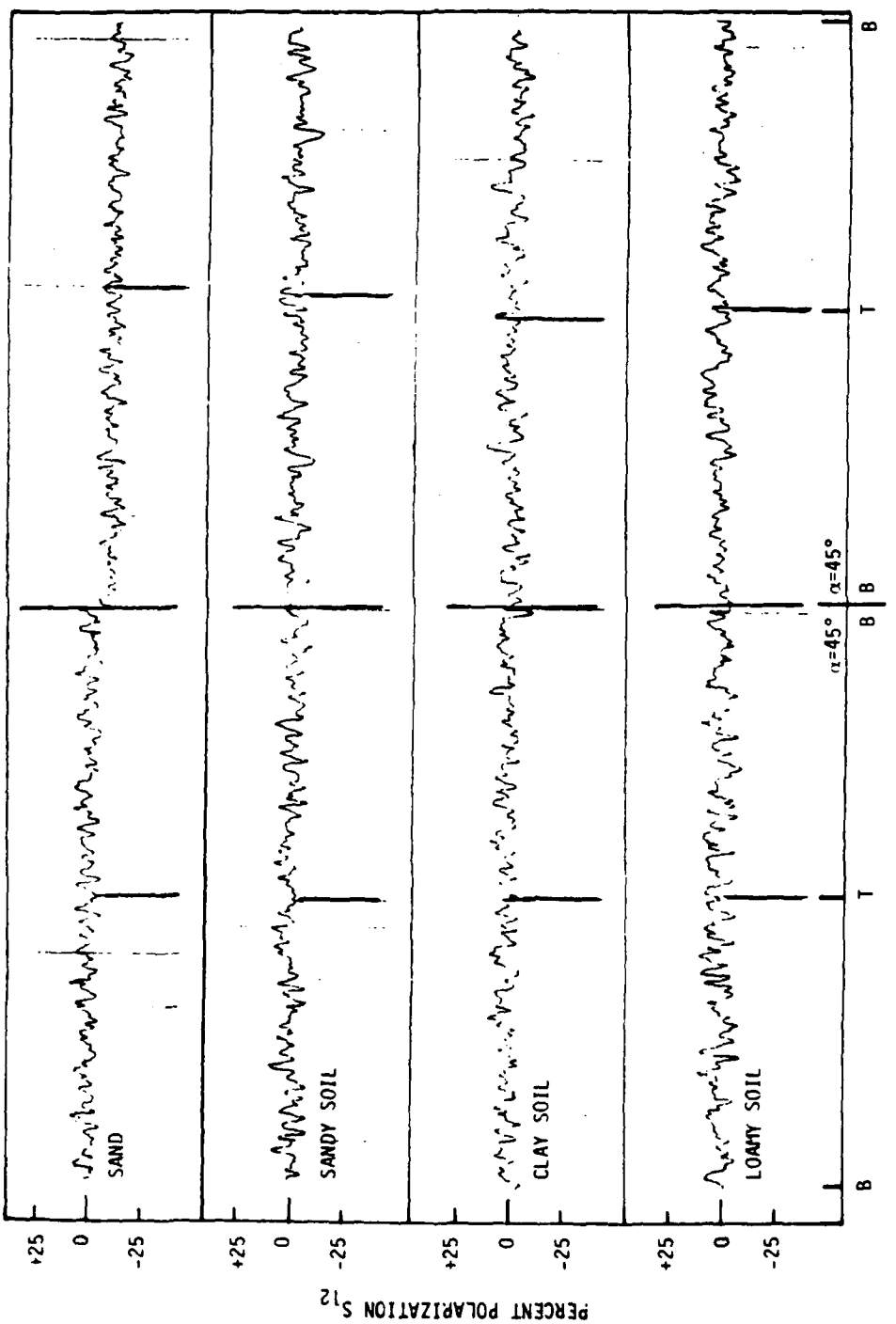

FIGURE 30. Fluctuations in S_{12} as a function of illumination position and illumination angle α for the four soils.

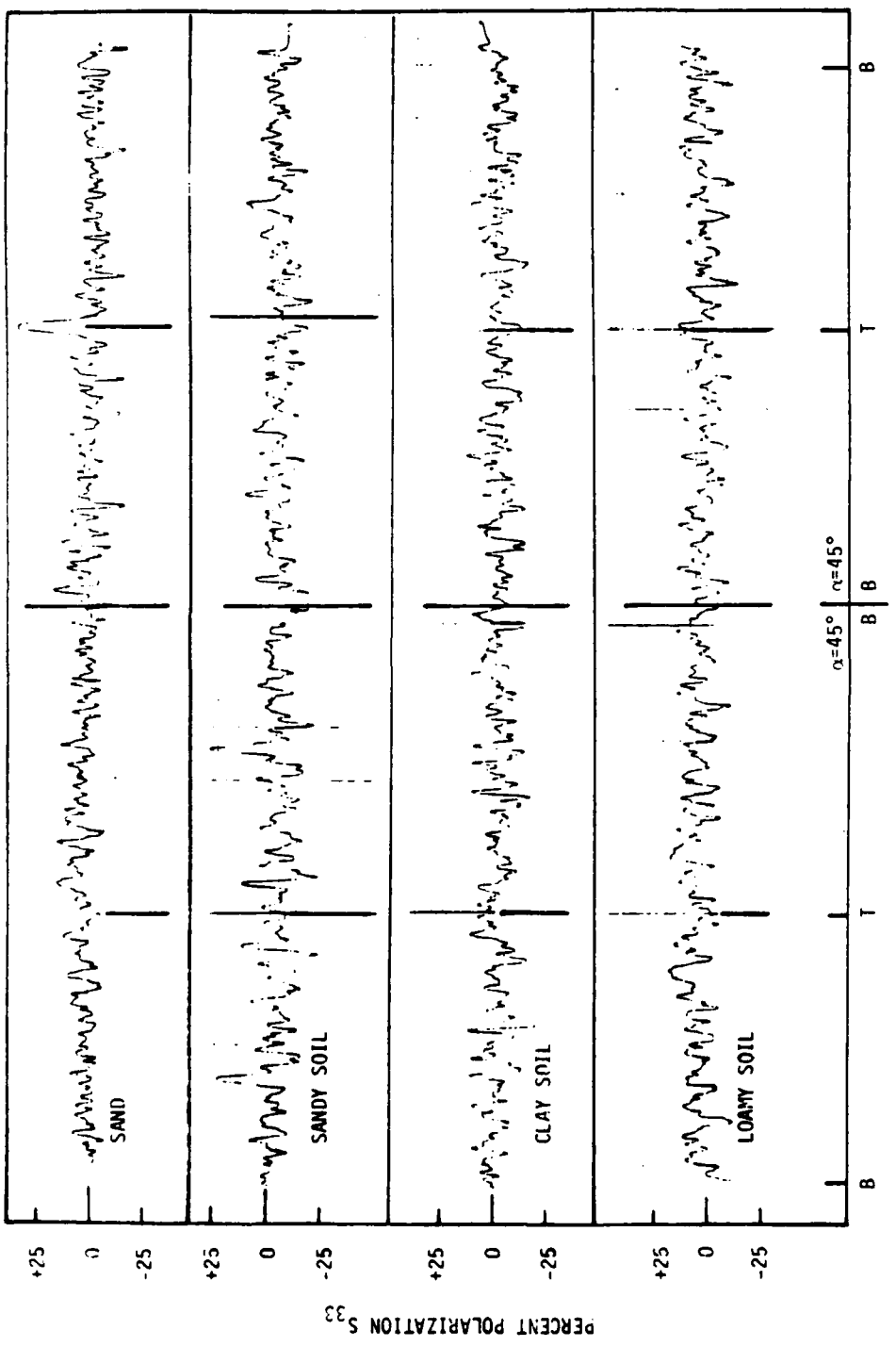

FIGURE 31. Fluctuations in S_{33} as a function of illumination position and illumination angle α for the four soils.

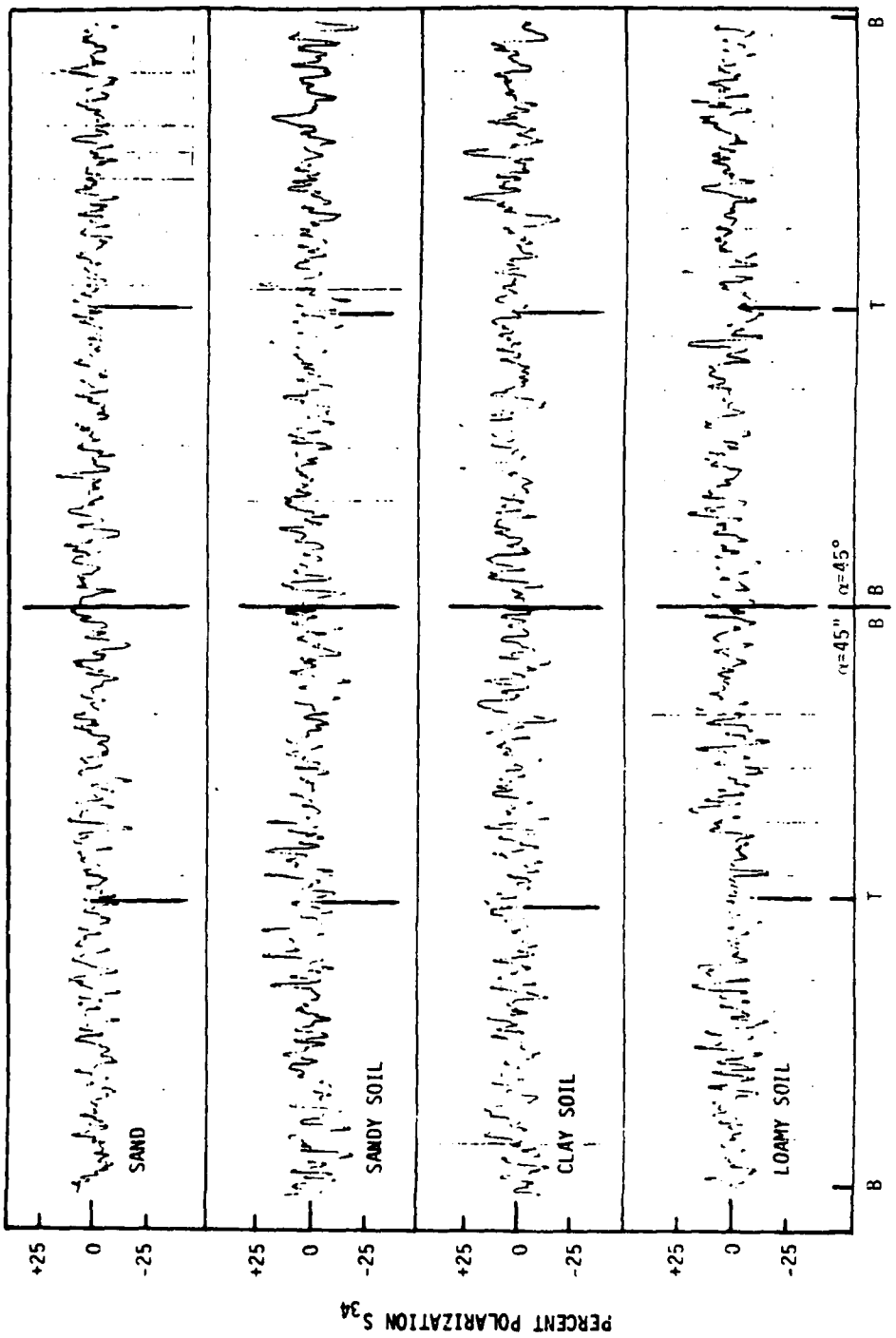

FIGURE 32. Fluctuations in S_{34} as a function of illumination position and illumination angle α for the four soils.

10. THE α-DEPENDENT BACKSCATTER SIGNALS AND REPRODUCIBILITY STUDIES FOR THE MATRIX ELEMENTS S_{11}, S_{12}, S_{33} AND S_{34} FOR THE FOUR SOILS

This group of curves was obtained by measuring the four matrix element signals S_{11}, S_{12}, S_{33} and S_{34} for the backscattered light (θ = 165°) as the illumination angle α varied from α = 0 to 180°. This yielded 160 backscatter curves for the same soil sample-matrix element combinations discussed in Section 8. Figure 33 shows the backscatter signals of the four matrix elements for three different soils. Note that matrix elements S_{11} and S_{33} can distinguish between the three different soils in the backscatter while S_{12} and S_{34} are zero and insensitive to soil type. Figures 34, 35, 36 and 37 show the four matrix elements for the four dry soil samples: Sand, Sandy Soil, Clay Soil, and Loamy Soil. Two curves for each S_{ij} as a function of illuminating angle α are plotted for two different but identically prepared samples to show the reproducibility from sample to sample.

Consider Figure 34 for sand as an example. Each matrix element signal contains two traces and each trace contains data from the same reference surface and a different soil surface indicated by "dry sample 2" and "dry sample 3." The data were taken as follows: A reference surface was placed back-to-back with the soil surface so that one α = 360° rotation of the sample holder exposed the reference surface for α = 0-180° and then the soil surface from α = 180-360° (indicated as α = 0-180° in the figure). We used this technique to ensure reproducible alignment of the sample holder. Reproducible reference scattering signals ensured that any changes in the soil scattering from sample to sample were due to sample difference and not misalignments when soil samples 2 and 3 were interchanged. Note for example the slight but real differences in the S_{11} signals for sand and clay soil.

The signals presented here are taken from identically prepared samples and therefore the variation in the matrix element curves are examples of the variation that can occur in real-world, natural, unprepared surfaces. These measurements and the results of similar measurements on the other samples indicate the reproducibility of the S_{ij} from sample to sample of the same soil. The results of these studies are summarized in Table V.

This table shows that the fluctuations are greatest for S_{11} and least for S_{12}. Consequently, all variations in S_{ij} due to coating should be larger than these fluctuations if the remote sensing is to detect the difference between a coated or non-coated surface (i.e., to detect whether the soil is coated or not).

TABLE V
MAXIMUM FLUCTUATION (PERCENT) IN THE BACKSCATTER FROM TWO DIFFERENT (IDENTICALLY PREPARED) SOIL SAMPLES

S_{ij}	Sand	Sandy soil	Clay soil	Loamy soil
S_{11}	80	50	90	30
S_{12}	6	5	5	5
S_{33}	8	6	12	14
S_{34}	6	8	8	9

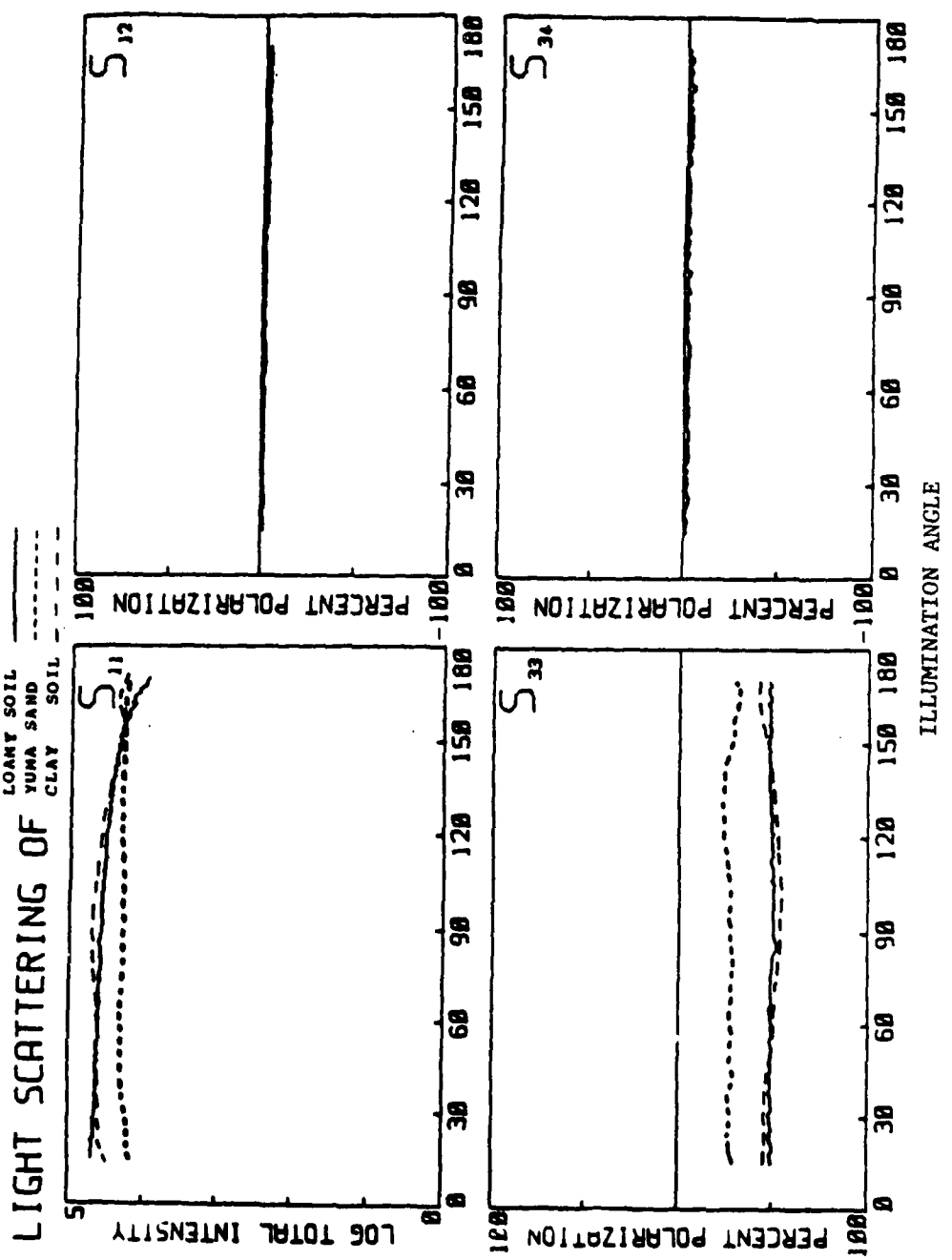

FIGURE 33. Matrix elements in the backscatter for three soils as a function of illumination angle α.

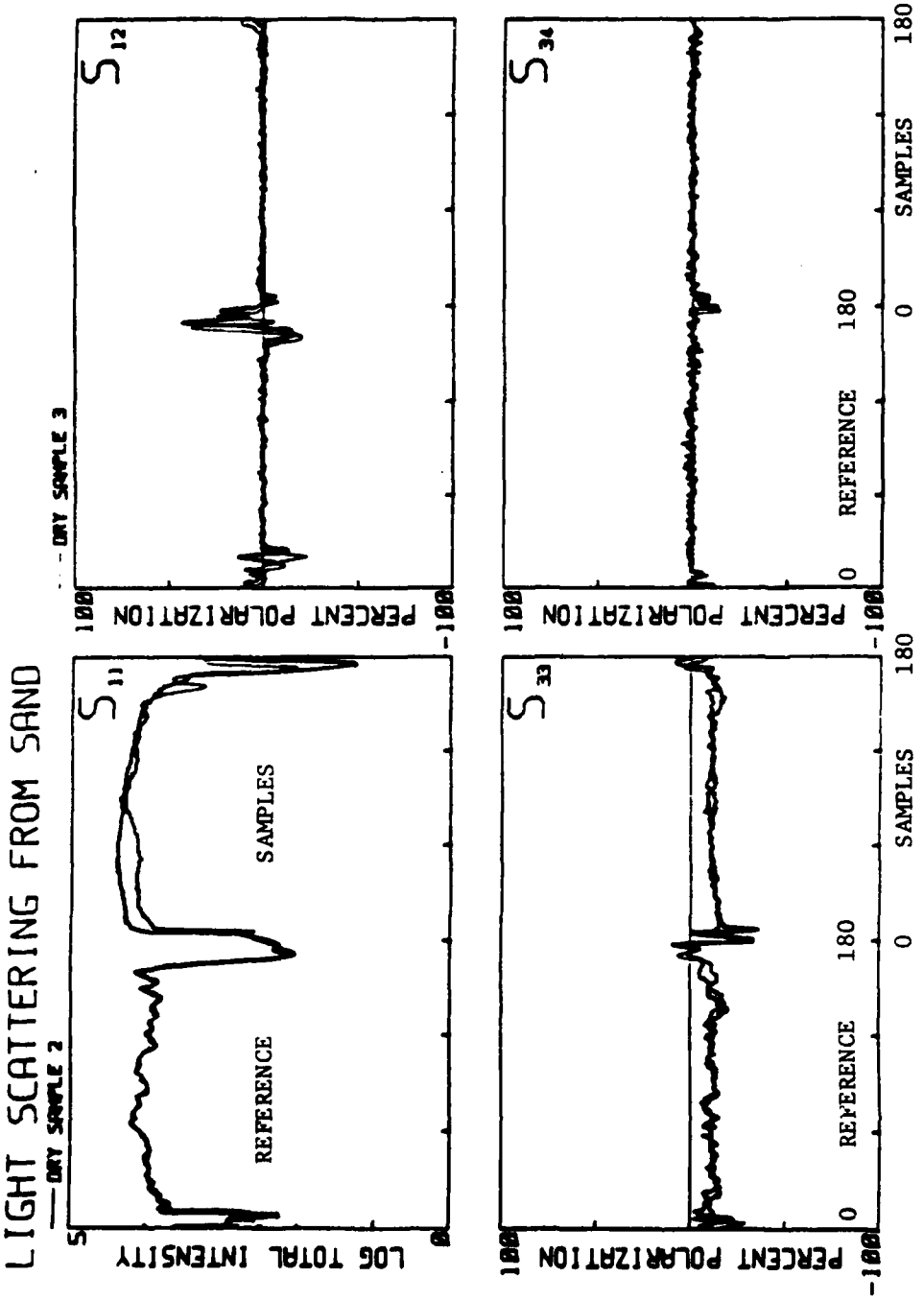

FIGURE 34. Matrix elements in the backscatter for two different sand surfaces as a function of illumination angle α.

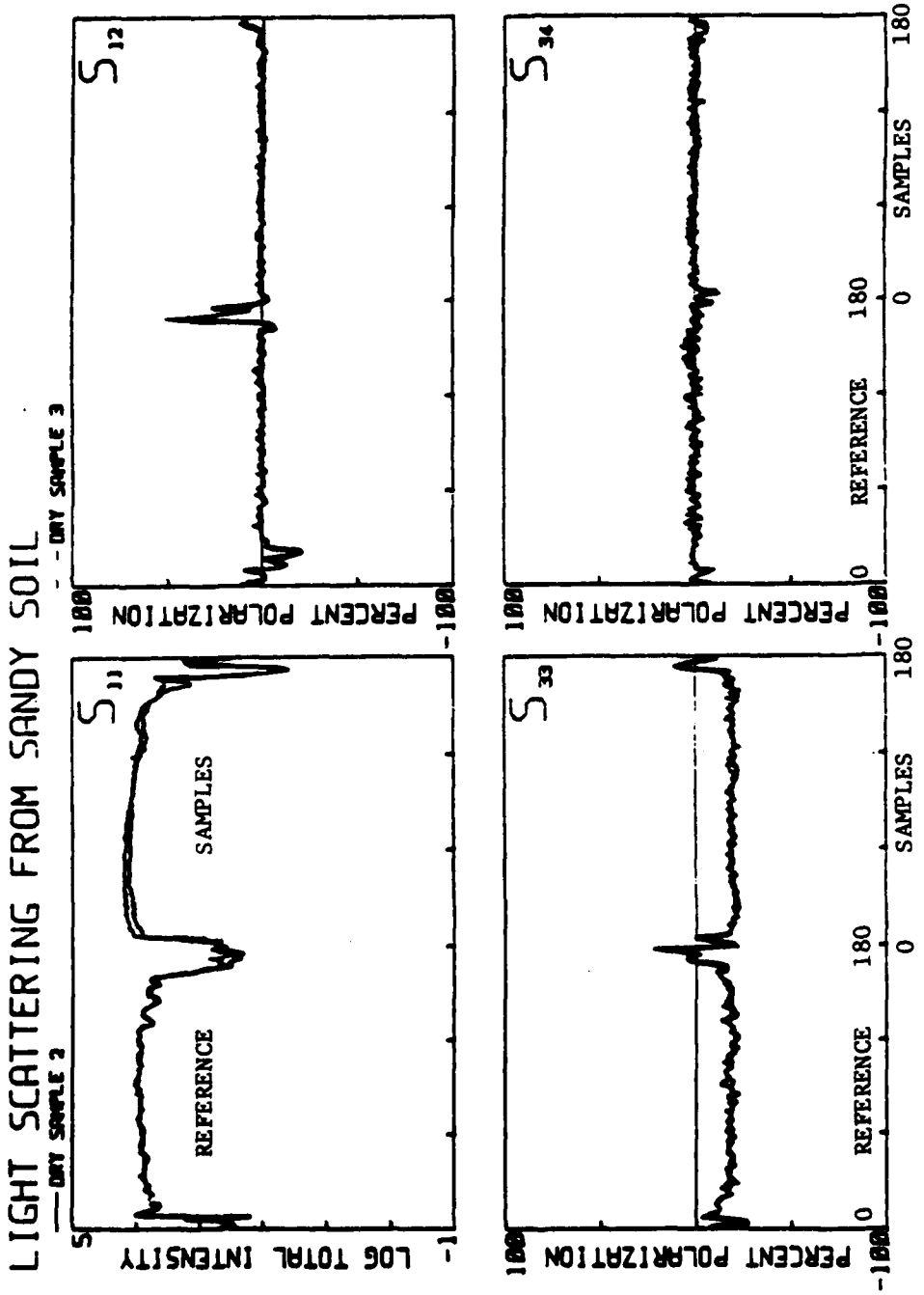

FIGURE 35. Matrix elements in the backscatter for two different sandy soil surfaces as a function of illumination angle α.

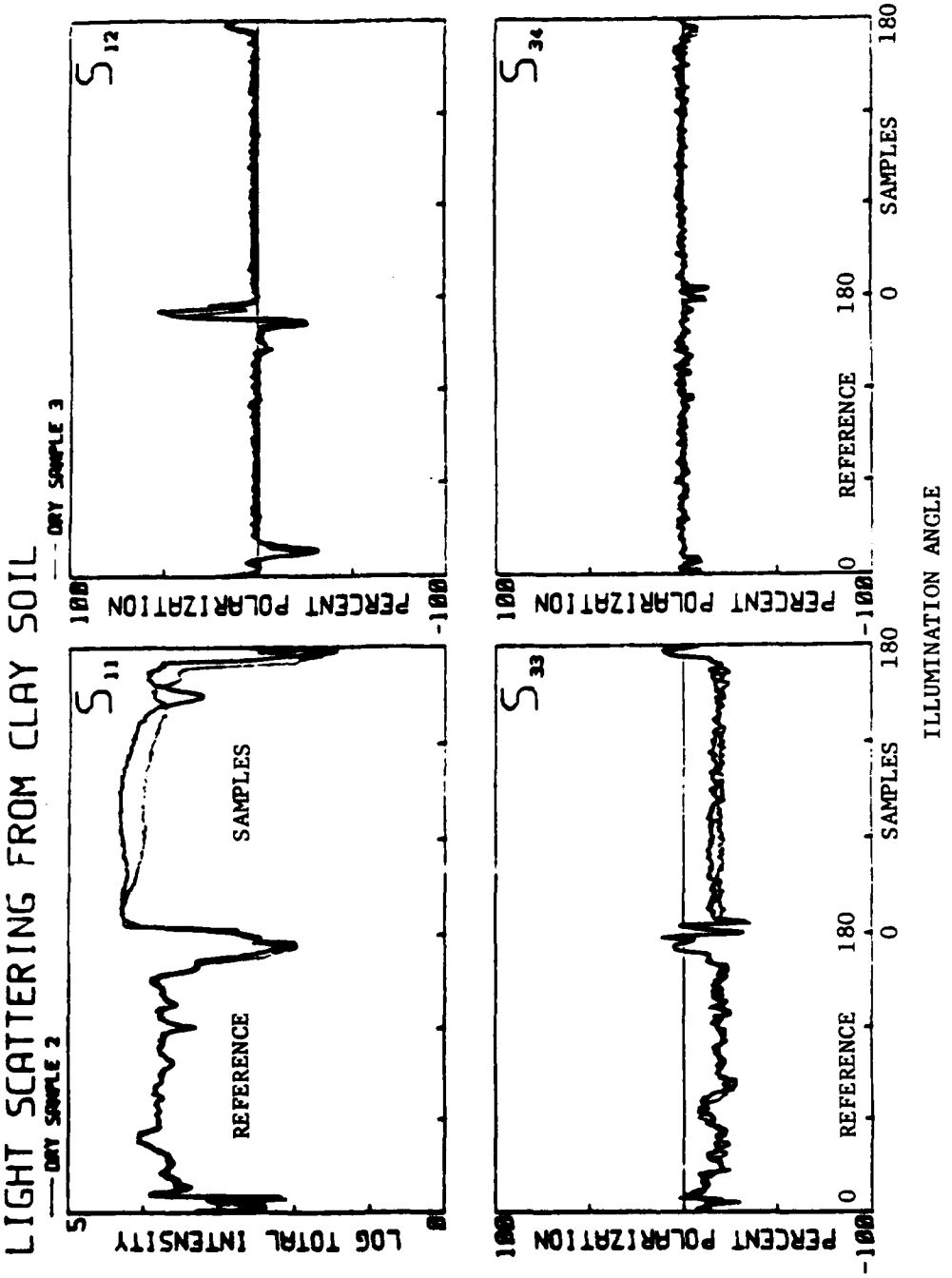

FIGURE 36. Matrix elements in the backscatter for two different clay soil surfaces as a function of illumination angle α.

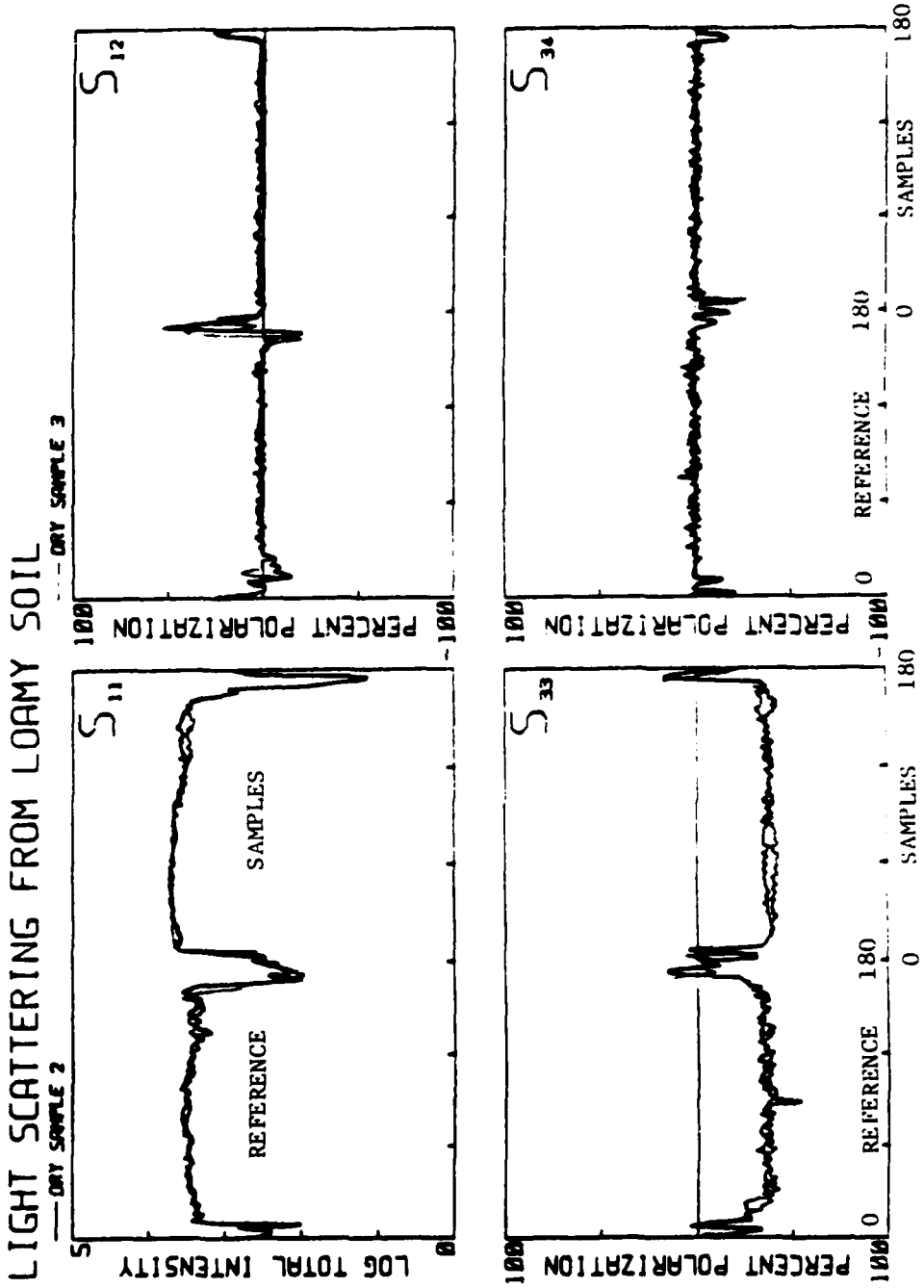

FIGURE 37. Matrix elements in the backscatter for two different loamy soil surfaces as a function of illumination angle α.

11. PROPERTIES OF THE LIGHT AND DARK OILS

The four soil samples were coated with two different oils -- one that was absorbing at the probe wavelength and one that was not. For the non-absorbing light oil we used standard Pennzoil SAE30. The absorbing dark oil was made from the light oil by dissolving an opaque tar-like material into it.

We had to create a special absorbing oil after we examined a number of commercially available dark oils that we thought would be suitable for the absorption studies. The oil had to satisfy several requirements:

1. The viscosities be similar,
2. The vapor pressures be low,
3. The refractive indices be similar,
4. The oils be free of particulates, and
5. The absorption coefficients be different.

The main problem with most dark oils was the presence of particulates. The dark quality was caused by the absorption of very fine (>100 microns) irregular black particles suspended in a light (transparent) oil base. These particles caused excessive scatter.

Heating, ultrasonificating, filtering, redissolving and grinding the small particles did not solve the problem of particulate scatter. We therefore created a dark oil solution by dissolving a "black hydrocarbon tar" in toluene ($C_6H_5CH_3$), which was then added to the light oil. This technique worked well and resulted in two similar oils that were used to coat the soil samples. The absorption coefficients of the two oils were experimentally determined by measuring the transmitted intensity at the probe wavelength through an oil layer of known thickness. Lambert's Law related the absorption coefficient to the intensity change. The properties of the light and dark oils are given in Table VI below.

The oils were sprayed onto the soil samples with a high pressure atomizer that created a fine oil mist. The amount of oil sprayed onto each sample was determined the following way.

The sample to be sprayed was placed on platform between two clean microscope slides of known weight. As the platform rotated 1 rotation per second, the sample and both microscope slides were simultaneously sprayed with the oil for a certain length of time. The clean slides with the oil on them were weighed and from their known area and new weight, the aeral density (micro liters/cm^2) of oil on the soil surface was determined. This technique could create oil surfaces as thin as 10^{-5} grams/cm^2 or less than one micron thick. The spraying time, air pressure and the distance between nozzle and surface could be adjusted to lay down coatings as slow as 10^{-5} grams/cm^2/sec.

TABLE VI
PROPERTIES OF THE LIGHT AND DARK OILS

	Absorption coefficient (cm^{-1}) Blue λ4416 Å	Red λ6328 Å	Vapor pressure (mmHg)	Viscosity (CSt)	Density (g/cm^3)
Light oil	1.68	28.76	$<10^{-3}$	120.3	0.9953
Dark oil	20.25	32.16	$<10^{-3}$	120.3	0.9678

12. LONG-TERM TIME DEPENDENCE OF OIL COATED SOILS: THE MATRIX ELEMENTS OF SAND, CLAY SOIL, AND LOAMY SOIL WITH AND WITHOUT OIL COATINGS AS A FUNCTION OF TIME

In these experiments three soil surfaces -- sand, clay soil, and loamy soil -- were coated with light and dark oil. The backscattering signals (θ = 165°) from these three coated surfaces were measured at three different times: at t=0 immediately after coating, then at t = 12 hours and t = 24 hours after coating with oil. Four Mueller matrix elements S_{11}, S_{12}, S_{33}, and S_{34} were examined using He-Cd laser radiation at λ4416 Å We found that matrix element S_{33} is most sensitive to the presence of oil coatings.

The preparation and properties of the three soil samples have been described in Chapter 7. In order to observe the scattering difference between oil-coated and uncoated surfaces, we measured the light scattered from them at the same time, using the uncoated surface as a reference. A metal holder, as shown in Figure 38, was made to hold, back-to-back, the microscope slides containing the soil samples. The holder was connected to a motor which rotated at the rate of 4 rpm. During each rotation the reference surface (uncoated surface) and the coated surface were each illuminated by the incident laser beam in turn as the illumination angle continuously changed from α = 0 to 180°. The detector was set at θ = 165° to record the near backscatter signal. The four matrix elements S_{11}, S_{12}, S_{33}, and S_{34} were detected at t = 0, t = 12 hours and t = 24 hours after the surfaces were coated with the oil. The results of the backscatter measurements for the light oil are shown in Figures 39, 40 and 41. Those for the dark oil are shown in Figures 42, 43 and 44.

Each matrix element plot compares the three curves taken at t = 0, 12, and 24 hours respectively. No changes occur in the reference curves (uncoated samples) and only very small changes with time occur on the coated surfaces.

For the sand surface, only the S_{11} and S_{33} matrix elements for light oil coated surfaces show any differences as a function of time and these are very small. No significent differences occur for the other matrix elements for the other soils regardless of the light or dark oil coatings.

From these data we draw the following conclusions:

1. Matrix elements S_{11} and S_{33} are possible discriminators of uncoated and oil-coated soils.

2. Matrix elements S_{12} and S_{34} are essentially zero for all angles for all surfaces whether coated or uncoated.

3. Virtually no time dependence is seen in the scattered light in any matrix element over a period of 24 hours.

4. The data from this set of measurements cannot distinguish between the light and dark oil coatings.

5. Only matrix element S_{33} shows promise as a probe for time dependence.

We also studied sand and loamy soil as a function of time after rapidly coating them with water. The solid lines of Figure 45 show the four matrix elements for sand uncoated and coated with water. The dotted line is the matrix element value sixty minutes later after substantial evaporation and soaking has occurred. Figure 46 shows similar results obtained with loamy soil.

These water and oil experiments show that surface scattering depends on whether the surface is coated or not and on the kind of coating. The light and dark oils are evidently too similar to see an appreciable difference between their scattering. The water is significantly different from the oils and its evaporation eventually returns the surface to its initial condition. The oil with higher viscosity and low vapor pressure does not evaporate or diffuse enough after initial application to show long term effects.

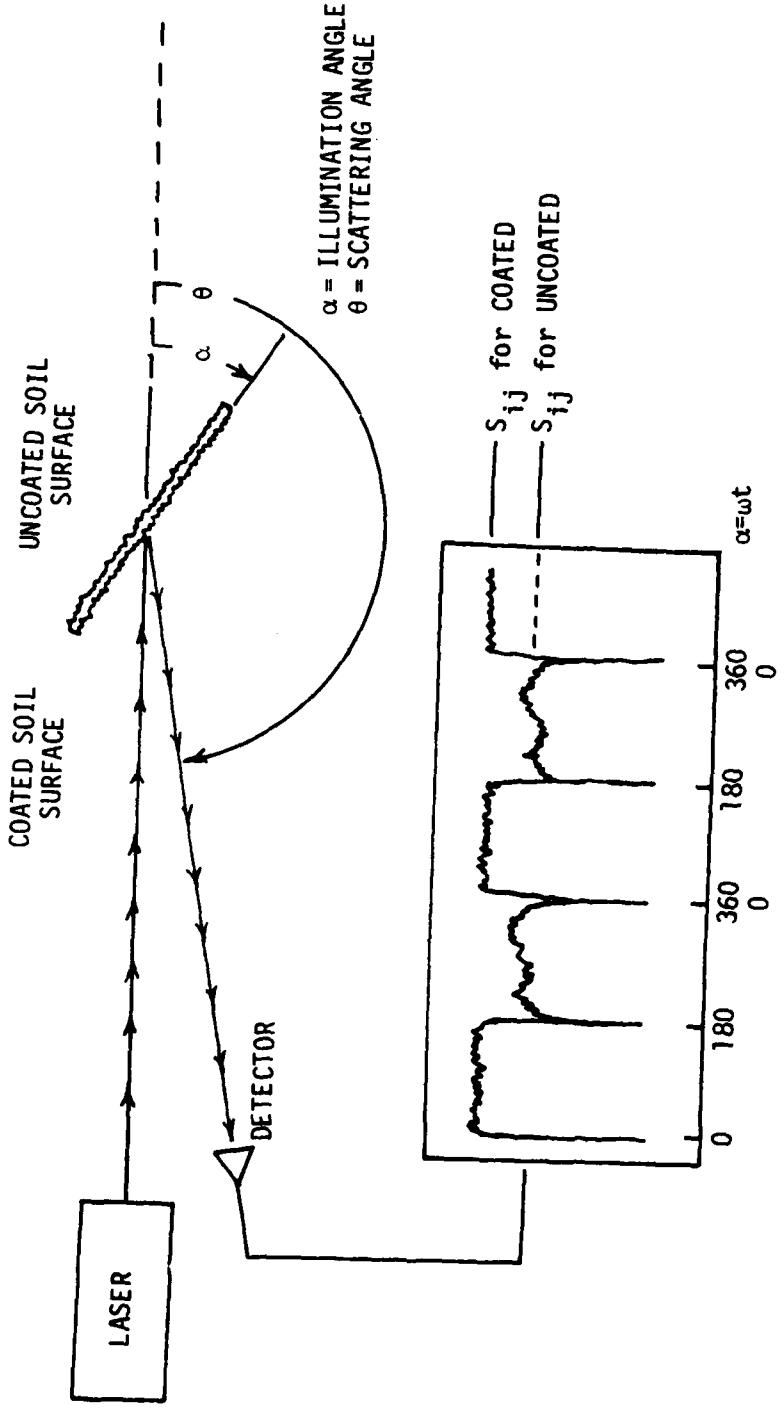

FIGURE 38. Geometry showing the relation between illumination angle α and scattering angle θ for the measurement of coated and uncoated soil surfaces.

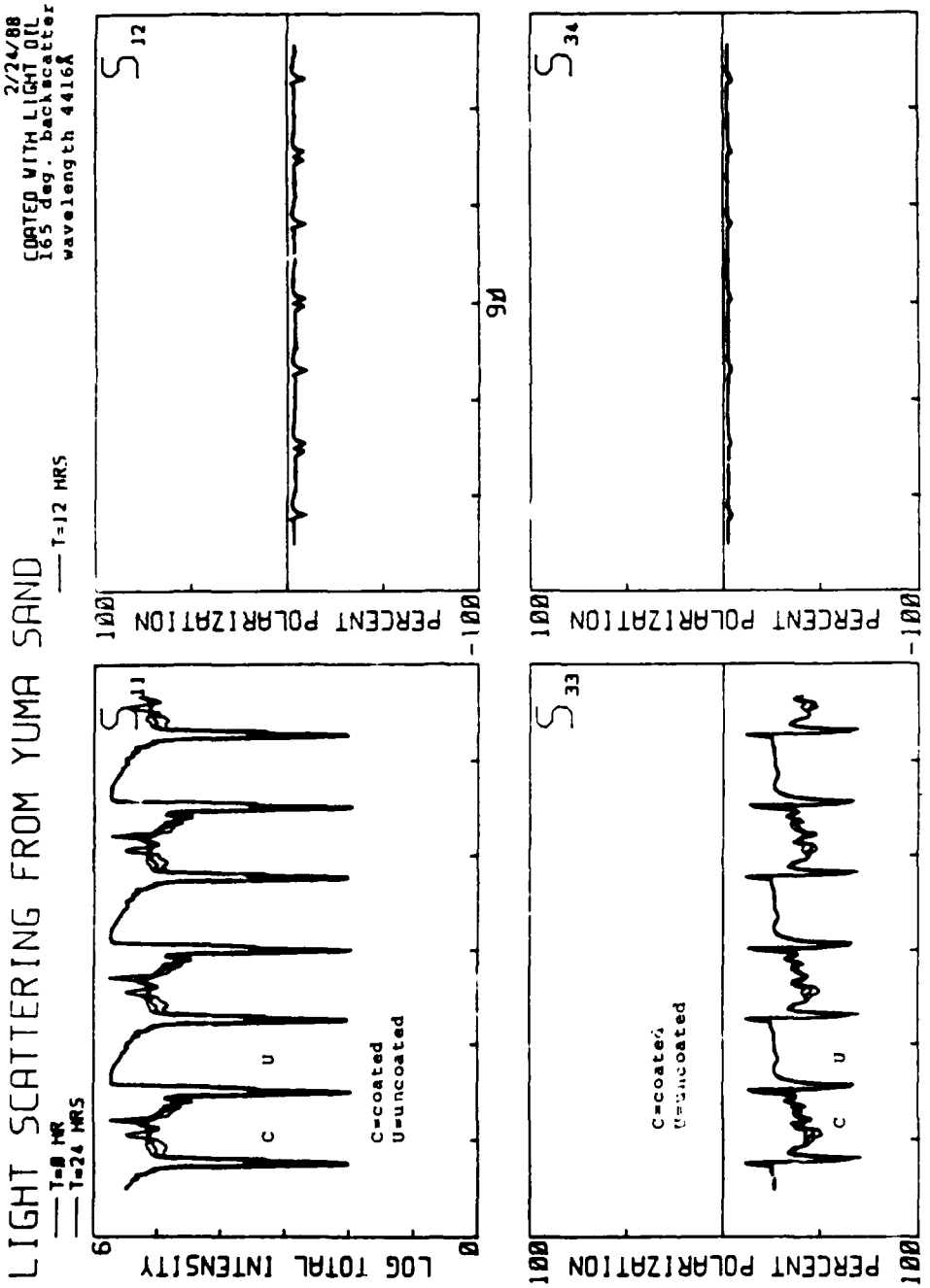

FIGURE 39. Matrix elements of light oil coated sand surfaces as a function of time and illumination angle α.

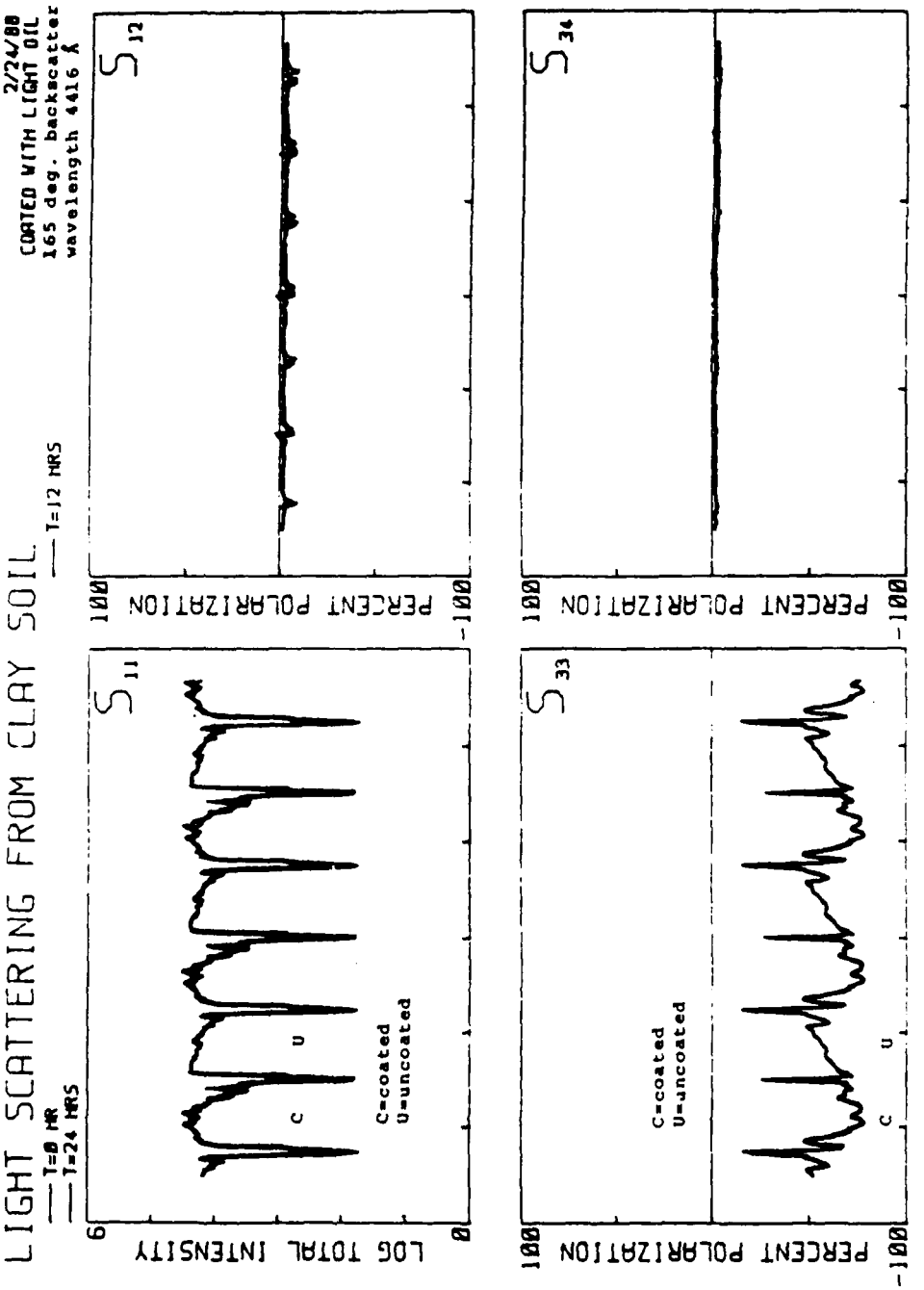

FIGURE 40. Matrix elements of light oil coated clay soil surfaces as a function of time and illumination angle α.

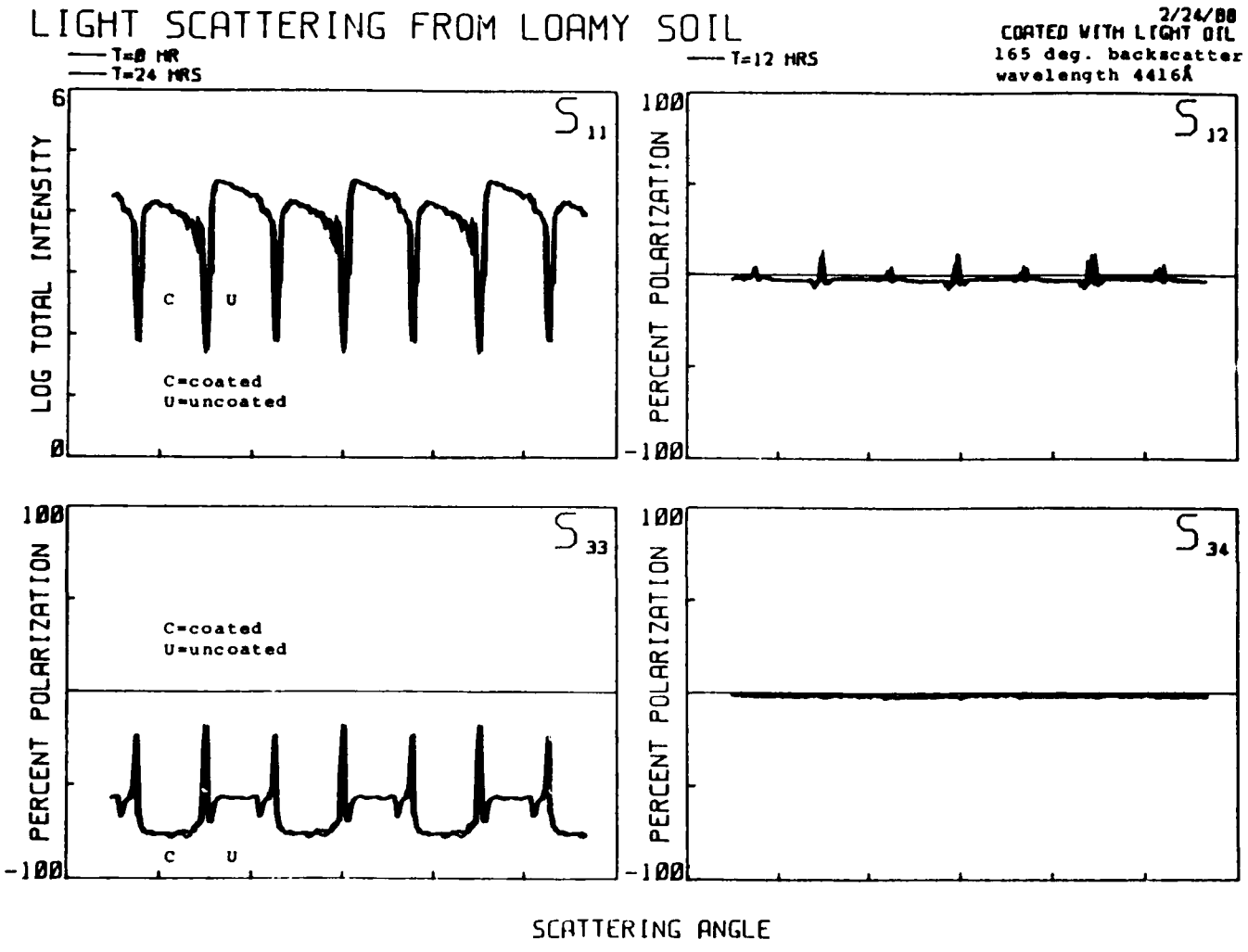

FIGURE 41. Matrix elements of light oil coated loamy soil surfaces as a function of time and illumination angle α.

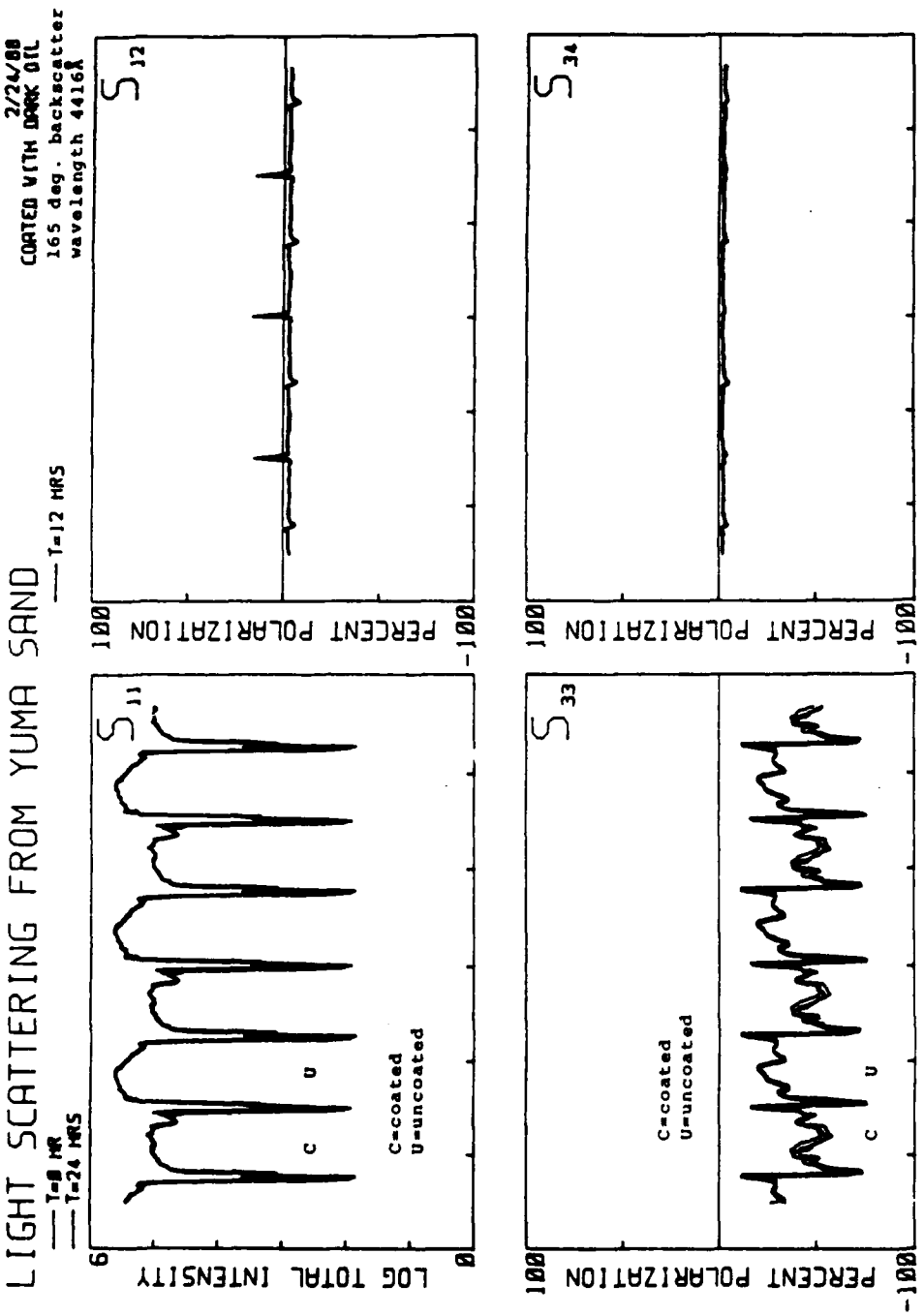

FIGURE 42. Matrix elements of dark oil coated sand surfaces as a function of time and illumination angle α.

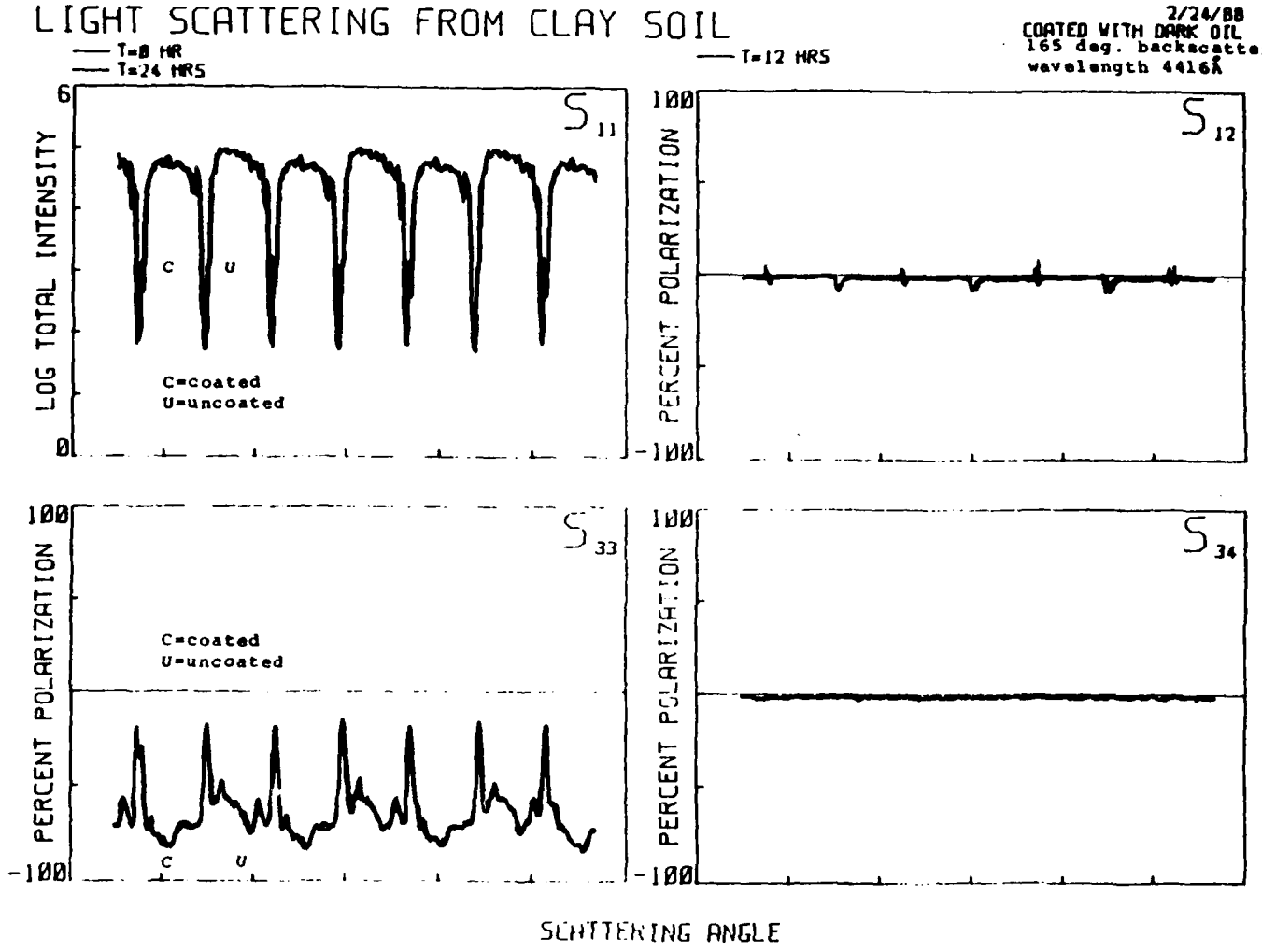

FIGURE 43. Matrix elements of dark oil coated clay soil surfaces as a function of time and illumination angle α.

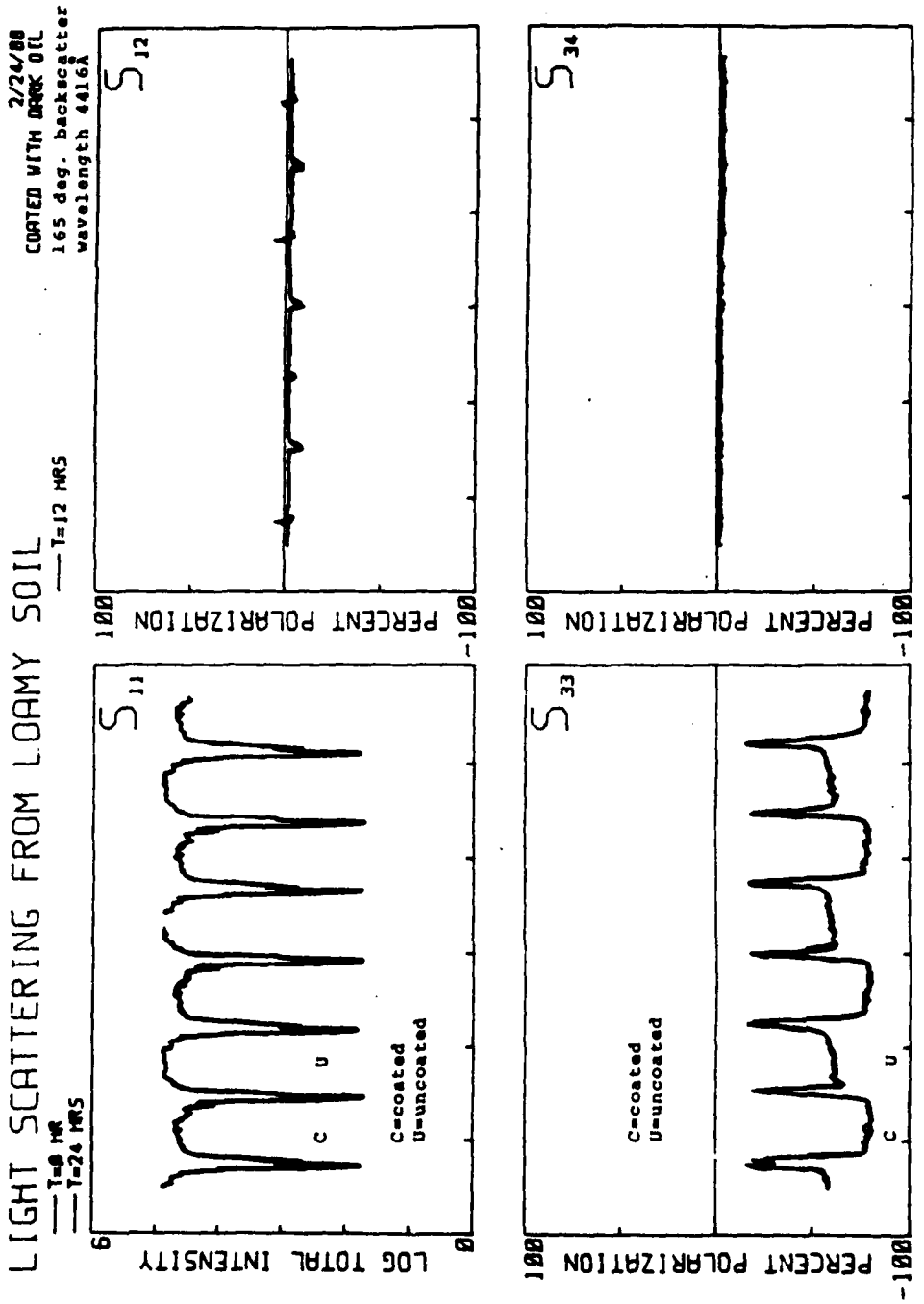

FIGURE 44. Matrix elements of dark oil coated loamy soil surfaces as a function of time and illumination angle α.

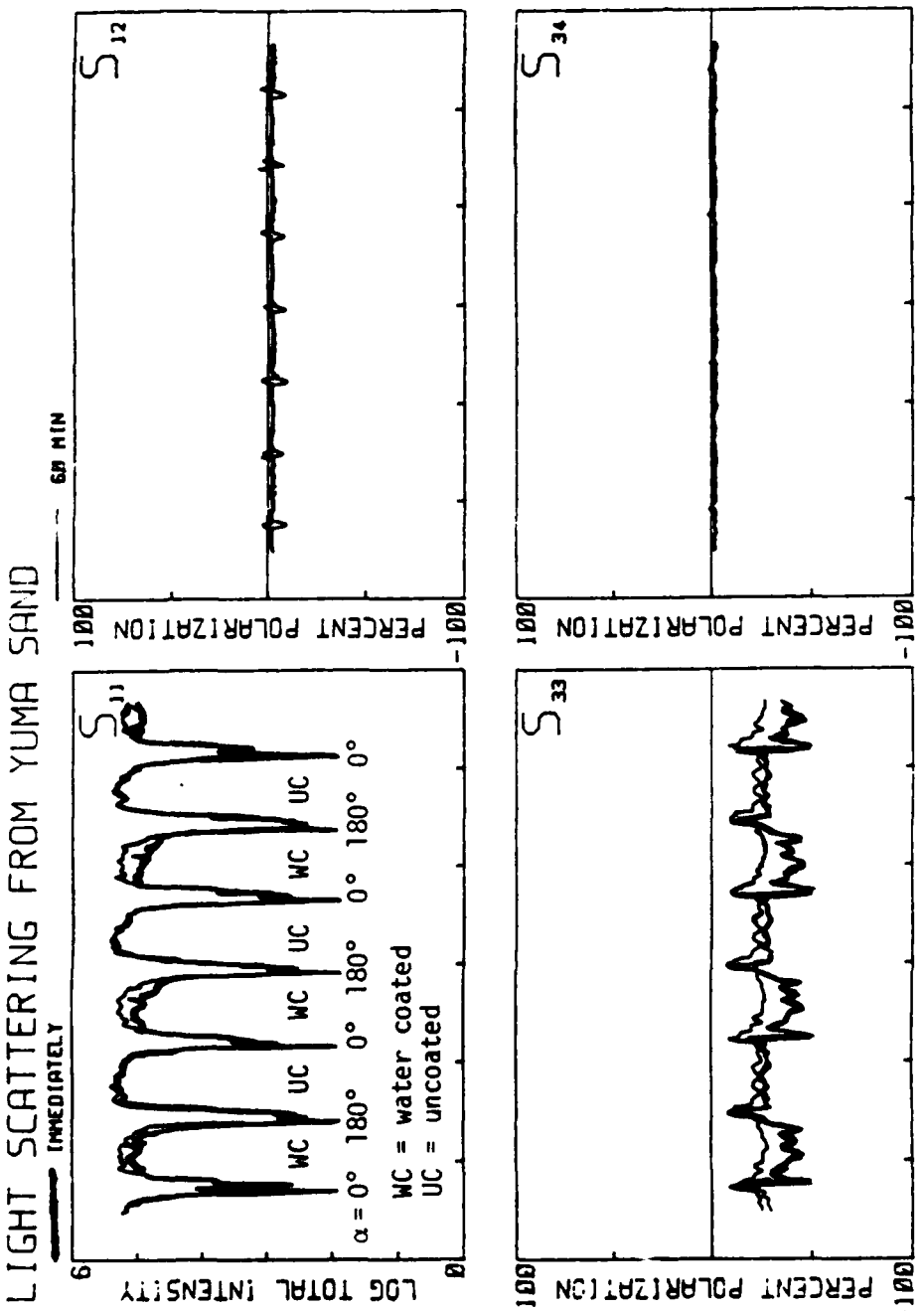

FIGURE 45. Matrix elements of water coated sand surfaces as a function of time and illumination angle α.

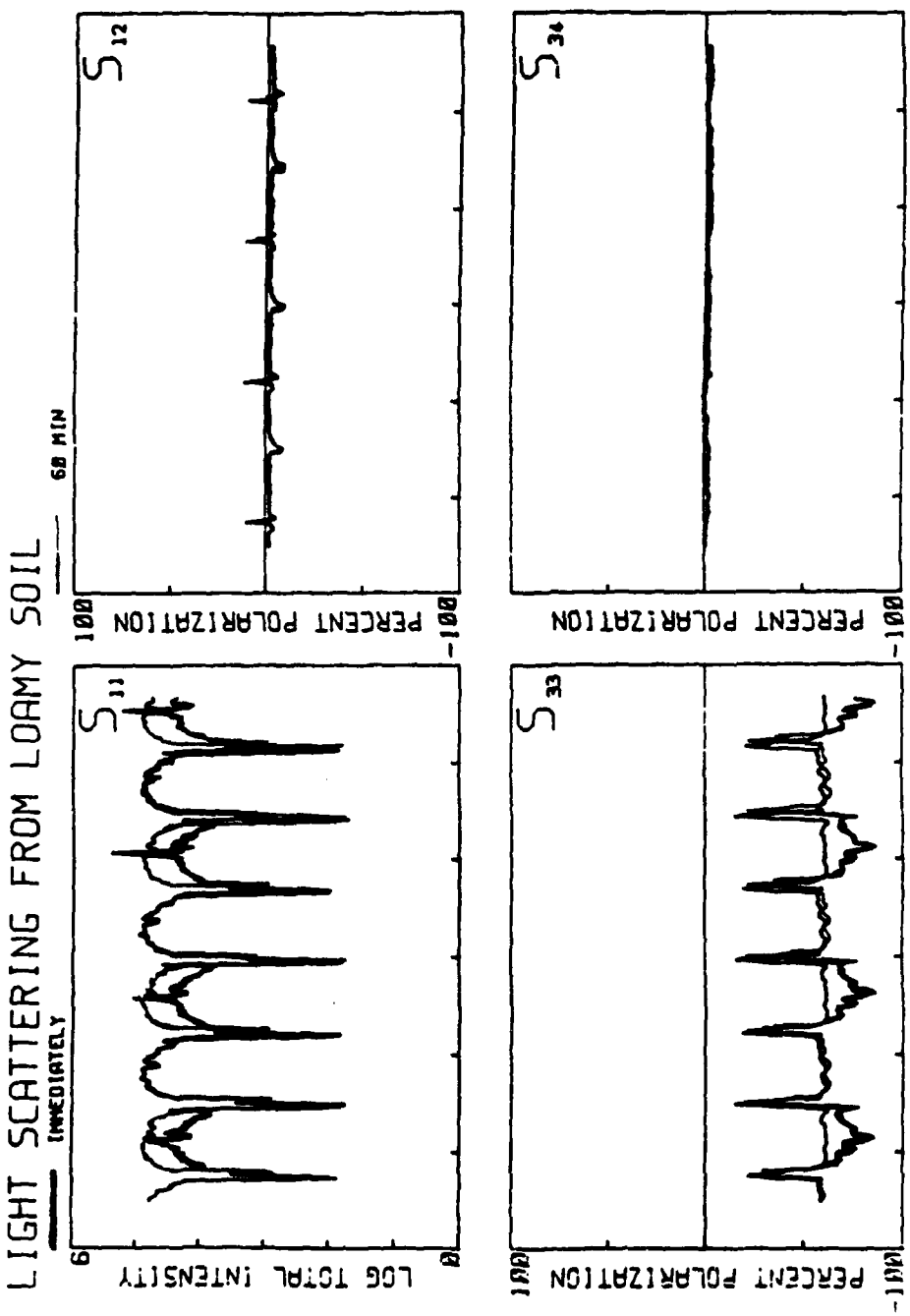

FIGURE 46. Matrix elements of water coated loamy soil surfaces as a function of time and illumination angle α.

13. SHORT-TERM TIME-DEPENDENCE OF OIL COATED SOILS

After looking at the long term (t > 1 hour) time effects discussed in the previous section, we investigated the short term (t < 5 min) time response of the S_{ij} after various thickness oil layers were quickly applied to the four soils. The largest change in any matrix element occurred within 10 minutes after coating. Among other things the length of time it takes for a surface to reach equilibrium after being coated depends on the amount of oil applied. Relaxation times ranged from 10^{-2} seconds, when thicknesses of several microns were applied, to minutes for much thicker coatings. After coating the time dependence of the various matrix elements are characterized by a definite lack of reproducibility.

Figure 47 shows the time dependence of S_{11} after identical amounts of light oil were sprayed onto four different but identically prepared sand surfaces A, B, C and D. An initial decrease in the scattered light occurs followed by an abrupt recovery and then a return to a value slightly lower than that of the uncoated surface. The new equilibrium value is reached within 3 seconds.

Figure 48 shows the time dependence of S_{11} after different amounts of sand were sprinkled onto a surface coated with equal amounts of light oil. The backscatter decreases about a factor of three within 3 seconds.

Relaxation times this short are not useful indicators of the type of coatings sprayed on the surface. We found the relaxation times to be strong functions of the soil type, soil compaction and liquid viscosity. Even without a systematic study of the relationship among these parameters, we have demonstrated that the largest signal changes occur in the first few minutes after oil application and that tne functional dependence of the relaxation is not reproducible enough to be used as a probe to determine the kind of thickness or coating.

Experiments dealing with the time dependence of the light scattering from the oil coated soil surfaces were the most difficult and least reproducible of all the experiments done for this project.

The problem of surface coating is related to the role of capillarity in controlling the behavior of wet particulate systems. This is an area of considerable technological importance. Some applications include moisture retention of soil systems, adhesion of small particles, and the drying of filters. Characterization of these systems demands that the geometric and physical-chemical nature of the particulate and fluid phases be defined, and that the liquid configuration and forces acting on the system be known. The starting point for studying such systems is to calculate the volume and surface area of the liquid ring between two unequal sized touching spheres. Since most real particulate systems consist of particles with a size distribution, a description of the real system requires an understanding of the bond interaction between unequal sized particles. The analysis becomes even more complex when the particles have shapes other than spherical — as with light scattering, where in general a mathematical description of the irregular shapes is not possible.

The soil surfaces of this research are characterized by a collection of size-polydispersed irregular particles that touch each other at random places. The porosity of the system depends on the ratio of air-space volume to solid-material volume. Figures 49(a,b,c) illustrate a cross section of the soil surface for various coating thicknesses.

When a small volume of liquid is sprayed onto the surface, the top surface of the upper layer of particulates becomes coated with small droplets which then form a film of thickness t. As the individual drops touch the surface, the surface tension causes them to spread and if they can touch each other they can flow together to create a thin film coating on the top surface of each particulate (Figure 49(a)). Depending on surface tension and

viscosity, this coating can stabilize in times as short as microseconds. The oil film cannot soak far into the surface since the liquid volume is conserved and adhesion forces establish a minimum film thickness at any place on the top surface.

If an additional volume of liquid is sprayed on to the surface, the drops will make contact with the initial film and flow along the surface and down inside until again equilibrium is reached and flow is stopped (Figure 49(b)). The liquid film on the top surface will have the same thickness as the first case.

Adding more oil will cause the above described process to repeat until the soil surface becomes saturated. When this occurs the flow downward ceases and the thickness of the oil coat on the upper surface will increase (Figure 49(c)).

Two time scales can be identified. The shortest one occurs when a small volume of oil is sprayed onto the surface leaving small individual droplets or small droplets that touch each other. The liquid redistribution to equilibrium will be rapid with time scales of the order of microseconds to milliseconds. The longer time scale occurs when a substantial volume of oil already exists on the surface (several particle layers deep) and an additional small volume is added or if a large volume of oil is initially sprayed onto the uncoated surface. In both cases the fluid must flow over large distances (depths) in order to establish equilibrium via capillary action. This model explains why the time dependence for the light and dark oils were essentially the same. Their liquid properties were identical and flow rates were equivalent. The final thin film thickness on the top surface is the same for both oils when small volumes were sprayed on. Subsequent soaking of additional oil via capillary action leaves surface film thickness the same. With surface films thinner than 100 microns, our light scattering experiments were not able to discern a substantial (useful) difference between the light and dark oil coatings. Only at saturation, where surface oil coatings were thick, did the light and dark oils make a difference in scattered light.

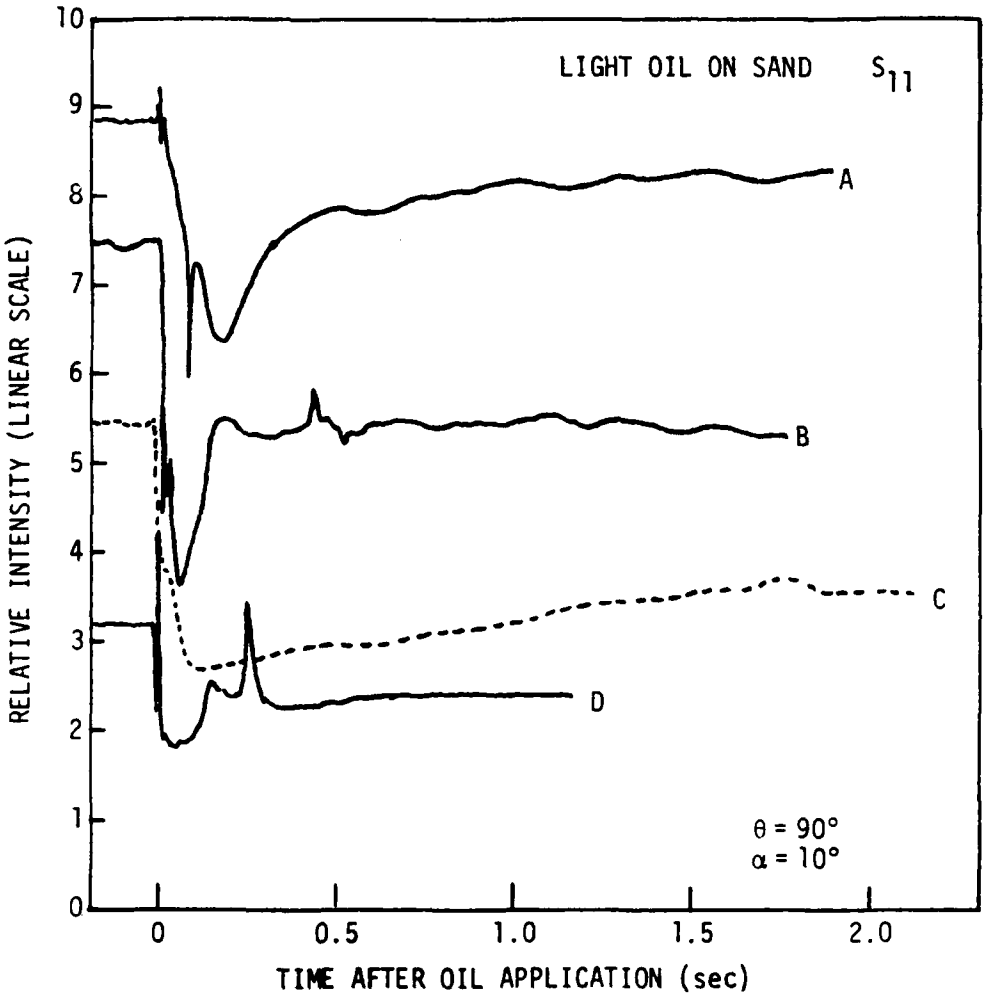

FIGURE 47. Short term time dependence of S_{11} for light oil sprayed on sand.

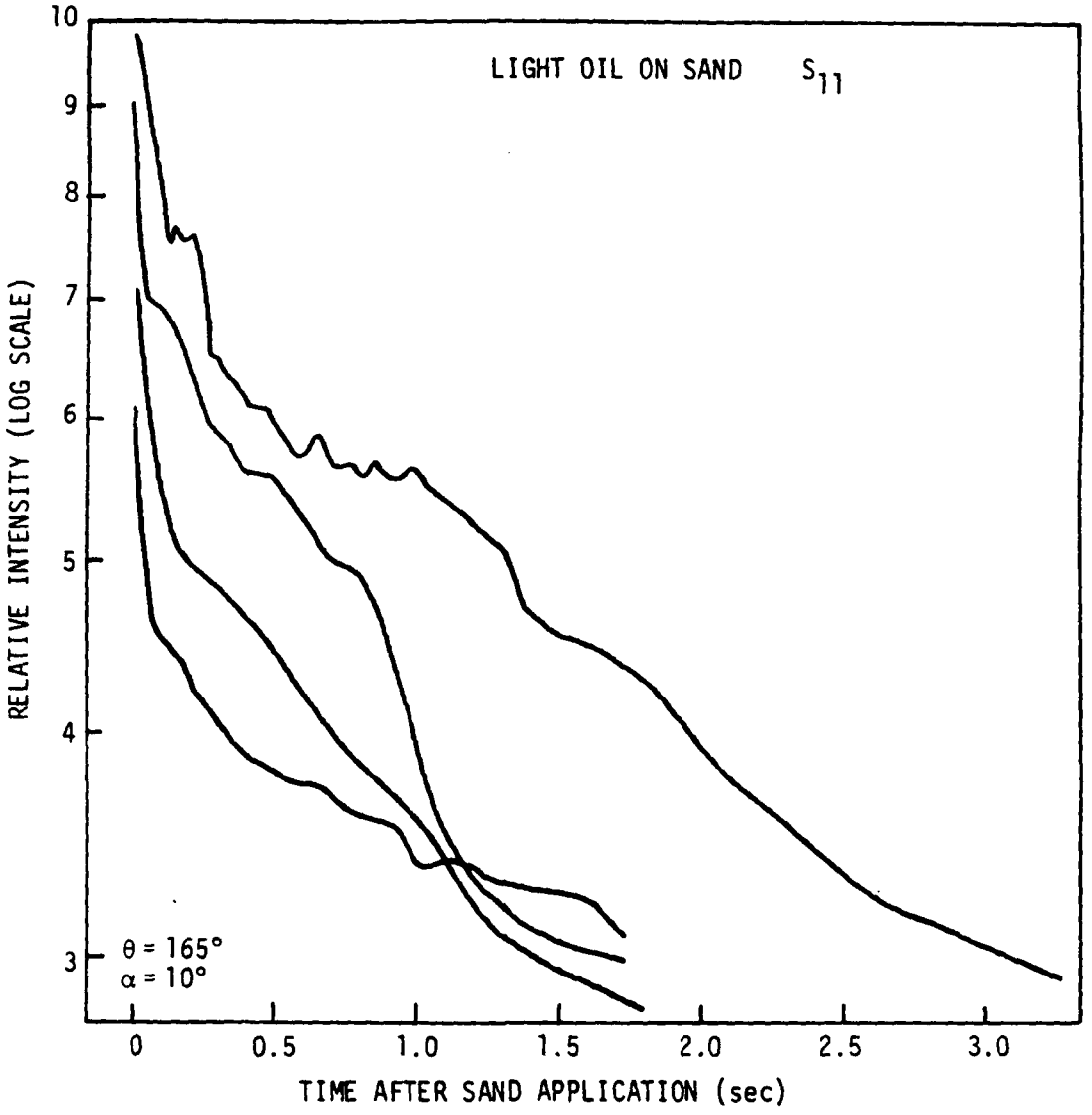

FIGURE 48. Short term time dependence of S_{11} for sand applied to a light oil film.

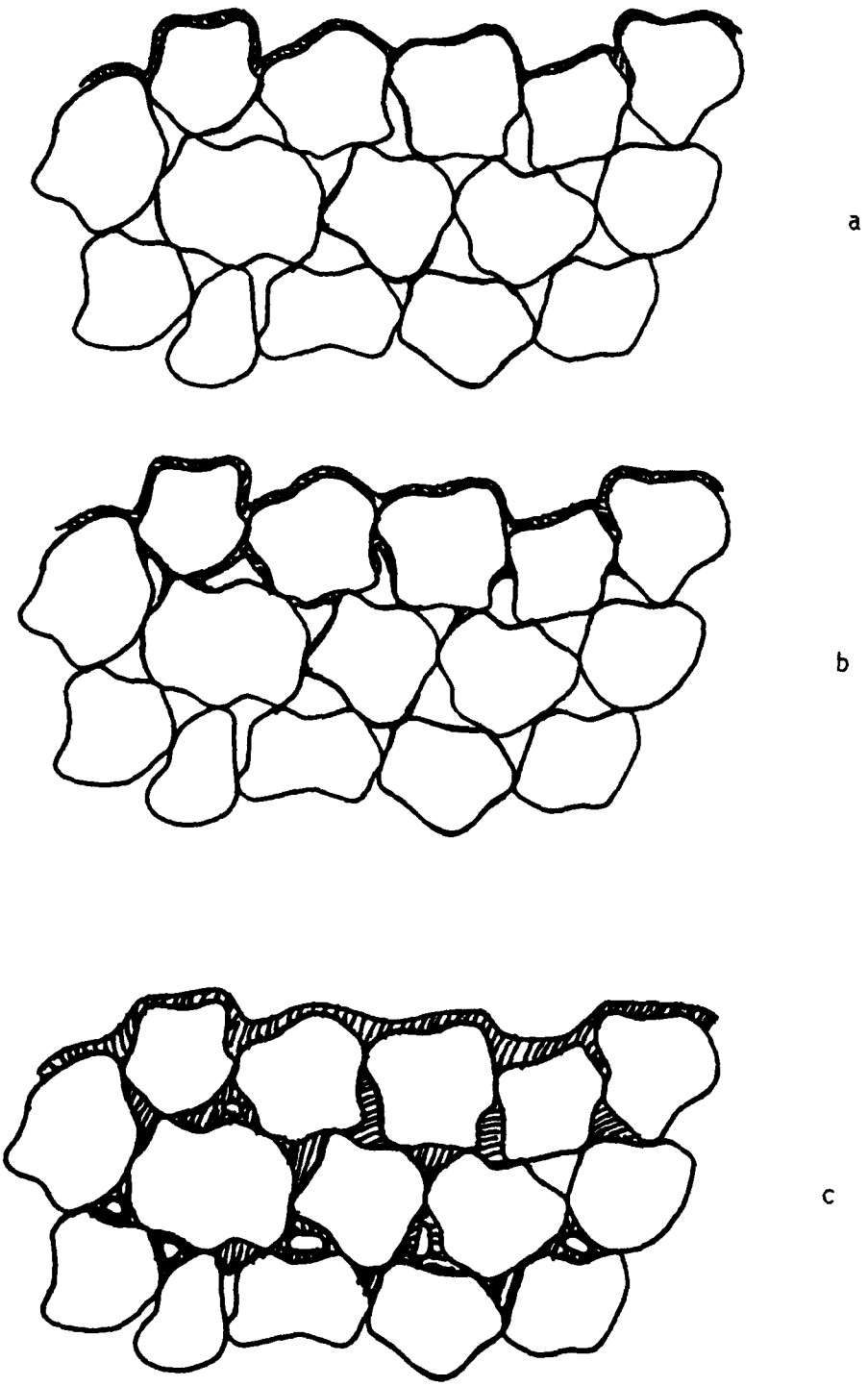

FIGURE 49. Geometrical representation of a liquid soaking into a porous surface. Thin coat (a). Thicker coat (b). Heavy coat (c).

14. MATRIX ELEMENTS OF THE FOUR SOIL SURFACES COVERED WITH BLACK (OPAQUE) PAINT

Because the light scattering differences between the light and dark oil-coated surfaces were small, we compared light scattering from the four uncoated surfaces with the same surfaces coated with flat black paint. After the paint dried, the particulates left on the surface by the paint were much smaller than the average size of the soil particles. Therefore the painted surface had essentially the same roughness as the unpainted surface. This set of black coated surfaces forms the extreme case of surface absorption of the incident laser radiation. The light scattering data for these surfaces are shown in Figures 50 to 57. We made two sets of measurements. One set measured the four matrix elements as a function of scattering angle θ for the samples illuminated at $\alpha = 10^{\circ}$. These are shown in Figures 50, 51, 52, and 53. The other set measured the backscatter at $\theta = 165^{\circ}$ as a function of illumination angle α by rotating the sample from 0 to 180°. These are shown in Figures 54, 55, 56, and 57.

A quick survey of the matrix element curves shows that virtually all matrix elements from all soils can distinguish between the uncoated and black coated surfaces. The one exception is matrix element S_{34} for loamy soil where signal differences are smaller than the signal fluctuation.

In general, coating the soils with black paint affects the light scattering signals in the following ways:

1. Decreases S_{11} for all soils at all angles with the exception of the clay soil where the major difference occurs in the backscatter.

2. Makes S_{12} more negative. This matrix element is very close to zero for all θ for the uncoated soils.

3. Increases S_{33} in the forward scatter and decreases S_{33} in the backscatter. The curves for the black and uncoated surfaces cross near $\theta = 65^{\circ}$ for all soils.

4. Increases S_{34} only slightly from its uncoated value of nearly zero.

We also note the following:

1. S_{12} and S_{34} cannot distinguish between the black and uncoated surfaces for $\theta > 150^{\circ}$.

2. The main differences between the black and uncoated surfaces occur in the forward scatter ($30 < \theta < 90^{\circ}$) for S_{12} and S_{34}.

3. S_{33} shows the largest response to surface absorption and the largest differences occur in the backscatter.

4. For each soil the shape of the S_{11} curves for black and uncoated surfaces are similar. The black surface absorbs more and scatters less light.

These data show that the polarization matrix element S_{34} is the least sensitive to absorption differences whereas S_{12} and S_{33} are good discriminators of surface absorption.

The unnormalized total intensity matrix element S_{11} responds as it should to increasing surface absorption but it is not as useful as the polarization for characterizing surface

absorption.

The backscatter data taken at $\theta = 165°$ as a function of illumination angle α is shown in Figures 54, 55, 56, and 57. Backscatter measurements are more useful than the matrix element curves since they are the actual measurement made "in the field." As a scatterometer flies over a field (surface) the laser beam can be aimed to illuminate a section of the surface at any angle while the detected signal must always be received near the backscatter ($\theta \approx 180°$).

A quick survey of the backscatter curves shows that matrix elements S_{12} and S_{34} at $\theta = 165°$ are zero for all soils, for all α and for both surfaces (black and uncoated). Only matrix elements S_{11} and S_{33} survive as useful discriminators for surface absorption.

Specifically we note that increasing surface absorption decreases the backscatter intensity S_{11} at all θ, and it drives the S_{33} matrix element even more negative than the one for the uncoated surface.

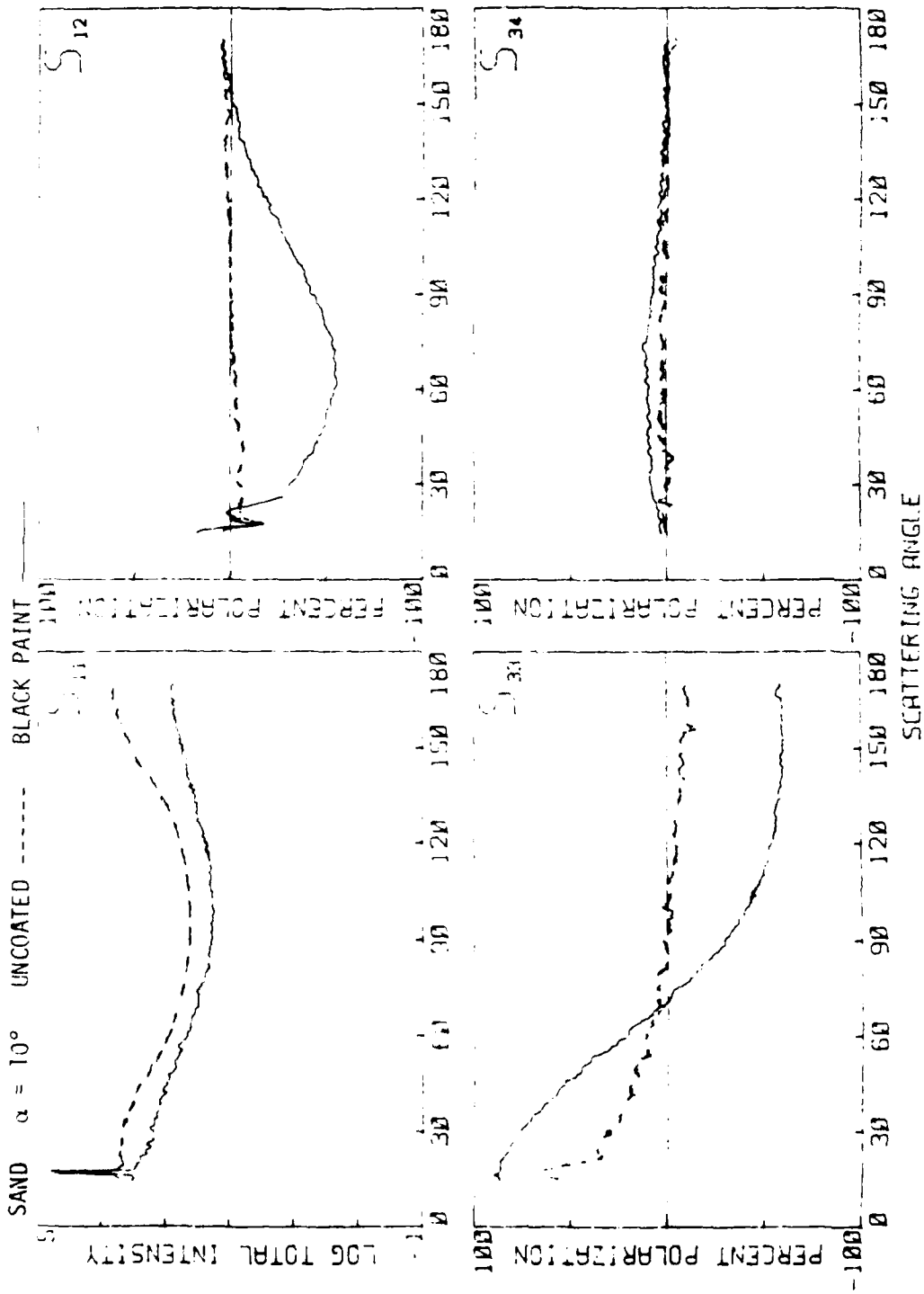

FIGURE 50. Matrix elements for an uncoated sand surface and a sand surface coated with black paint.

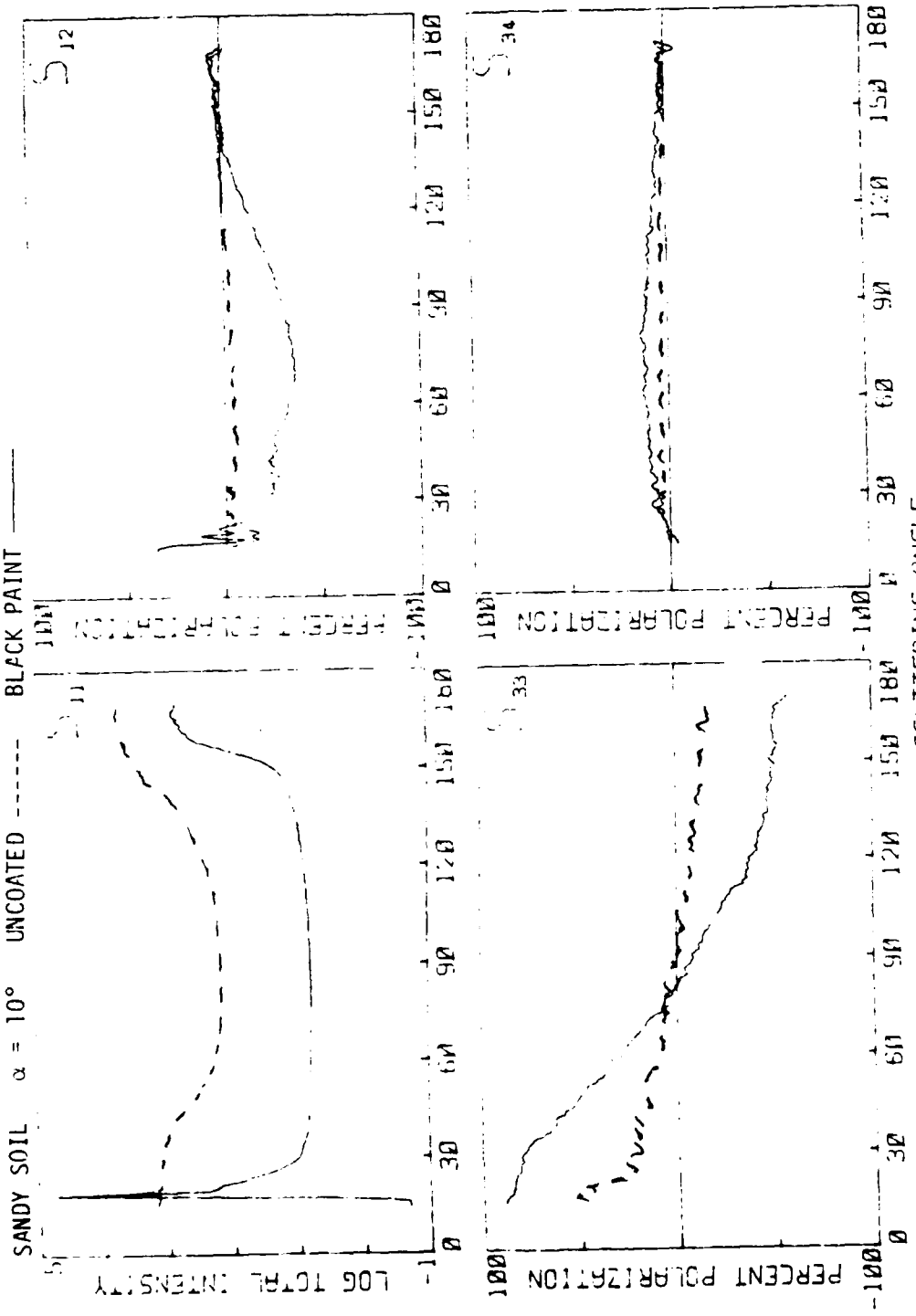

FIGURE 51. Matrix elements for an uncoated sandy soil surface and a sandy soil surface coated with black paint.

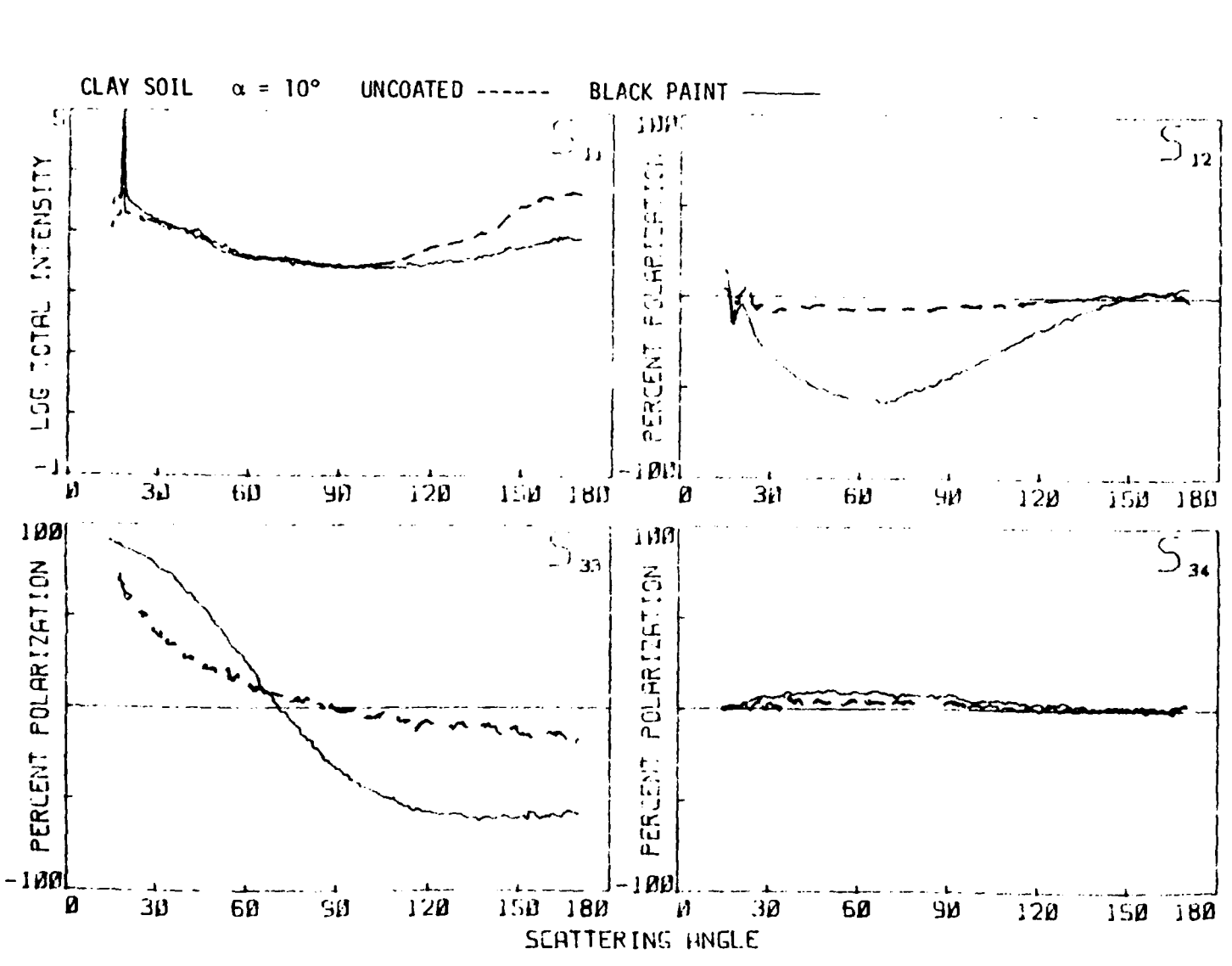

FIGURE 52. Matrix elements for an uncoated clay soil surface and a clay soil surface coated with black paint.

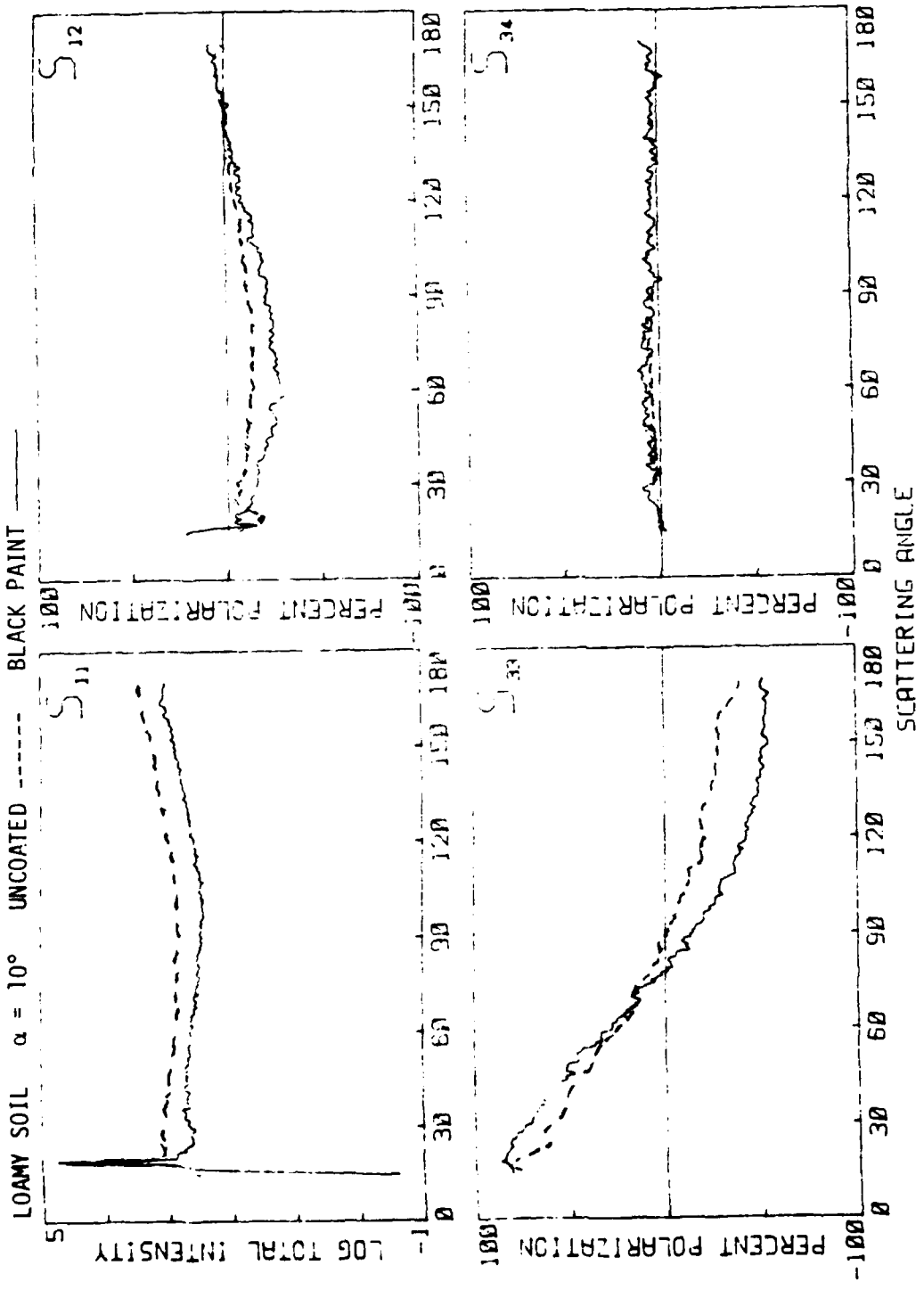

FIGURE 53. **Matrix elements for an uncoated loamy soil surface and a loamy soil surface coated with black paint.**

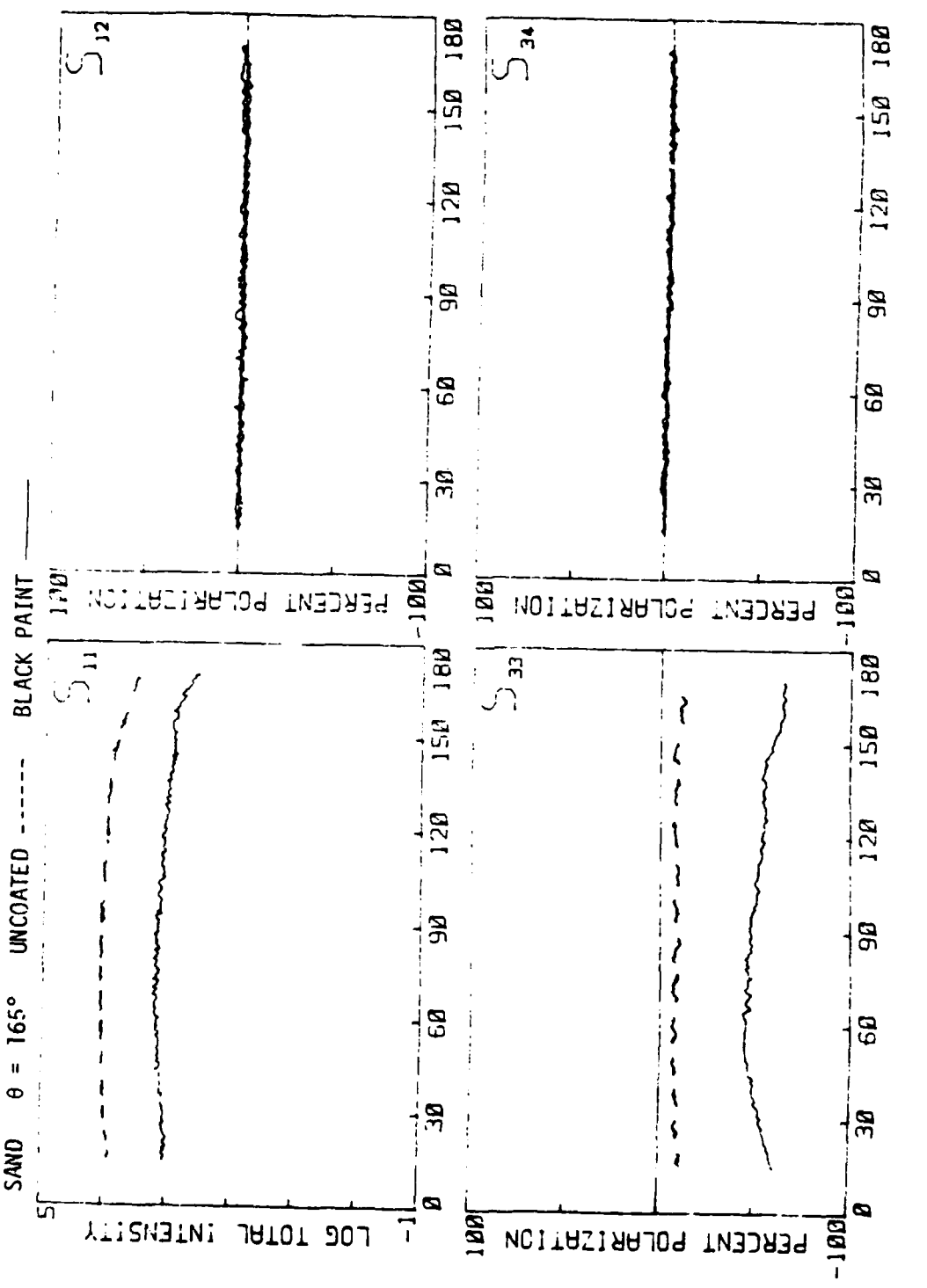

FIGURE 54. Backscatter measurements for an uncoated sand surface and a sand surface coated with black paint.

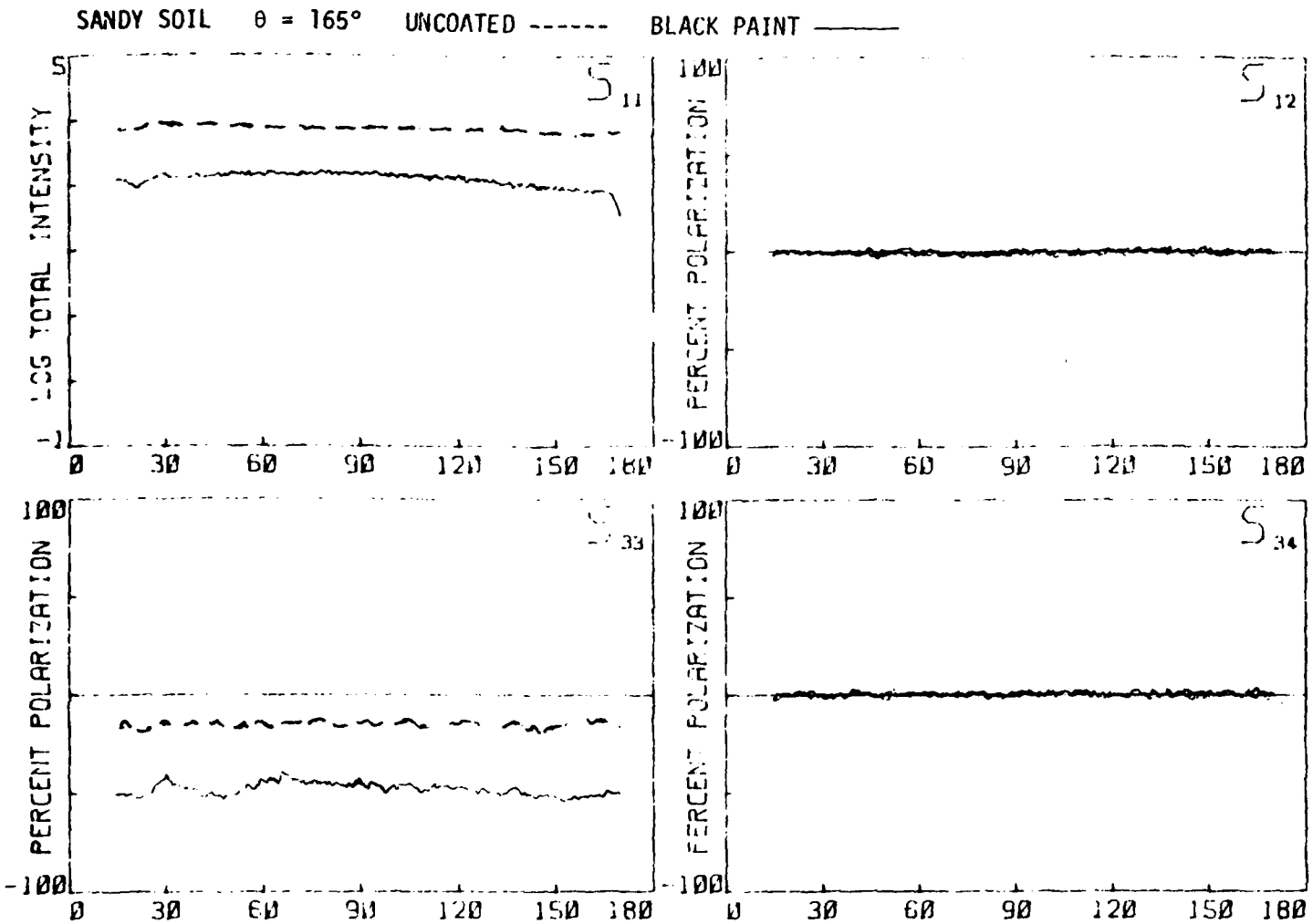

FIGURE 55. Backscatter measurements for an uncoated sandy soil surface and a sandy soil surface coated with black paint.

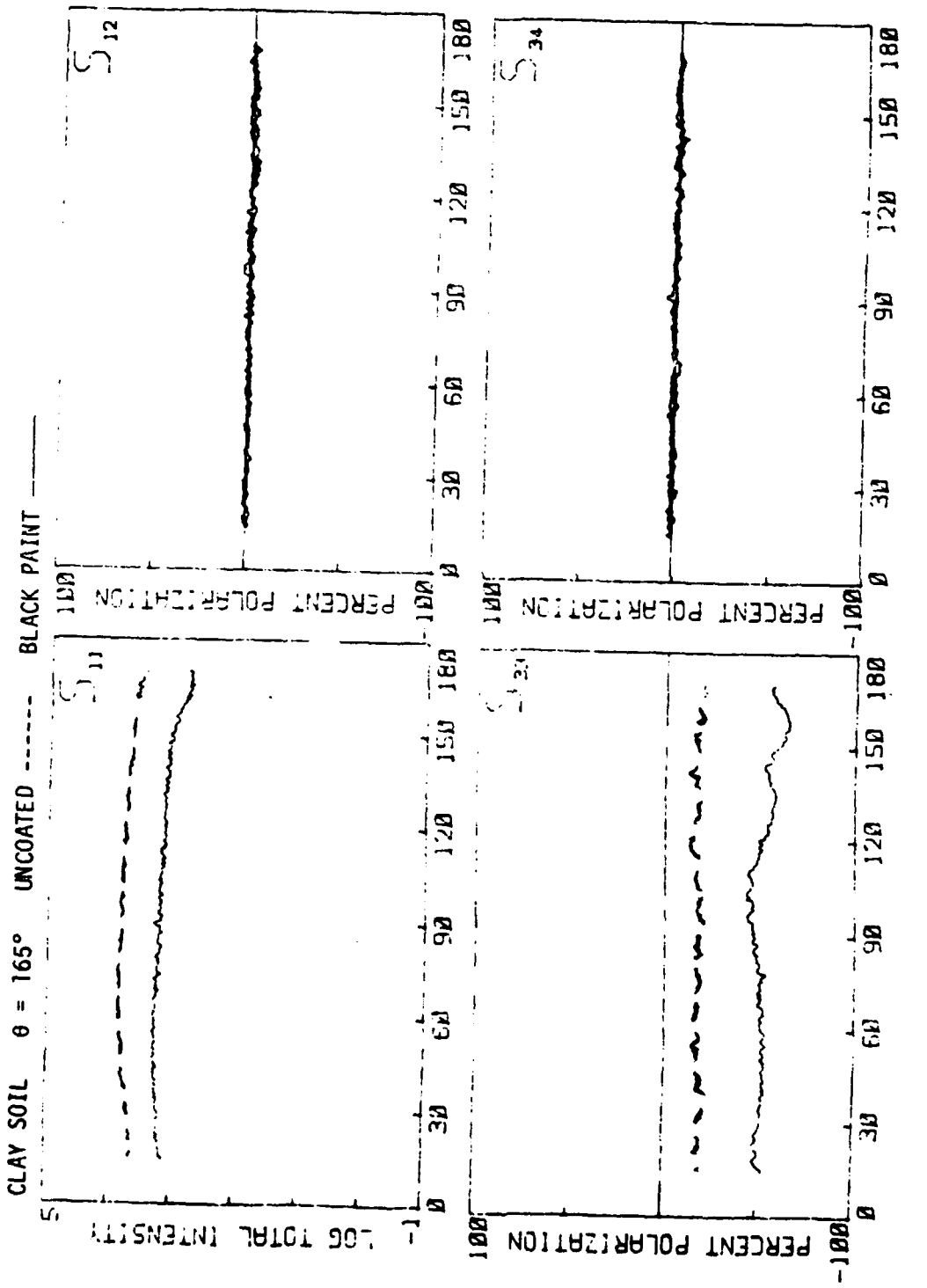

FIGURE 56. Backscatter measurements for an uncoated clay soil surface and a clay soil surface coated with black paint.

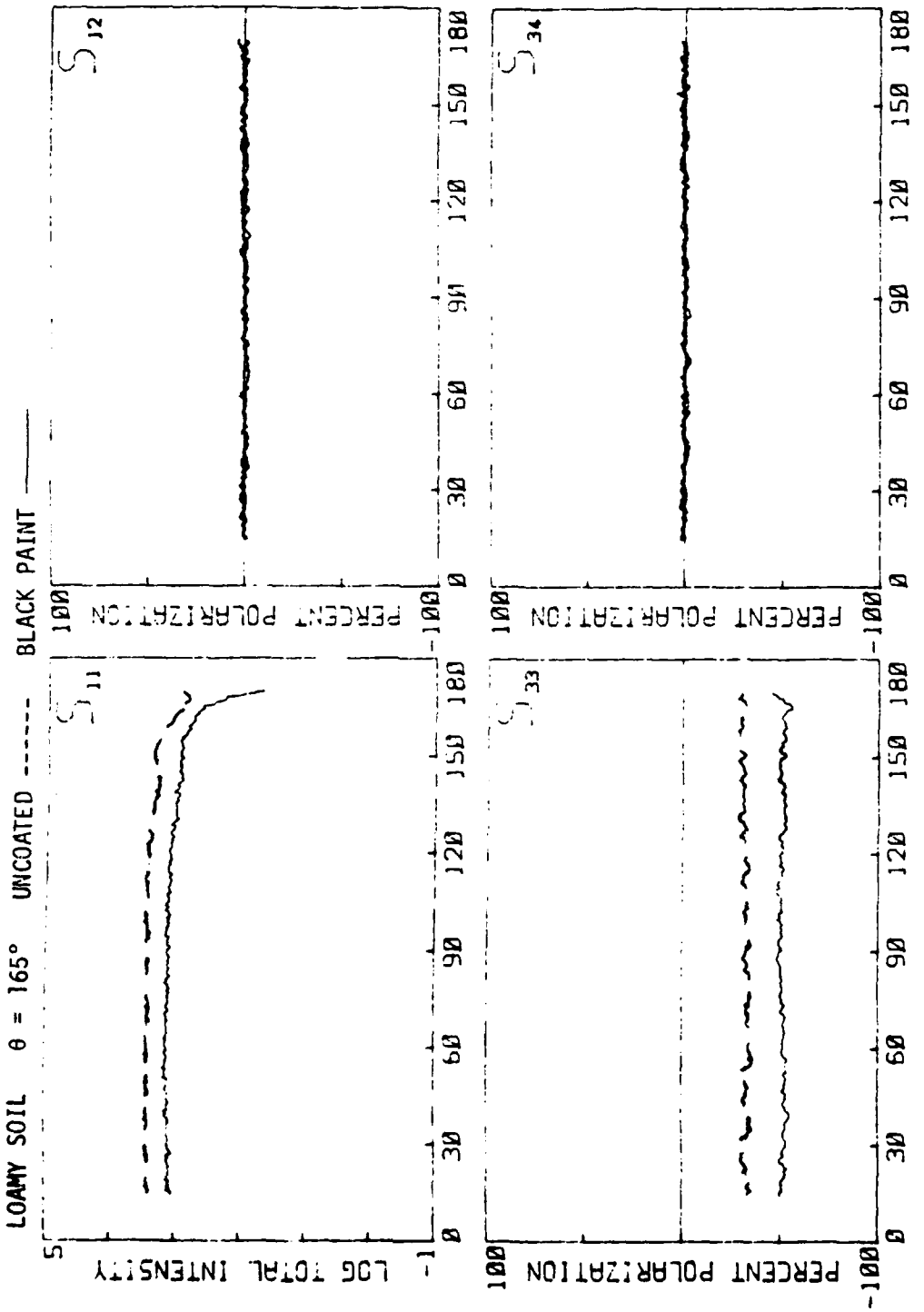

FIGURE 57. Backscatter measurements for an uncoated loamy soil surface and a loamy soil surface coated with black paint.

15. SAND SURFACES: MATRIX ELEMENTS S_{11} AND S_{33} AND BACKSCATTER STUDIES OF SAND SURFACES COATED WITH LIGHT AND DARK OILS

This section shows the results of five measurements on sand involving the matrix elements S_{11} and S_{33}:

1. $S_{ij}(\alpha = 45°, \theta = 165°)$ as a function of light and dark oil thickness.
2. Matrix element $S_{ij}(\theta)$ ($\alpha = 10°$) for three different thicknesses of light oil.
3. Matrix elements $S_{ij}(\theta)$ ($\alpha = 10°$) for three different thicknesses of dark oil.
4. Matrix element $S_{ij}(\alpha)$ ($\theta = 165°$) for three different thicknesses of light oil.
5. Matrix element $S_{ij}(\alpha)$ ($\theta = 165°$) for three different thicknesses of dark oil.

The next three sections -- 16, 17, and 18 -- describe the same measurements with sandy soil, clay soil and loamy soil, respectively. We describe how each measurement was made and some observations regarding the data. Final conclusions drawn from the entire study will be given in the last section.

Figure 58 shows the backscatter value of S_{11} ($\theta = 165°$, $\alpha = 45°$) as a function of oil thickness for the light and dark oils. These data were taken from a single sand surface on which a linear gradient thickness of light (or dark) oil was sprayed. Using the technique described in Section 9, the surface was scanned from bottom (oil thickness = 0) to top (oil thickness = 55 microns). The three almost coinciding curves are shown for the light oil. Two of these were taken along two different paths from bottom to top to record the reproducibility of the signal for essentially identical surfaces, the third (middle curve) is the avearge of the first two. The scattered intensity from the surface coated with light oil is about a factor of 2 larger than that from the surface coated with dark oil. The scattered intensity at this angle increases slightly with thickness.

Figure 59 (TOP and BOTTOM) compares the $S_{11}(\theta)$ matrix elements at $\alpha = 10°$ for three different thicknesses of the light oil and dark oil, respectively.

Figure 60 (TOP and BOTTOM) compares the $S_{11}(\alpha)$ matrix elements at $\theta = 165°$ for three different thicknesses of the light oil and dark oil, respectively.

The data shown in Figures 59 and 60 were taken from separate but identically prepared sand surfaces where each individual surface was coated to the indicated thickness of light and dark oil.

Figure 61 shows the backscatter value of S_{33} ($\theta = 165°$, $\alpha = 45°$) as a function of oil thickness for the light and dark oils. These data were taken from the same single sand surface prepared with a linear gradient thickness of light (or dark) oil as described for Figure 58. The slight (<10%) variation of S_{33} with increasing thickness is equal to the ±10% variation in the signal due to surface roughness.

Figure 62 compares the $S_{33}(\theta)$ matrix elements at $\alpha = 10°$ for the light oil and dark oil, respectively.

Figure 63 compares the $S_{33}(\alpha)$ matrix elements at $\theta = 165°$ for the light oil and dark oil, respectively.

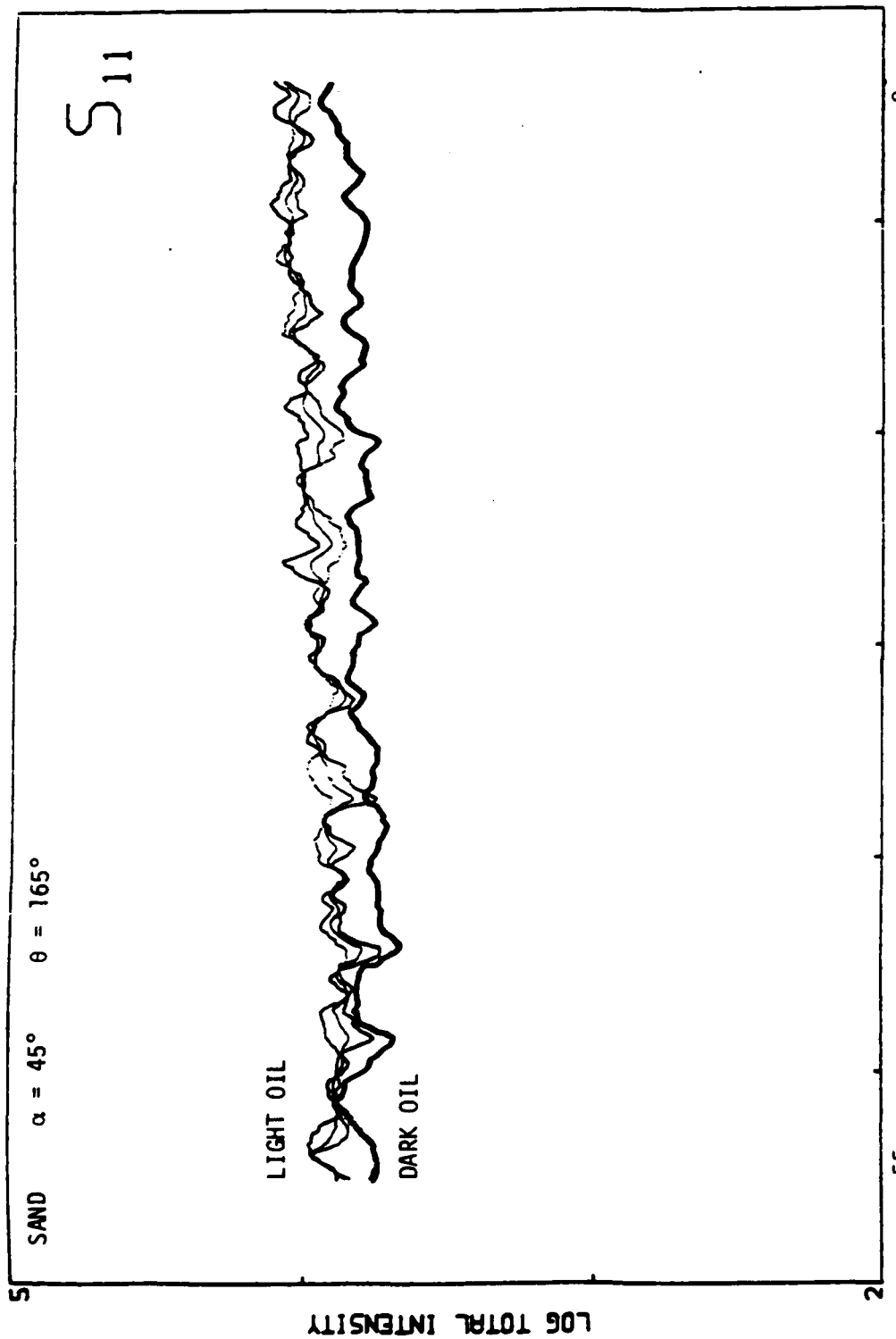

FIGURE 58. Backscatter of S_{11} for sand as a function of oil thickness for light oil and dark oil.

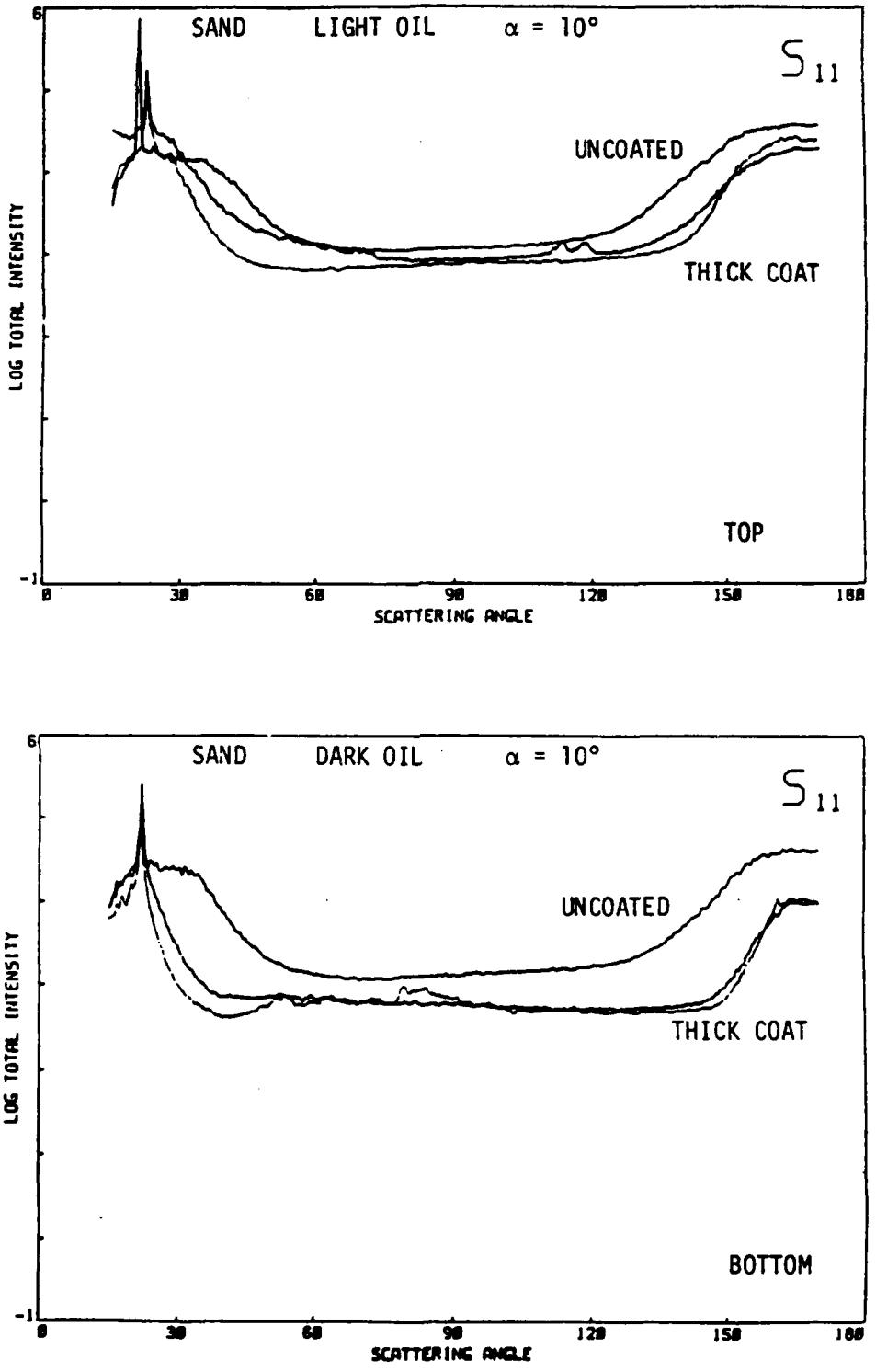

FIGURE 59. Matrix element S_{11} for sand coated with three different thicknesses of light oil (TOP) and of dark oil (BOTTOM).

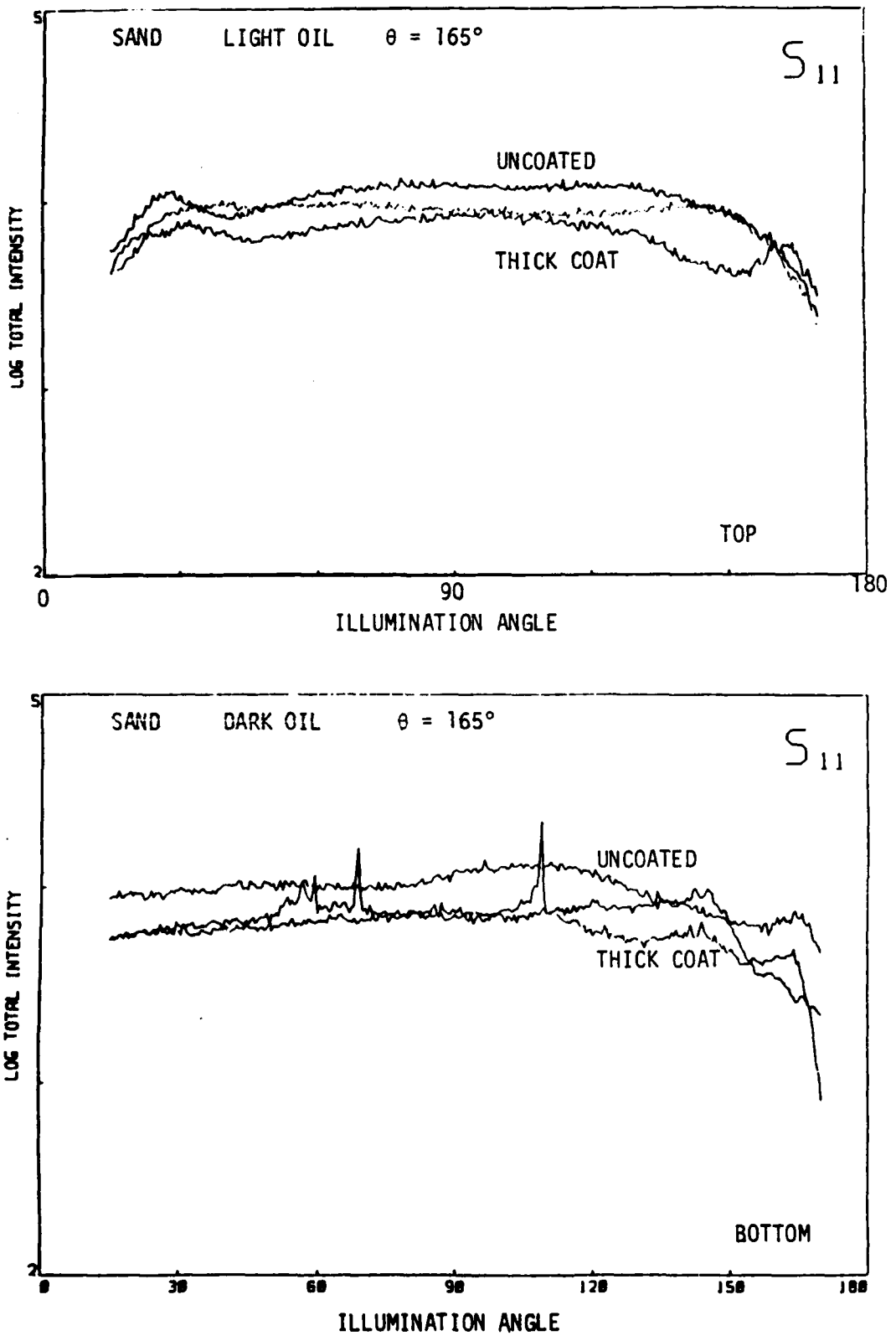

FIGURE 60. Backscatter of S_{11} for sand coated with three different thicknesses of light oil (TOP) and of dark oil (BOTTOM).

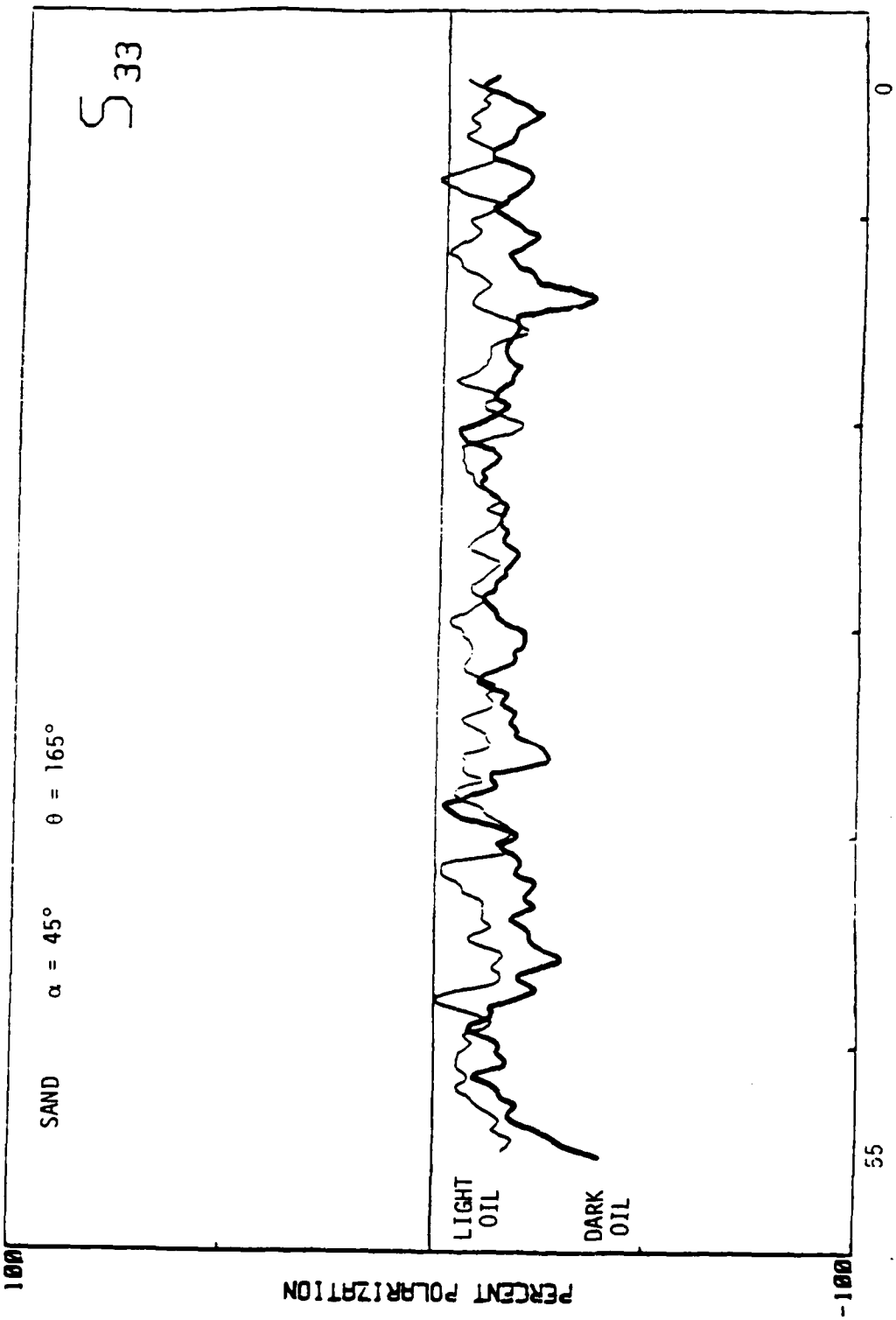

FIGURE 61. Backscatter of S_{33} for sand as a function of oil thickness for light oil and dark oil.

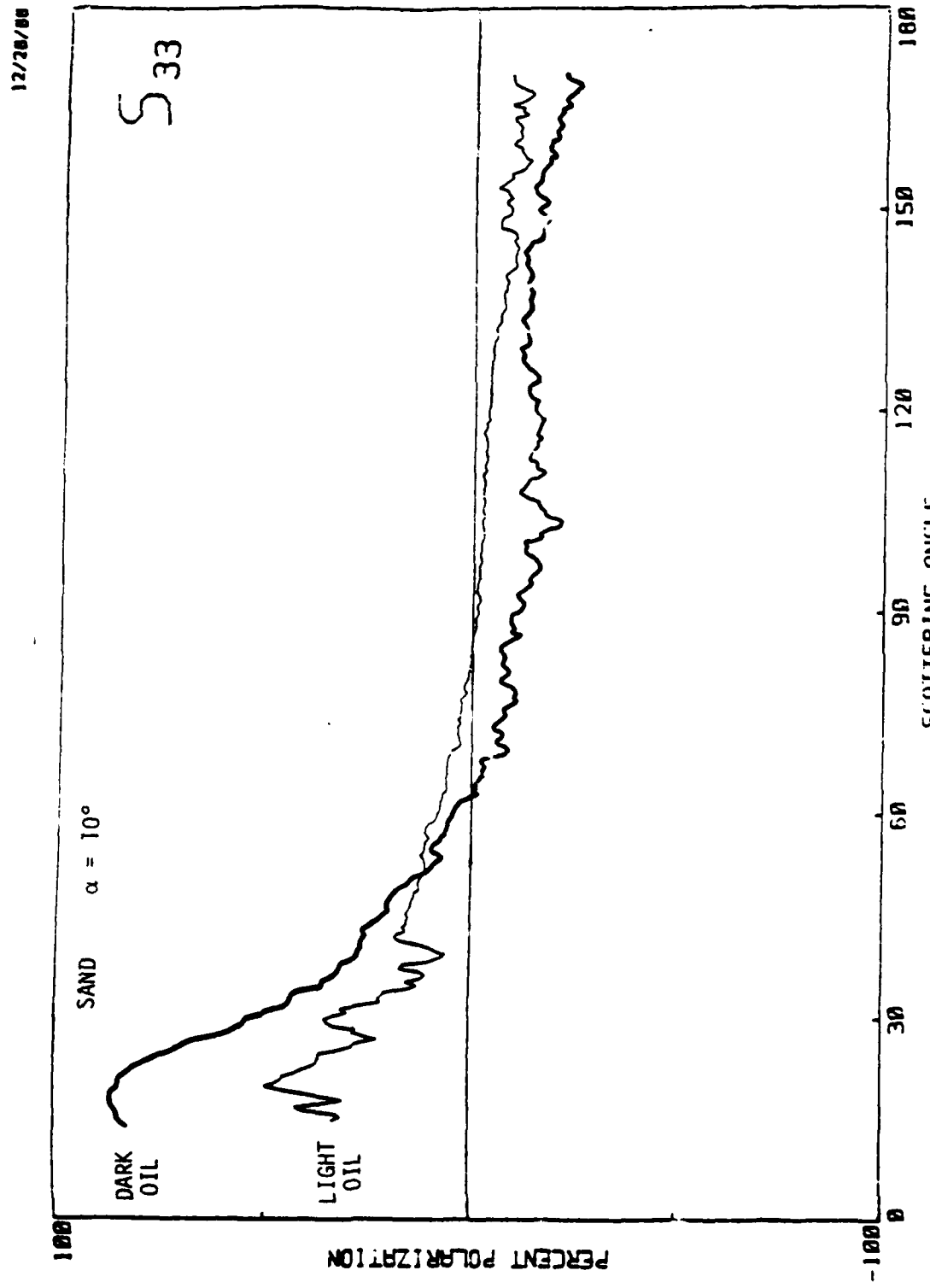

FIGURE 62. Matrix element S_{33} for sand coated with light oil and with dark oil.

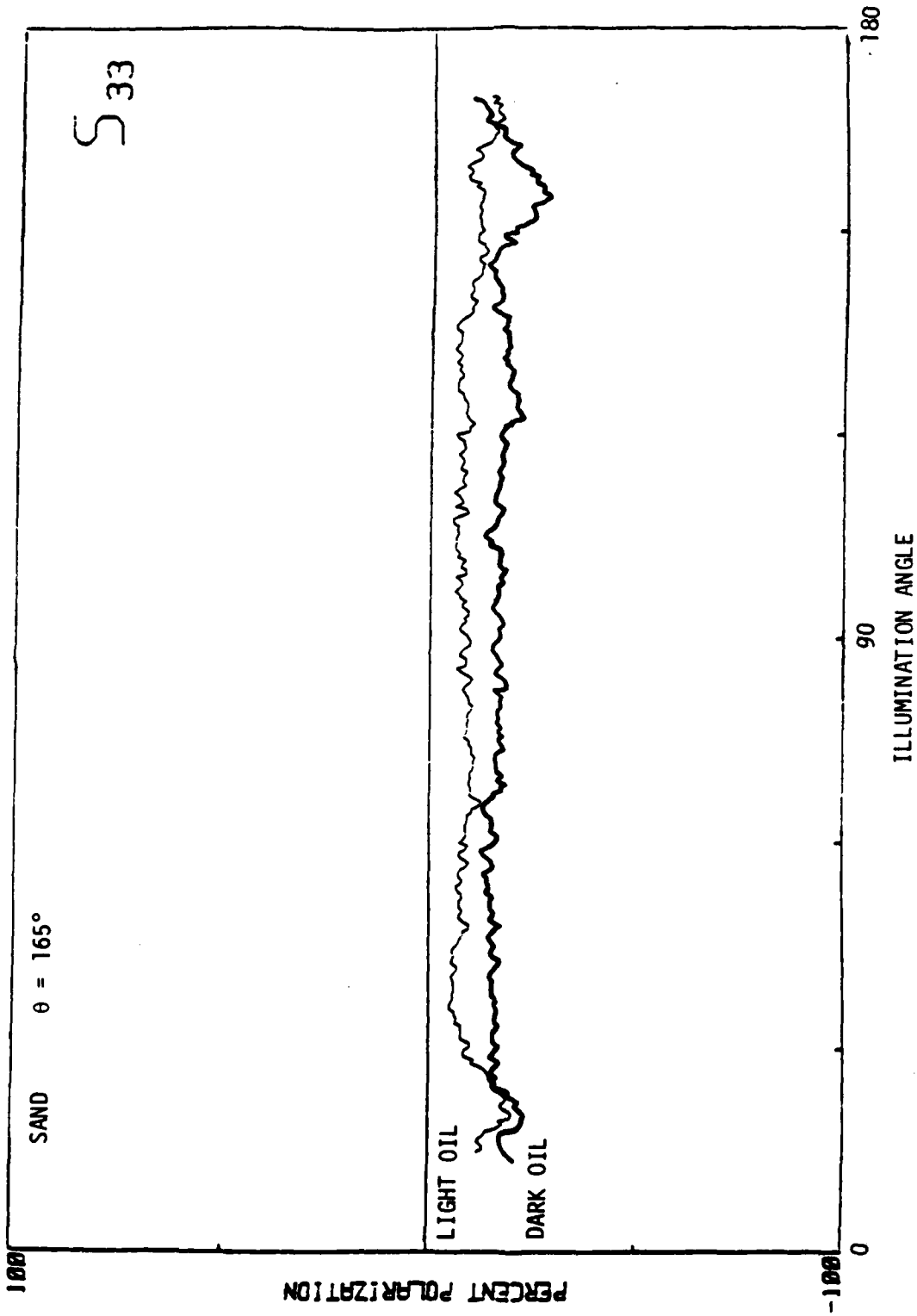

FIGURE 63. Backscatter of S_{33} for sand coated with light oil and with dark oil.

16. SANDY-SOIL SURFACES: MATRIX ELEMENTS S_{11} AND S_{33} AND BACKSCATTER STUDIES OF SANDY-SOIL SURFACES COATED WITH LIGHT AND DARK OIL

This section shows the results of the five measurements on sandy soil involving the matrix elements S_{11} and S_{33}. They are identical to the five measurements just described for sand.

1. $S_{ij}(\alpha = 45°, \theta = 165°)$ as a function of light and dark oil thickness.
2. Matrix element $S_{ij}(\theta)$ ($\alpha = 10°$) for three different thicknesses of light oil.
3. Matrix elements $S_{ij}(\theta)$ ($\alpha = 10°$) for three different thicknesses of dark oil.
4. Matrix element $S_{ij}(\alpha)$ ($\theta = 165°$) for three different thicknesses of light oil.
5. Matrix element $S_{ij}(\alpha)$ ($\theta = 165°$) for three different thicknesses of dark oil.

Figure 64 shows the backscatter of S_{11} ($\theta = 165°$, $\alpha = 45°$) as a function of thickness of the light and dark oils. The surface was prepared with a linear gradient oil thickness as was done for sand. In this case we show just one curve for the light and dark oils. For this surface (at these angles) the total intensity is unable to distinguish between light and dark oil coatings or thickness variations.

Figure 65 (TOP and BOTTOM) compares the $S_{11}(\theta)$ matrix elements at $\alpha = 10°$ for the three different thicknesses of light oil and dark oil, respectively. Figure 66 (TOP and BOTTOM) compares the $S_{11}(\alpha)$ matrix elements at $\theta = 165°$ for three different thicknesses of light oil and dark oil, respectively.

The data shown in Figures 65 and 66 were taken from separate but identically prepared sandy-soil surfaces where each individual surface was coated to the indicated thickness of light and dark oil.

Figure 67 shows the backscatter value of S_{33} ($\theta = 165°$, $\alpha = 45°$) as a function of oil thickness for the light and dark oils. These data were taken from the same single sandy-soil surface prepared with a linear gradient thickness of light (or dark) oil as described in Figure 58. The light oil gives a slightly more negative polarization than the dark oil; however, differences are not larger than the fluctuations due to surface roughness.

Figure 68 compares the $S_{33}(\theta)$ matrix element at $\alpha = 10°$ for light oil and dark oil, respectively.

Figure 69 compares the $S_{33}(\alpha)$ matrix elements at $\theta = 165°$ for the light oil and dark oil, respectively.

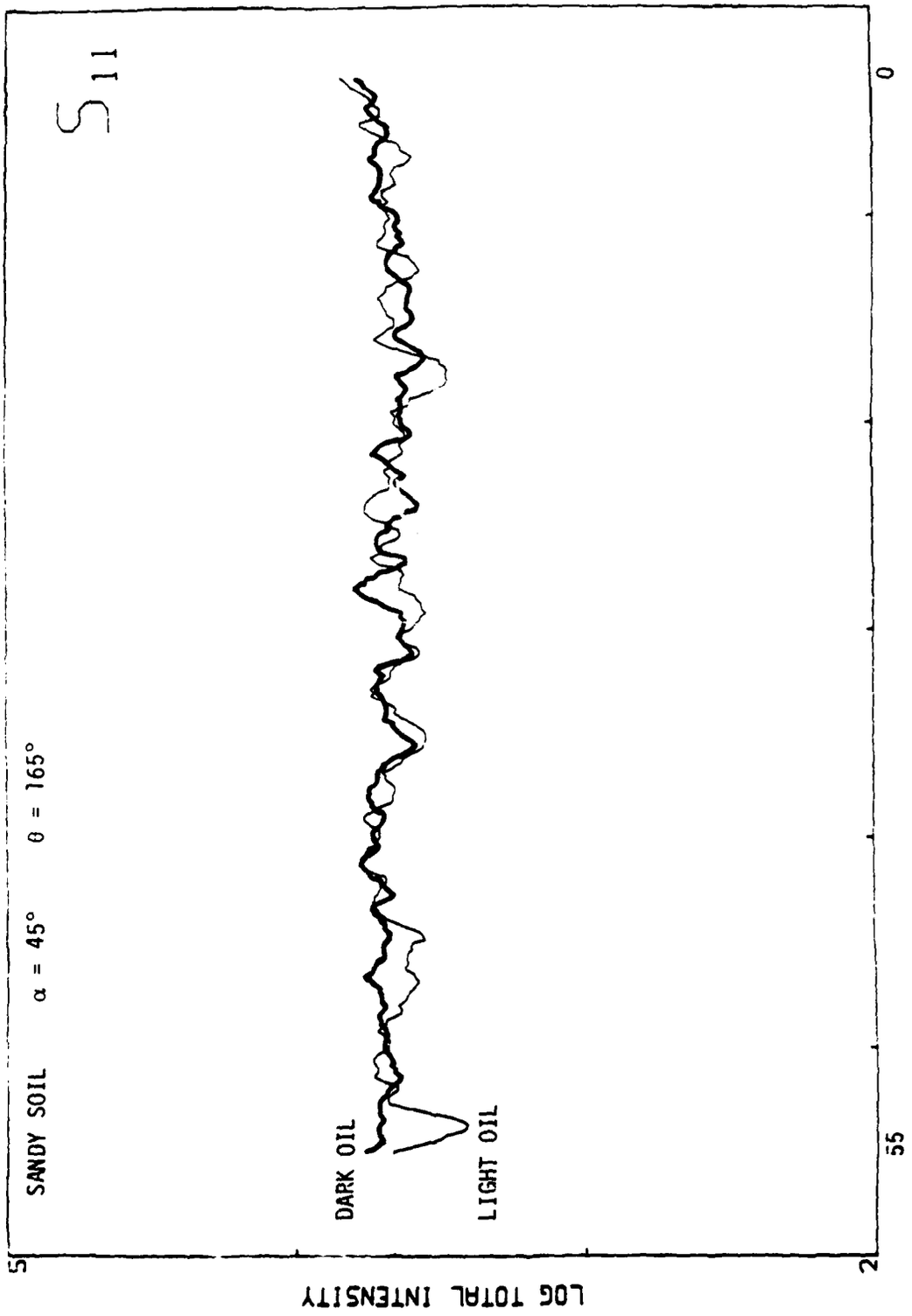

FIGURE 64. Backscatter of S_{11} for sandy soil as a function of oil thickness for light oil and dark oil.

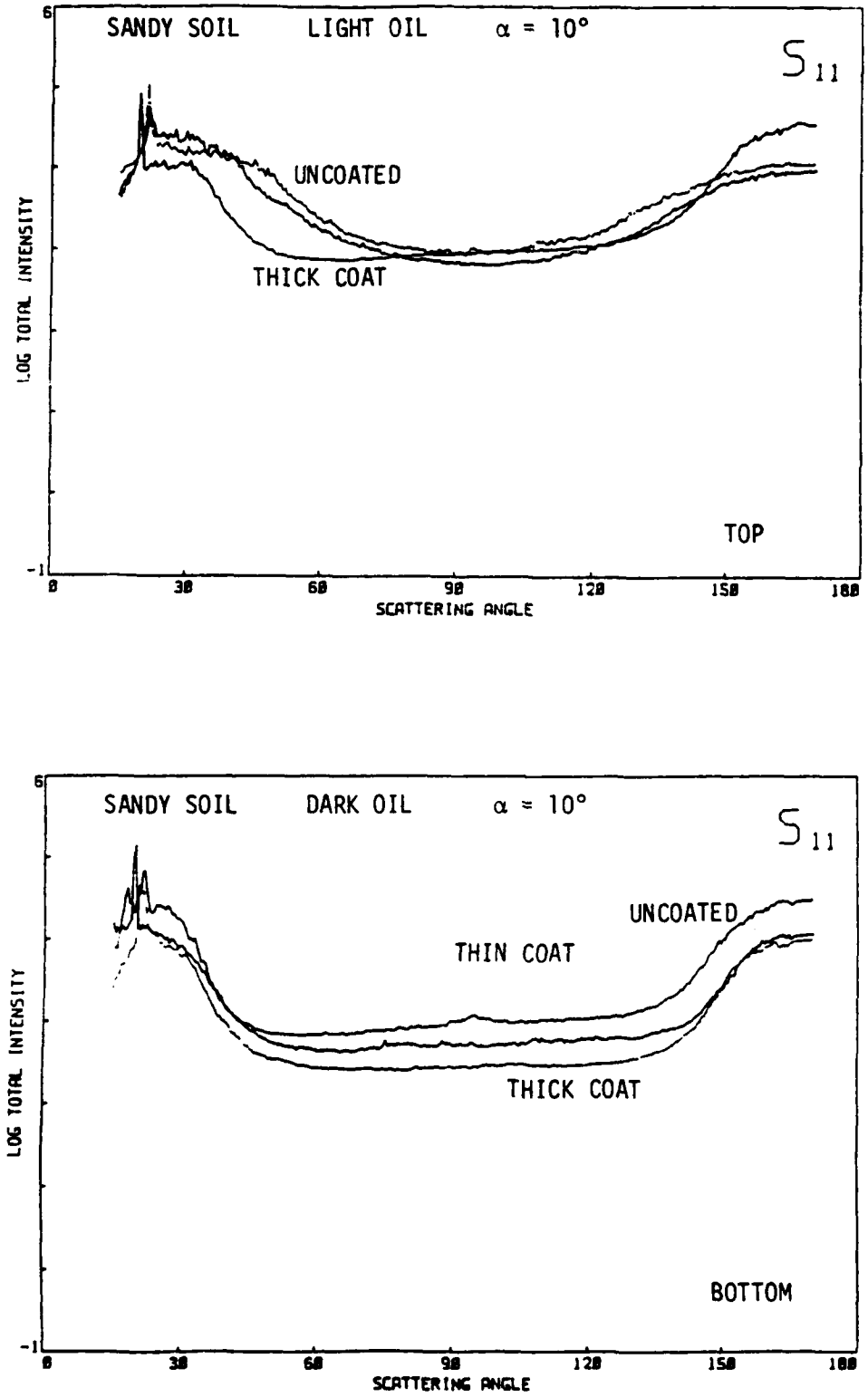

FIGURE 65. Matrix element S_{11} for sandy soil coated with three different thicknesses of light oil (TOP) and of dark oil (BOTTOM).

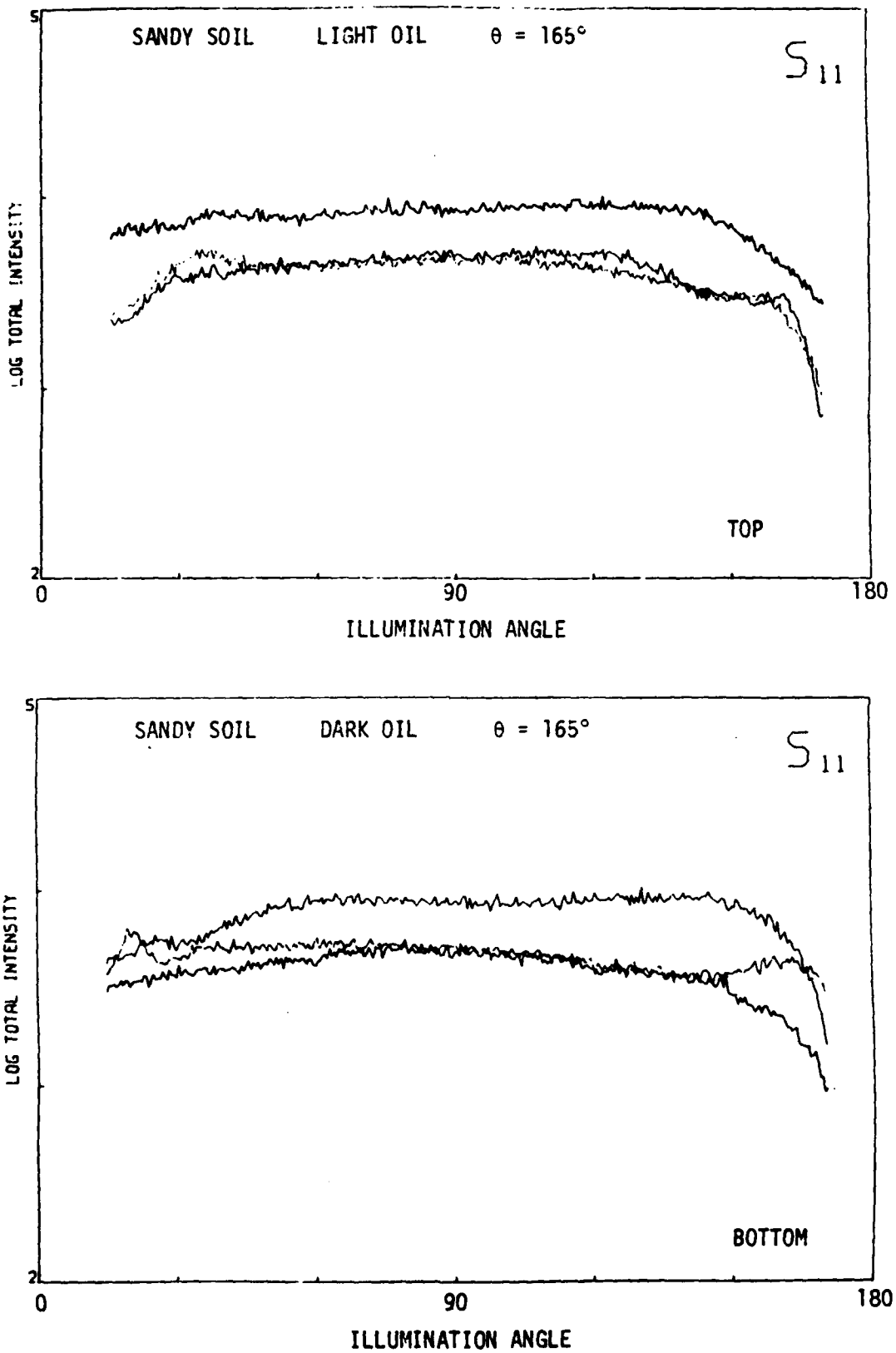

FIGURE 66. Backscatter of S_{11} for sandy soil coated with three different thicknesses of light oil (TOP) and of dark oil (BOTTOM).

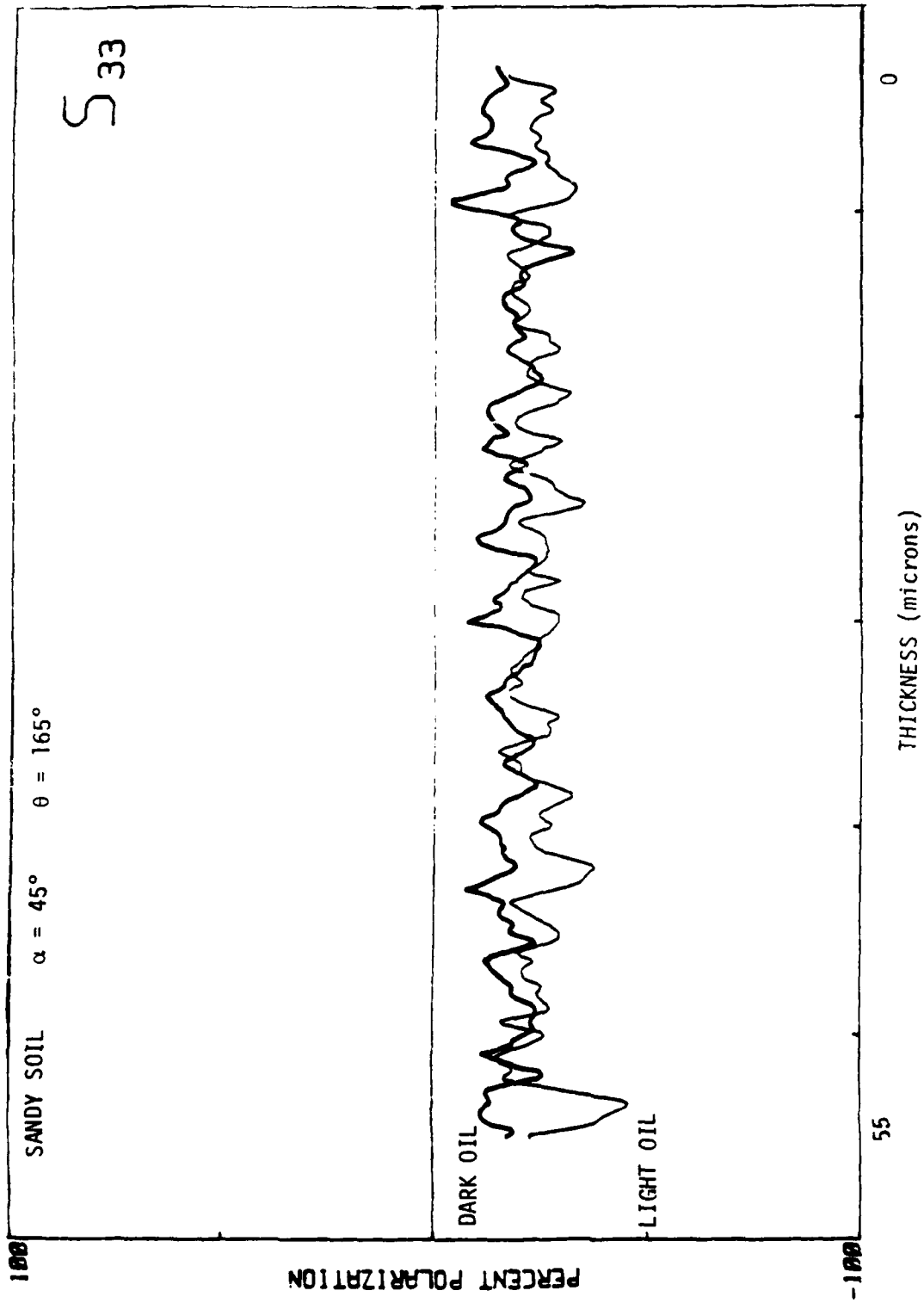

FIGURE 67. Backscatter of S_{33} for sandy soil as a function of oil thickness for light oil and dark oil.

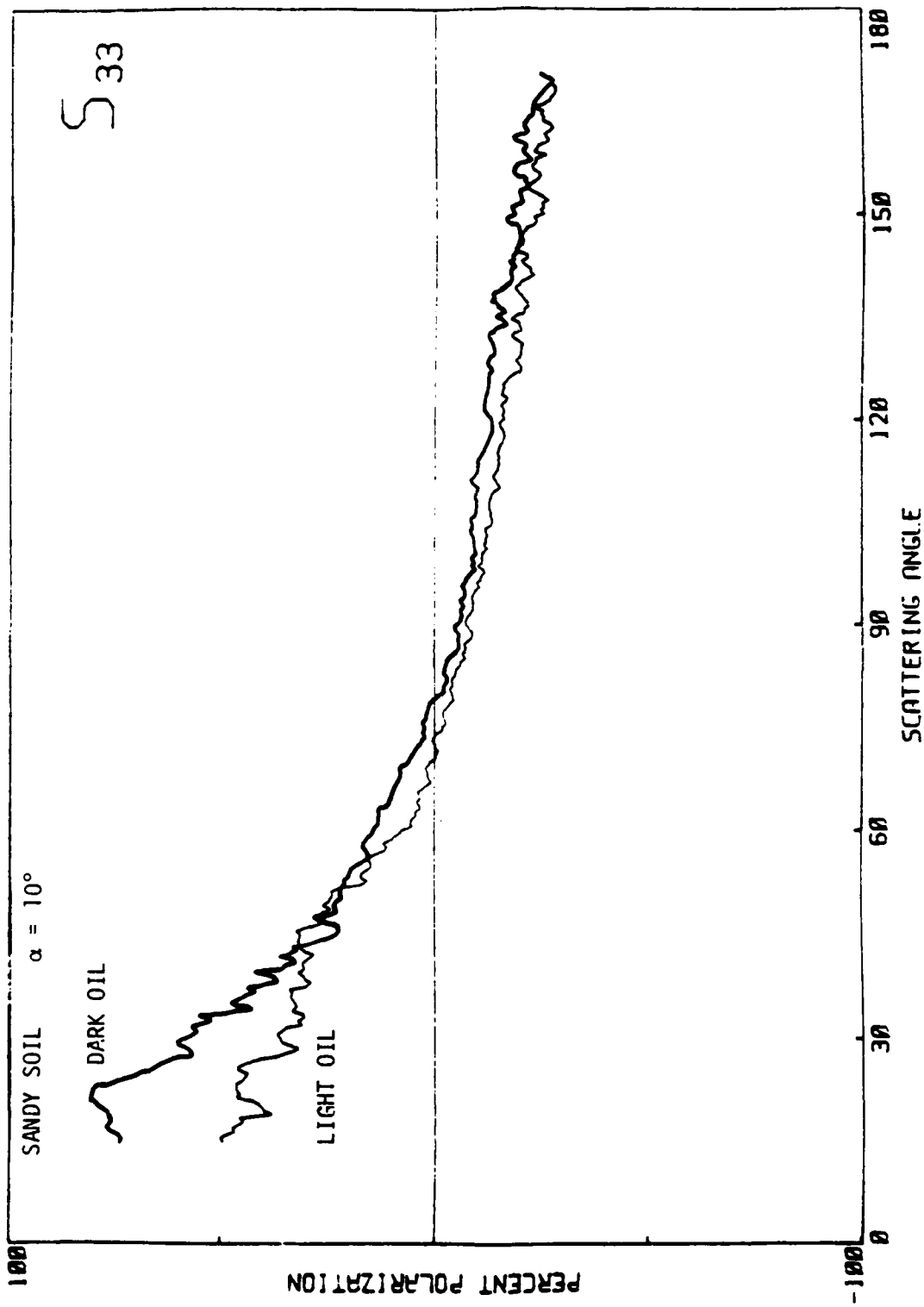

FIGURE 68. Matrix element S_{33} for sandy soil coated with light oil and with dark oil.

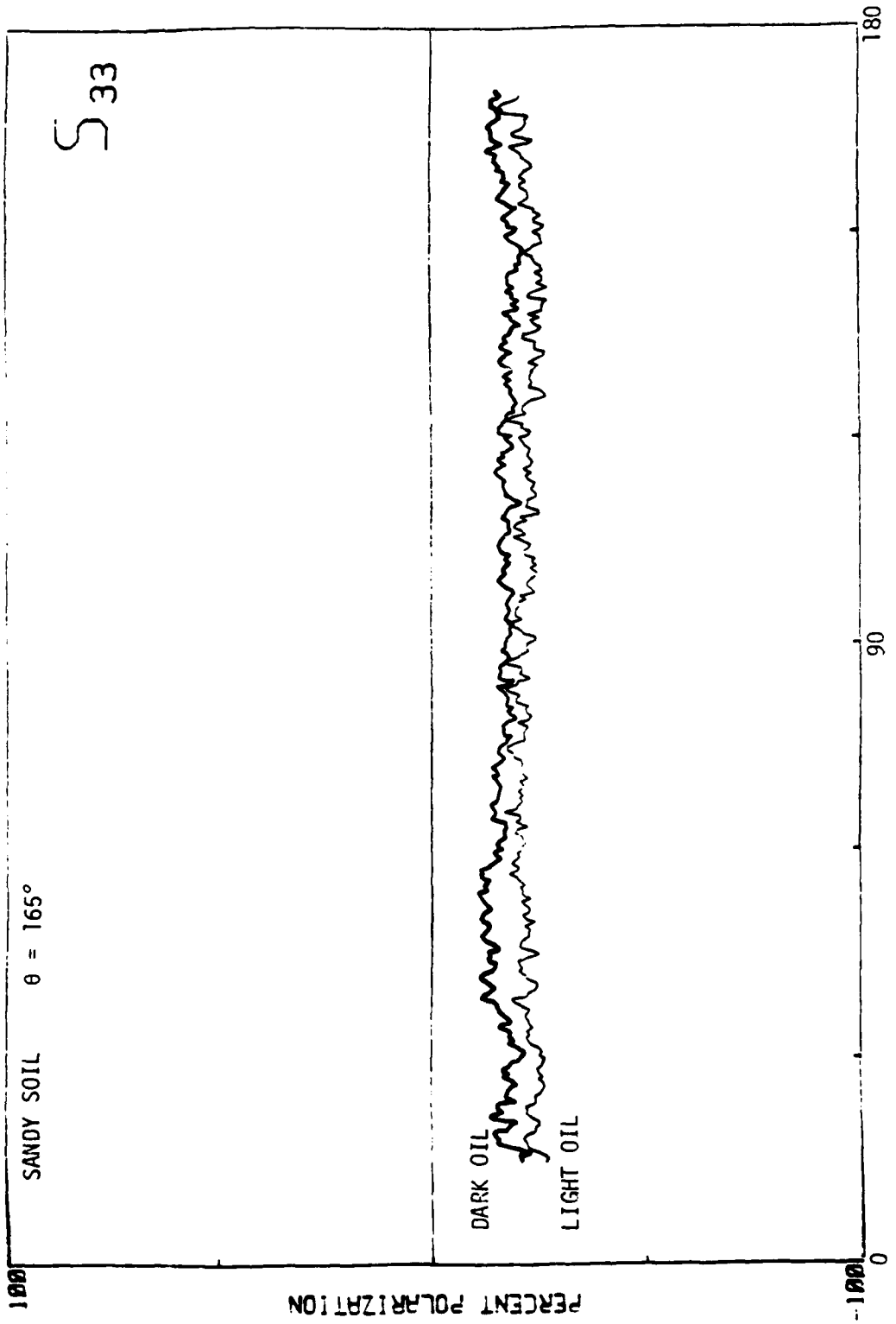

FIGURE 69. Backscatter of S_{33} for sandy soil coated with light oil and with dark oil.

17. CLAY-SOIL SURFACES: MATRIX ELEMENTS S_{11} AND S_{33} AND BACKSCATTER STUDIES OF SANDY-SOIL SURFACES COATED WITH LIGHT AND DARK OIL

This section shows the results of the five measurements on clay soil involving the matrix elements S_{11} and S_{33}. They are identical to the five measurements just described for sand.

1. $S_{ij}(\alpha = 45°, \theta = 165°)$ as a function of light and dark oil thickness.
2. Matrix element $S_{ij}(\theta)$ ($\alpha = 10°$) for three different thicknesses of light oil.
3. Matrix elements $S_{ij}(\theta)$ ($\alpha = 10°$) for three different thicknesses of dark oil.
4. Matrix element $S_{ij}(\alpha)$ ($\theta = 165°$) for three different thicknesses of light oil.
5. Matrix element $S_{ij}(\alpha)$ ($\theta = 165°$) for three different thicknesses of dark oil.

Figure 70 shows the backscatter of S_{11} ($\theta = 165°$, $\alpha = 45°$) as a function of thickness of the light and dark oils. The surface was prepared with a linear gradient oil thickness. In this case we show just one curve for the light and dark oils. For this surface (at these angles) the total intensity is unable to distinguish between light and dark oil coatings or thickness variations.

Figure 71 (TOP and BOTTOM) compares the $S_{11}(\theta)$ matrix elements at $\alpha = 10°$ for the three different thicknesses of light oil and dark oil, respectively. Figure 72 (TOP and BOTTOM) compares the $S_{11}(\alpha)$ matrix elements at $\theta = 165°$ for three different thicknesses of light oil and dark oil, respectively.

The data shown in Figures 71 and 72 were taken from separate clay-soil surfaces where each individual surface was coated to the indicated thickness of light and dark oil.

Figure 73 shows the backscatter value of S_{33} ($\theta = 165°$, $\alpha = 45°$) as a function of oil thickness for the light and dark oils. These data were taken from the same single sandy-soil surface prepared with a linear gradient thickness of light (or dark) oil, as described in Figure 58. The light oil gives a slightly more negative polarization than the dark oil; however, differences are not larger than the fluctuations due to surface roughness.

Figure 74 compares the $S_{33}(\theta)$ matrix element at $\alpha = 10°$ for light oil and dark oil, respectively.

Figure 75 compares the $S_{33}(\alpha)$ matrix elements at $\theta = 165°$ for the light oil and dark oil, respectively.

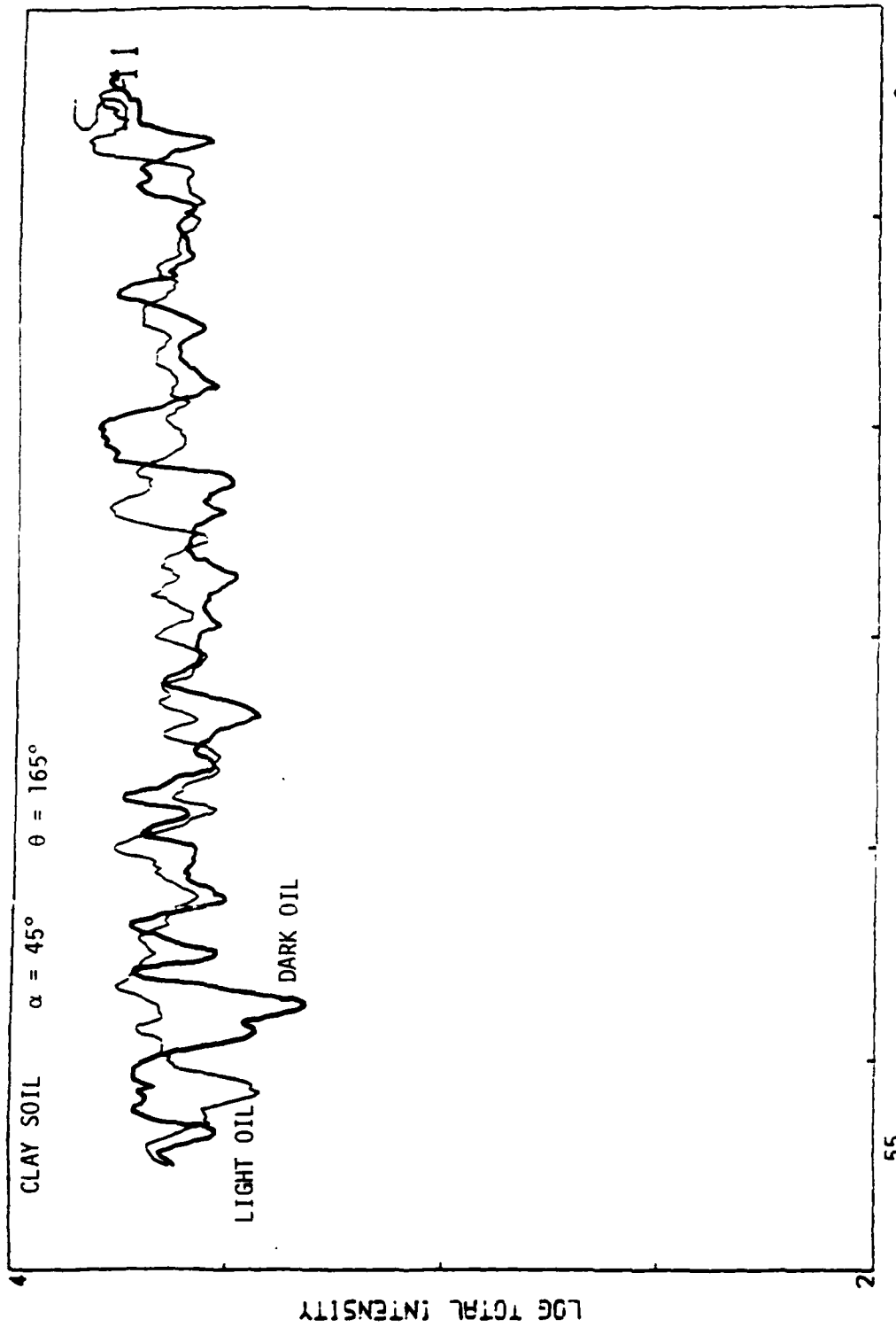

FIGURE 70. Backscatter of S_{11} for clay soil as a function of oil thickness for light oil and dark oil.

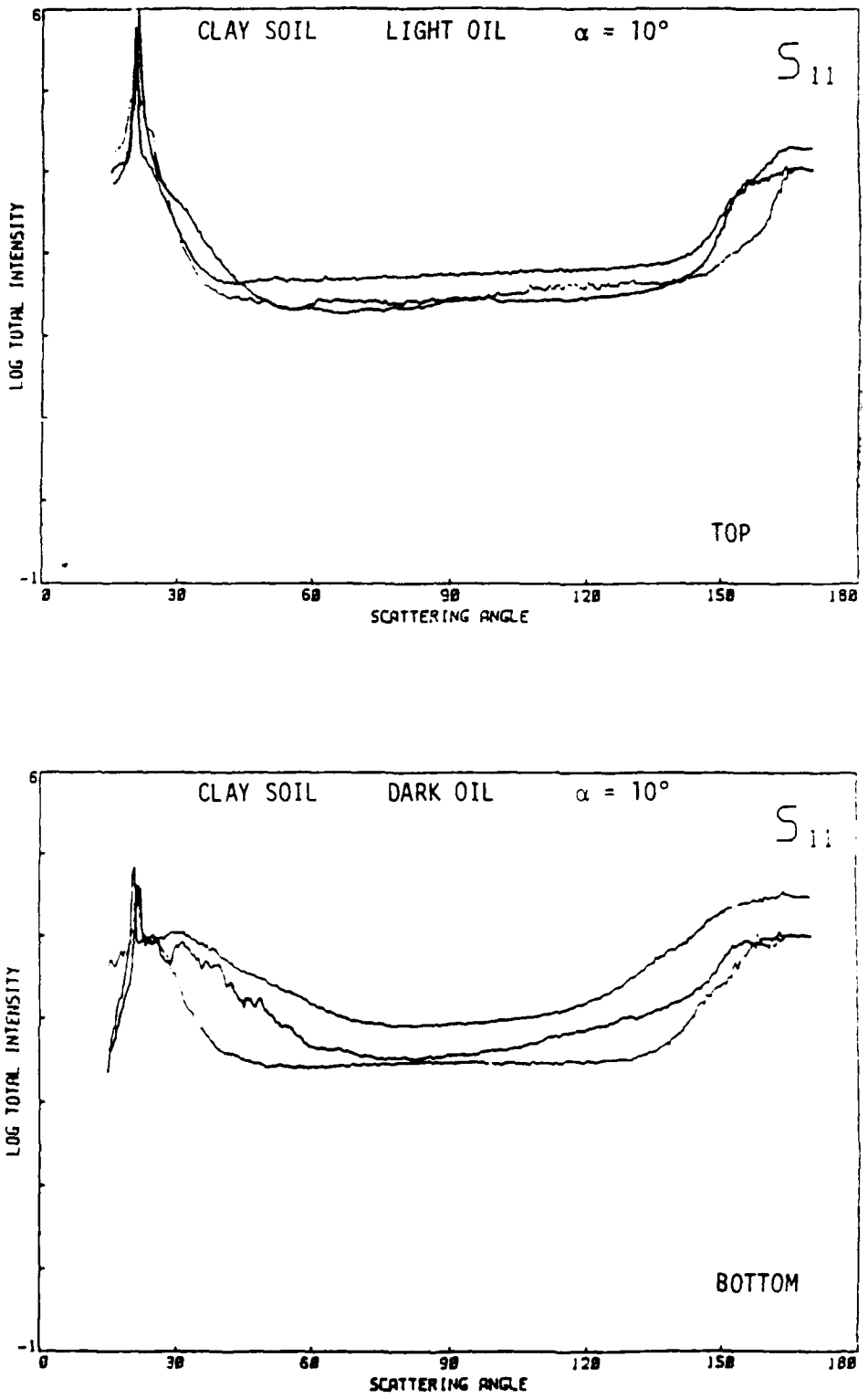

FIGURE 71. Matrix element S_{11} for clay soil coated with three different thicknesses of light oil (TOP) and of dark oil (BOTTOM).

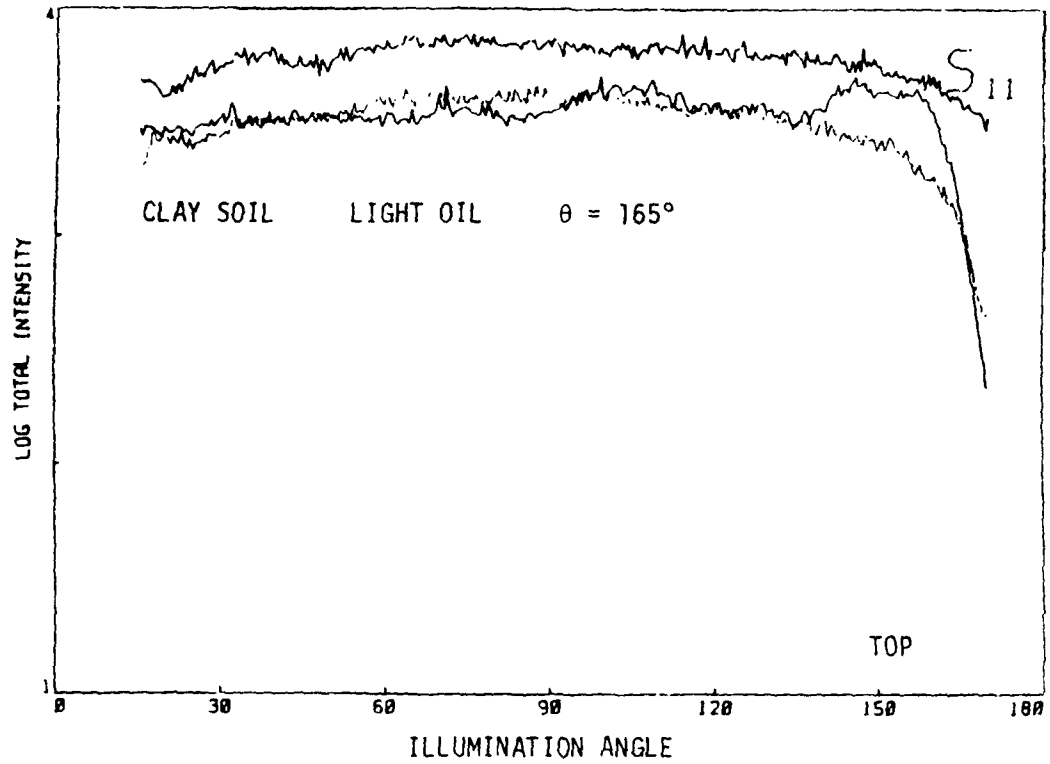

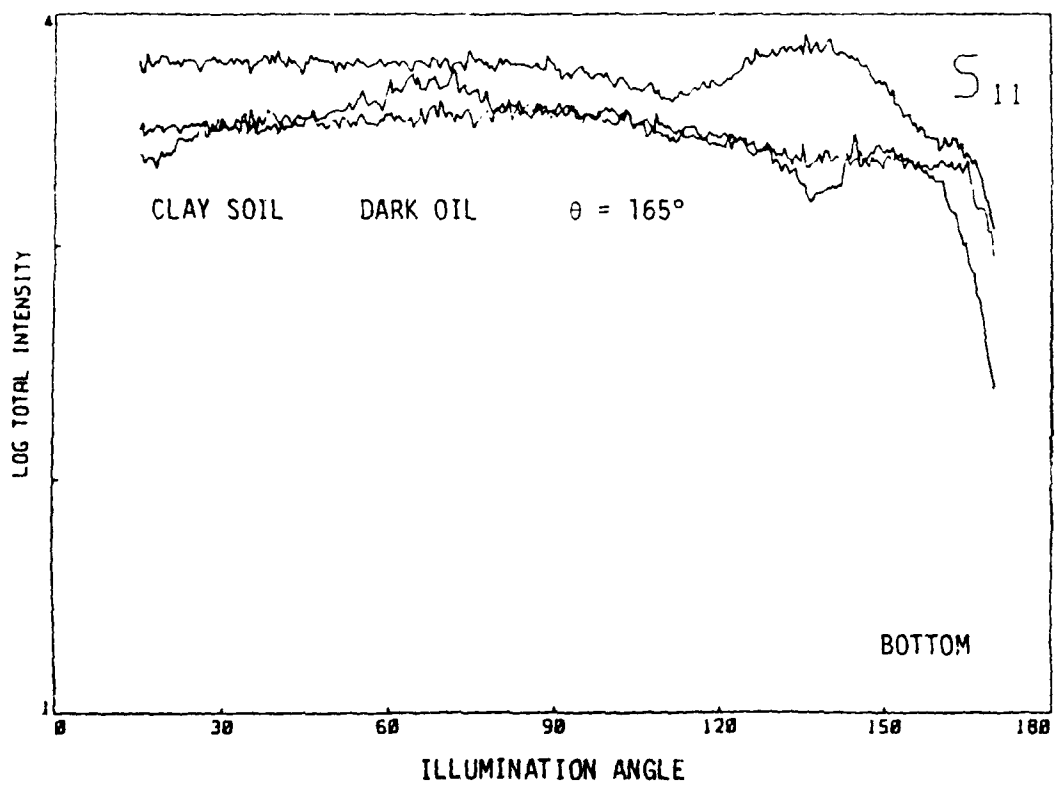

FIGURE 72. Backscatter of S_{11} for clay soil coated with three different thicknesses of light oil (TOP) and of dark oil (BOTTOM).

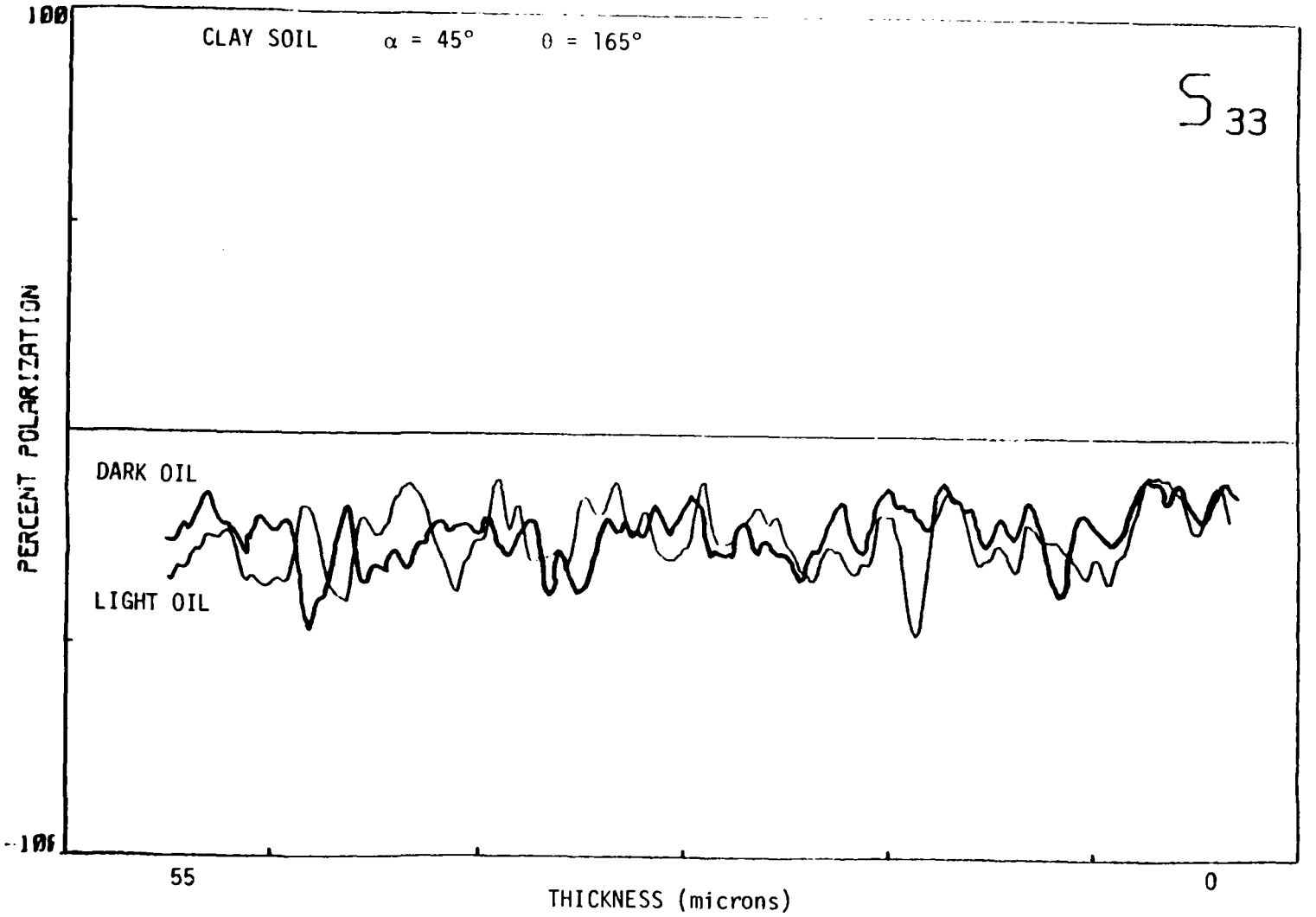

FIGURE 73. Backscatter of S_{33} for clay soil as a function of oil thickness for light oil and dark oil.

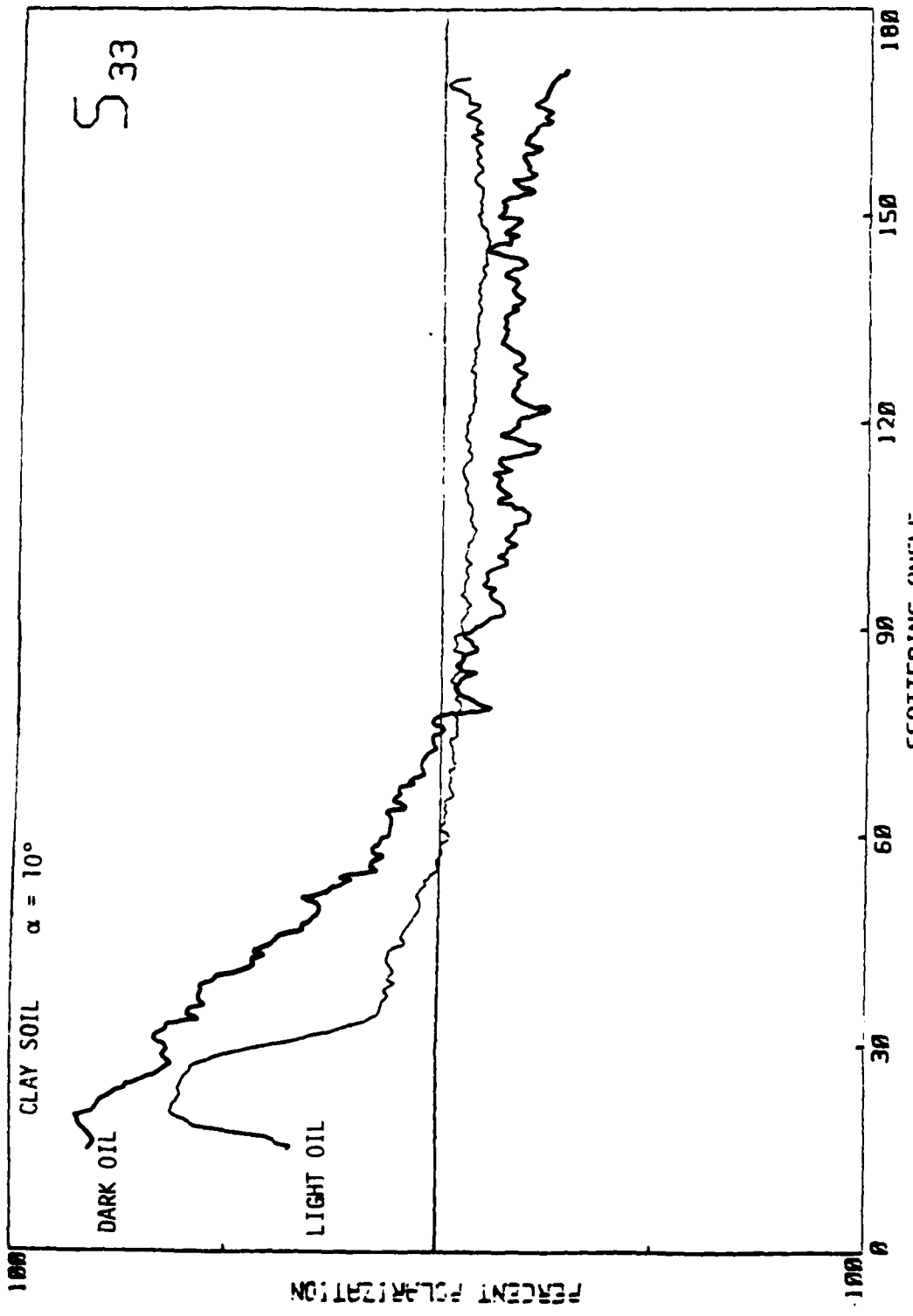

FIGURE 74. Matrix element S_{33} for clay soil coated with light oil and with dark oil.

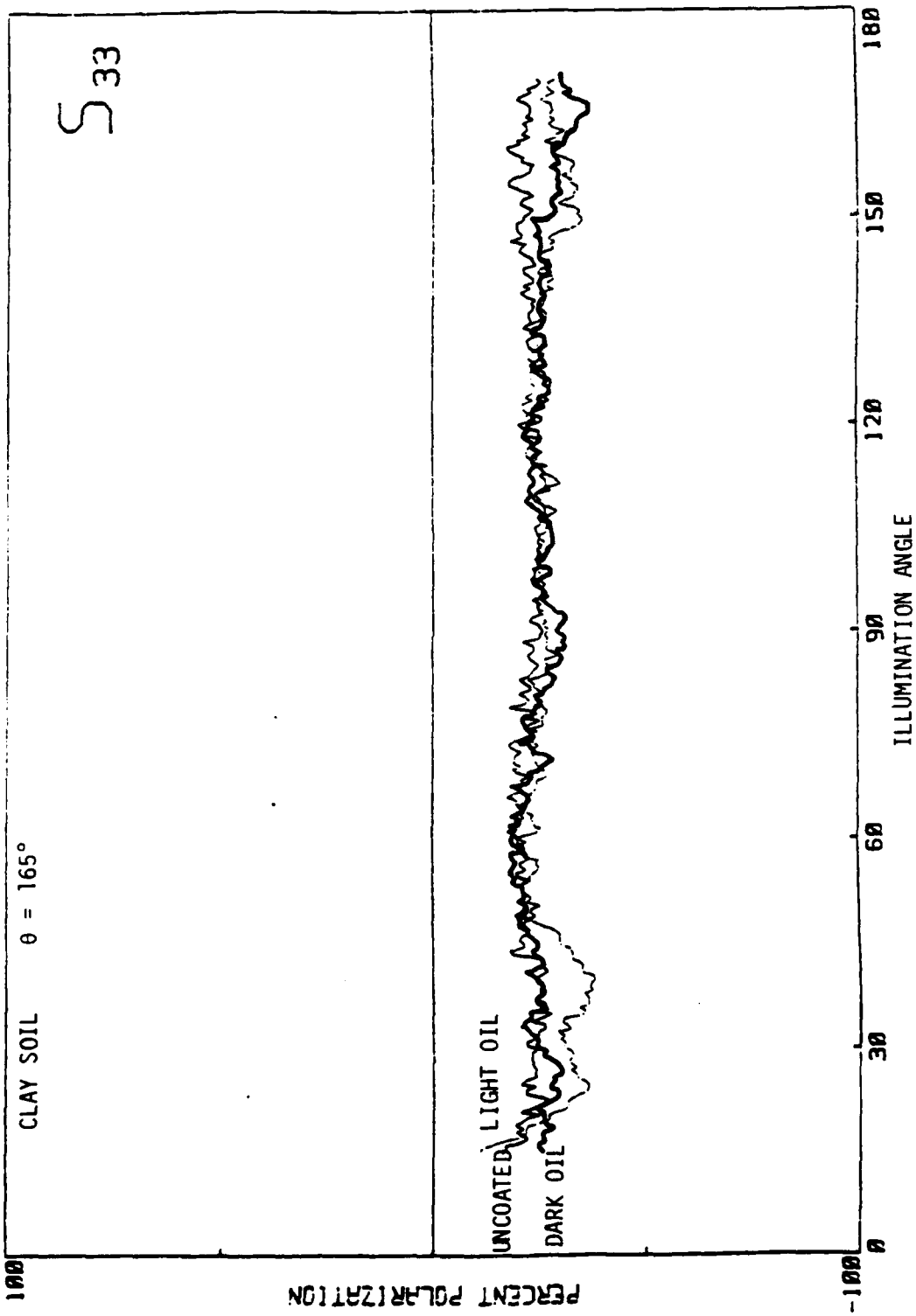

FIGURE 75. Backscatter of S_{33} for clay soil coated with light oil and with dark oil.

18. LOAMY-SOIL SURFACES: MATRIX ELEMENTS S_{11} AND S_{33} AND BACKSCATTER STUDIES OF SANDY-SOIL SURFACES COATED WITH LIGHT AND DARK OIL

This section shows the results of the five measurements on loamy soil involving the matrix elements S_{11} and S_{33}. They are identical to the five measurements just described for sand.

1. $S_{ij}(\alpha = 45^\circ, \theta = 165^\circ)$ as a function of light and dark oil thickness.
2. Matrix elements $S_{ij}(\theta)$ ($\alpha = 10^\circ$) for three different thicknesses of light oil.
3. Matrix elements $S_{ij}(\theta)$ ($\alpha = 10^\circ$) for three different thicknesses of dark oil.
4. Matrix elements $S_{ij}(\alpha)$ ($\theta = 165^\circ$) for three different thicknesses of light oil.
5. Matrix element $S_{ij}(\alpha)$ ($\theta = 165^\circ$) for three different thicknesses of dark oil.

Figure 76 shows the backscatter of S_{11} ($\theta = 165^\circ$, $\alpha = 45^\circ$) as a function of thickness of the light and dark oils. The surface was prepared with a linear gradient oil thickness. In this case we show just one curve for the light and dark oils. For this surface (at these angles) the total intensity is unable to distinguish between light and dark oil coatings or thickness variations.

Figure 77 (TOP and BOTTOM) compares the $S_{11}(\theta)$ matrix elements at $\alpha = 10^\circ$ for the three different thicknesses of light oil and dark oil, respectively. Figure 78 (TOP and BOTTOM) compares the $S_{11}(\alpha)$ matrix elements at $\theta = 165^\circ$ for three different thicknesses of light oil and dark oil, respectively.

The data shown in Figures 77 and 78 were taken from separate loamy-soil surfaces -- each individual surface was coated to the indicated thickness of light and dark oil.

Figure 79 shows the backscatter value of S_{33} ($\theta = 165^\circ$, $\alpha = 45^\circ$) as a function of oil thickness for the light and dark oils. These data were taken from the same single sandy-soil surface prepared with a linear gradient thickness of light (or dark) oil as described in Figure 58. The light oil gives a slightly more negative polarization than the dark oil; however, differences are not larger than the fluctuations due to surface roughness.

Figure 80 compares the $S_{33}(\theta)$ matrix element at $\alpha = 10^\circ$ for light oil and dark oil, respectively.

Figure 81 compares the $S_{33}(\alpha)$ matrix elements at $\theta = 165^\circ$ for the light oil and dark oil, respectively.

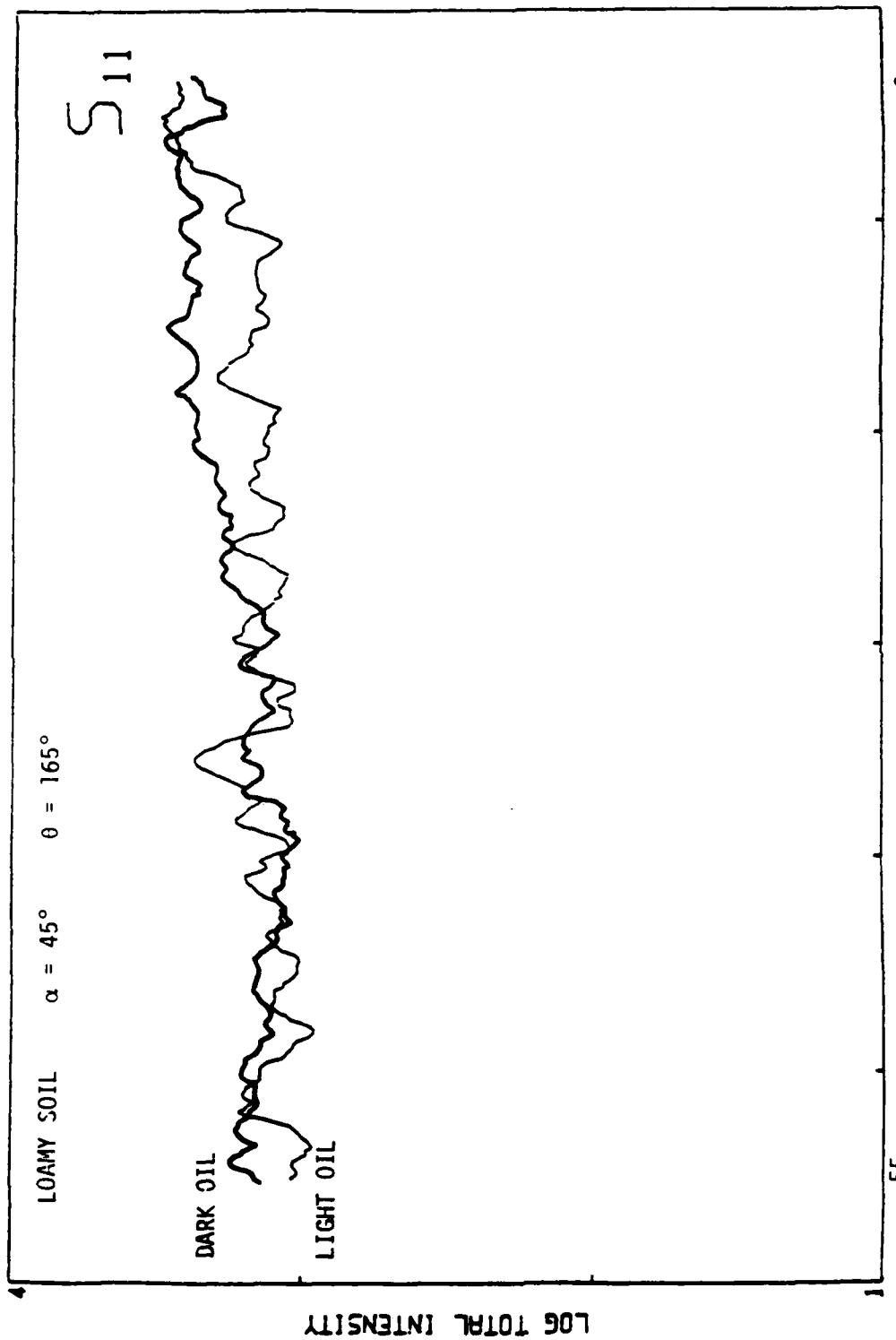

FIGURE 76. Backscatter of S_{11} for loamy soil as a function of oil thickness for light oil and dark oil.

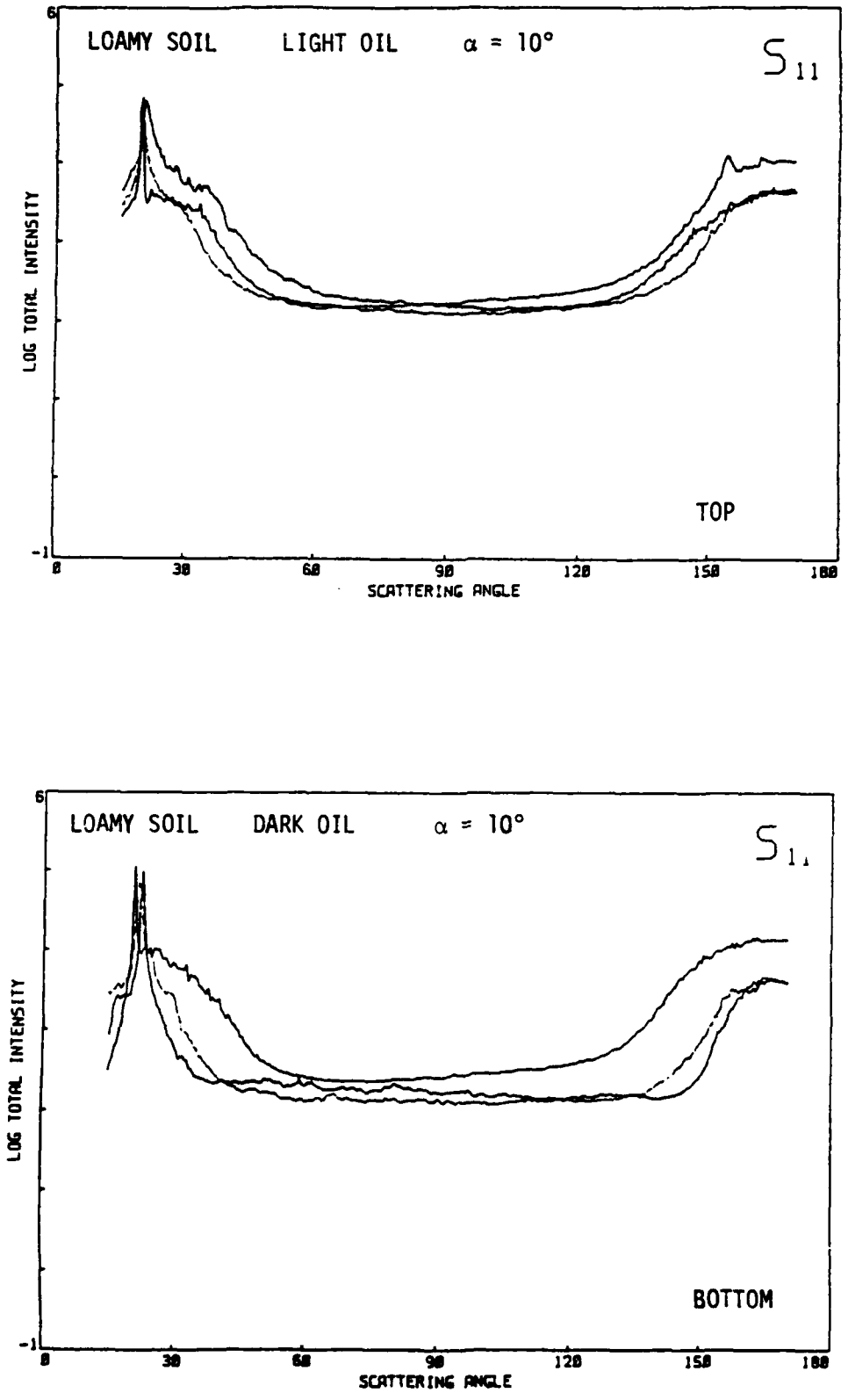

FIGURE 77. Matrix element S_{11} for loamy soil coated with three different thicknesses of light oil (TOP) and of dark oil (BOTTOM).

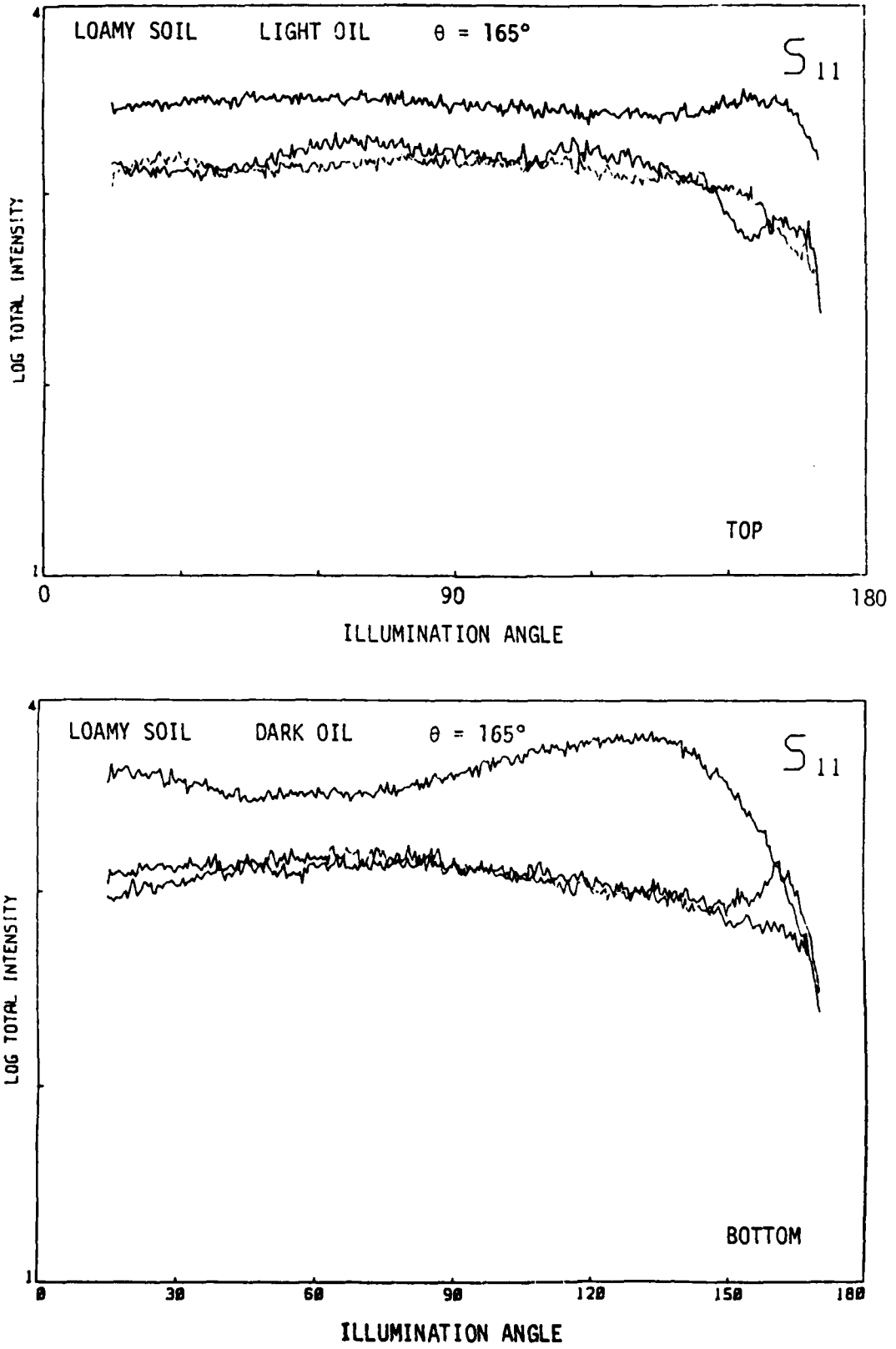

FIGURE 78. Backscatter of S_{11} for loamy soil coated with three different thicknesses of light oil (TOP) and of dark oil (BOTTOM).

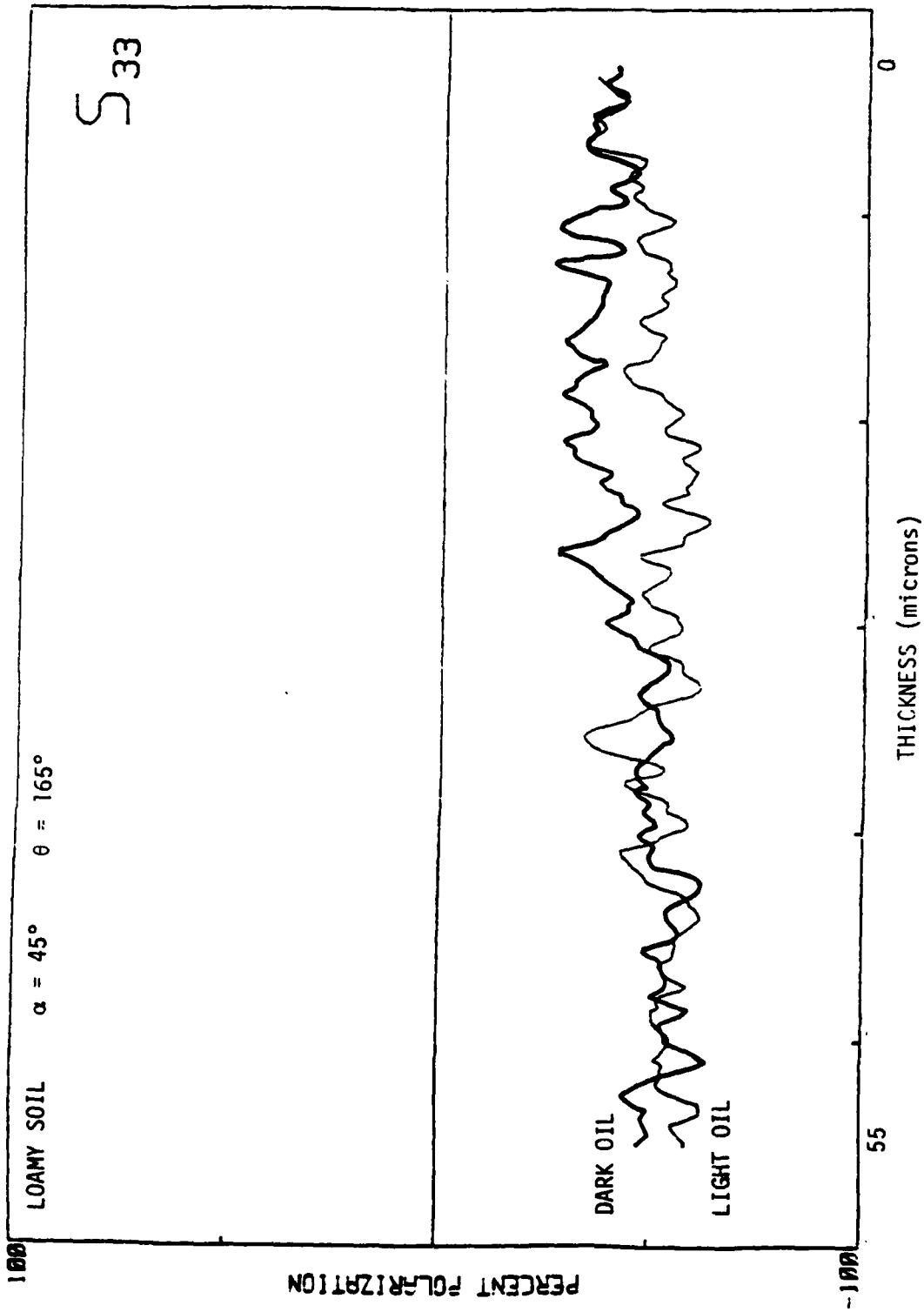

FIGURE 79. Backscatter of S_{33} for loamy soil as a function of oil thickness for light oil and dark oil.

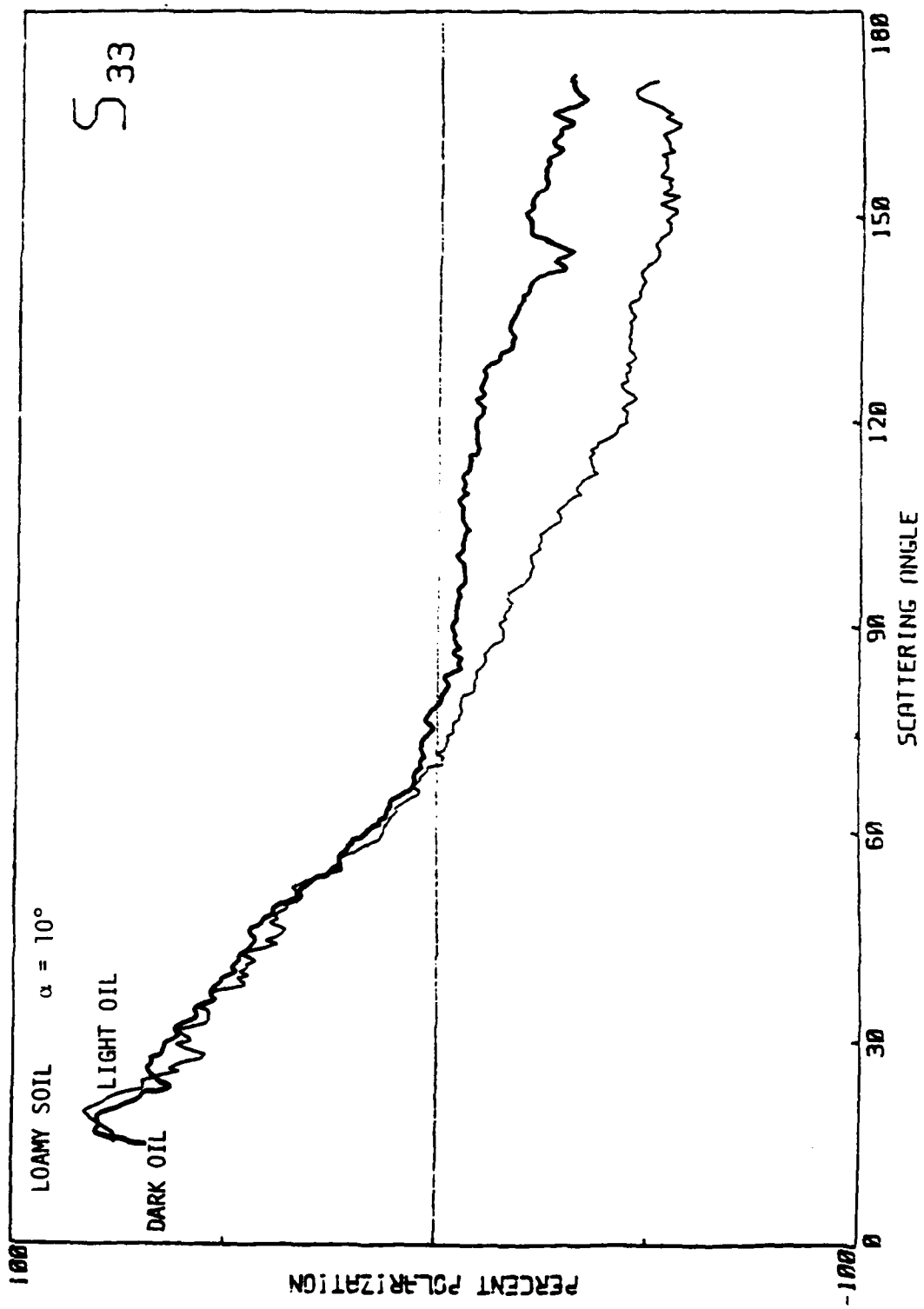

FIGURE 80. Matrix element S_{33} for loamy soil coated with light oil and with dark oil.

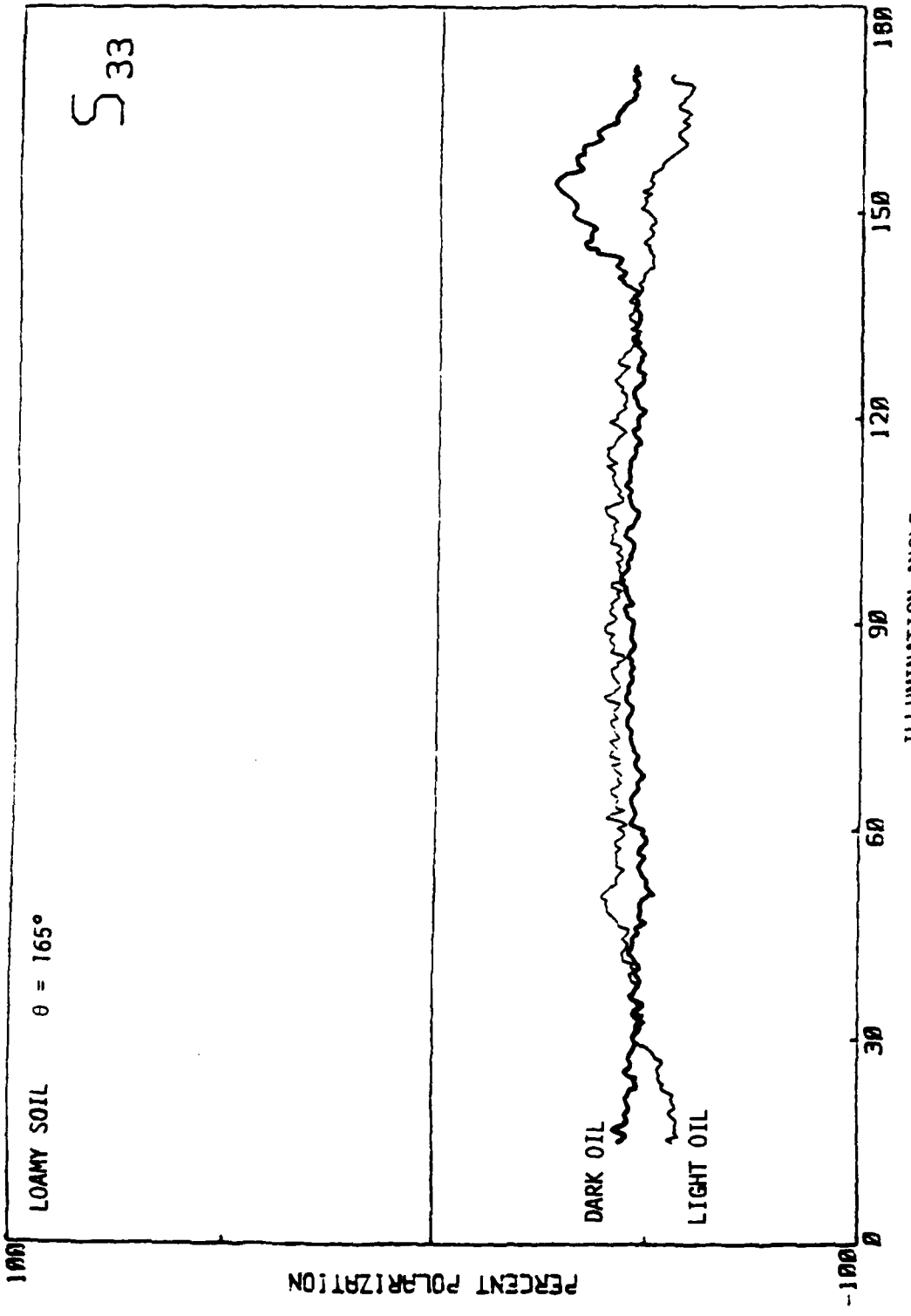

FIGURE 81. Backscatter of S_{33} for loamy soil coated with light oil and with dark oil.

19. MATRIX ELEMENTS S_{11} AND S_{33} AT λ4416 Å AS A FUNCTION OF ILLUMINATION ANGLE AND SCATTERING ANGLE FOR THE FOUR SOILS UNCOATED AND COATED WITH DARK OIL

This section shows the light-scattering signals for the four soil surfaces coated with dark (absorbing) oil illuminated with the He-Cd laser light at λ4416 Å Signals obtained from the dark oil coated surfaces are compared to the ones obtained from the uncoated surface. The following measurements were made on the four soils:

1. The matrix element $S_{11}(\theta)$ (α = 10°). These are shown in Figures 82 and 83.

2. The backscatter signals $S_{11}(\alpha)$ (θ = 165°). These are shown in Figures 84 and 85.

3. The matrix element $S_{33}(\theta)$ (α = 10°). These are shown in Figures 86 and 87.

4. The backscatter signals $S_{33}(\alpha)$ (θ = 165°). These are shown in Figures 88 and 89.

Figures 82 and 83 show that the total scattered intensity $S_{11}(\theta)$ from the dark oil coated surface is less than S_{11} for the uncoated surface. This is especially true in the backscatter where θ > 115 . However the dark oil coated surfaces scatter more into the forward direction except for the loamy soil. This is shown in Figures 82 (TOP and BOTTOM) and 83 (BOTTOM).

Figures 84 and 85 show that the backscatter signal $S_{11}(\ )$ from the dark oil coated surface is less than the uncoated surface for all illumination angles and all soil surfaces. The small signal differences between the uncoated and coated clay soil (Figure 83, BOTTOM, and Figure 85, BOTTOM) are not .gnificant.

Figures 86 and 87 show the $S_{33}(\theta)$ matrix elements for the uncoated and dark oil coated four soils. In the forward scatter the dark oil coated surface has the larger positive polarization. The curves cross near θ = 60° (in the forward scatter). In the backscatter the dark oil coated surface has the largest negative polarization. This is true for all four soils.

Figures 88 and 89 show the backscatter matrix element $S_{33}(\alpha)$ for the uncoated and dark oil coated four soils. For all four soils, the dark oil coated surfaces give larger negative polarizations.

The S_{33} signals from dark oil and uncoated clay soil surfaces are not significantly different from the S_{33} signals from the other soil surfaces. This is not the case for the S_{11} signals shown in Figures 83 (BOTTOM) and 85 (BOTTOM).

These curves compare remarkably well with those in Chapter 14 which were obtained from the four different soil surfaces coated with black (opaque) paint. Comparing corresponding matrix elements shows that there is little difference between the scattering properties of a black paint coated surface and one coated with an absorbing oil. This suggests that the role of surface absorption and scattering is independent of the nature of the coating on the surface and that the absorption coefficient is a relavent parameter. The curves in this chapter were taken from dark oil coated surfaces illuminated with He-Cd laser radiation at λ4416 Å The absorption coefficient for dark oil at this wavelength is significently higher then it is for the He-Ne laser radiation at λ6328 Å The curves in chapters 15, 16, 17 and 18 were taken from light oil and dark oil coated surfaces illuminated with λ6328 Å radiation. They show that low absorbing oil coatings have little effect on the scattered light.

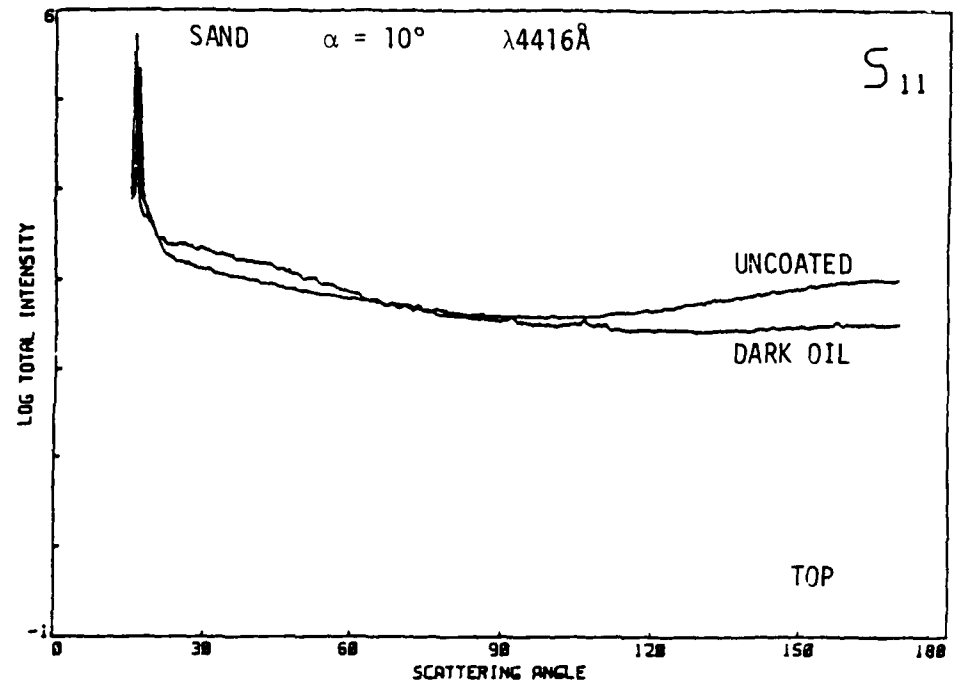

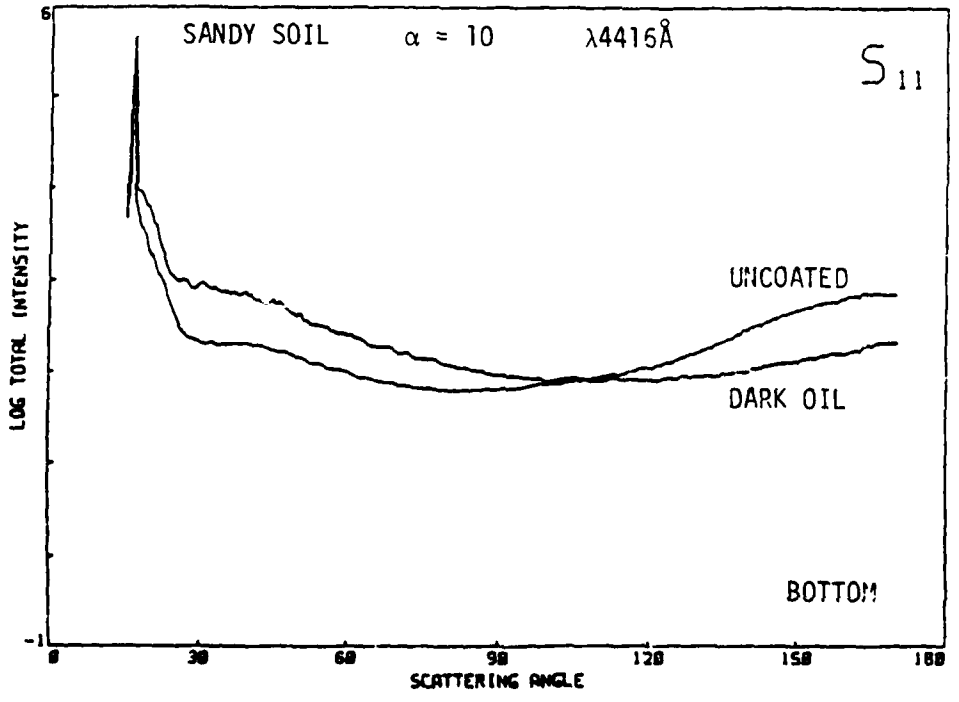

FIGURE 82. Matrix element S_{11} for uncoated and dark oil coated surfaces. Sand (TOP); Sandy soil (BOTTOM).

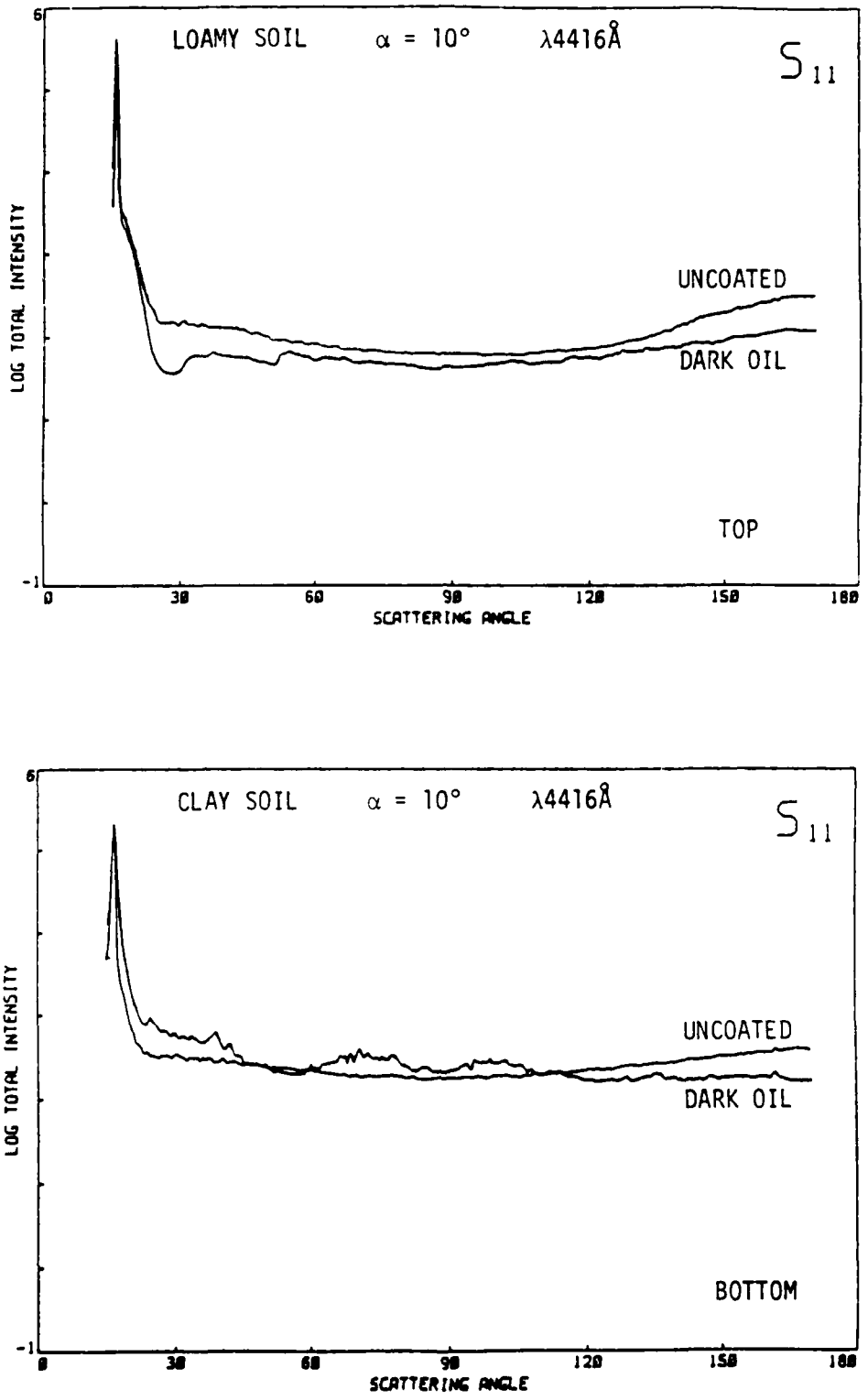

FIGURE 83. Matrix element S_{11} for uncoated and dark oil coated surfaces. Loamy soil (TOP); Clay soil (BOTTOM).

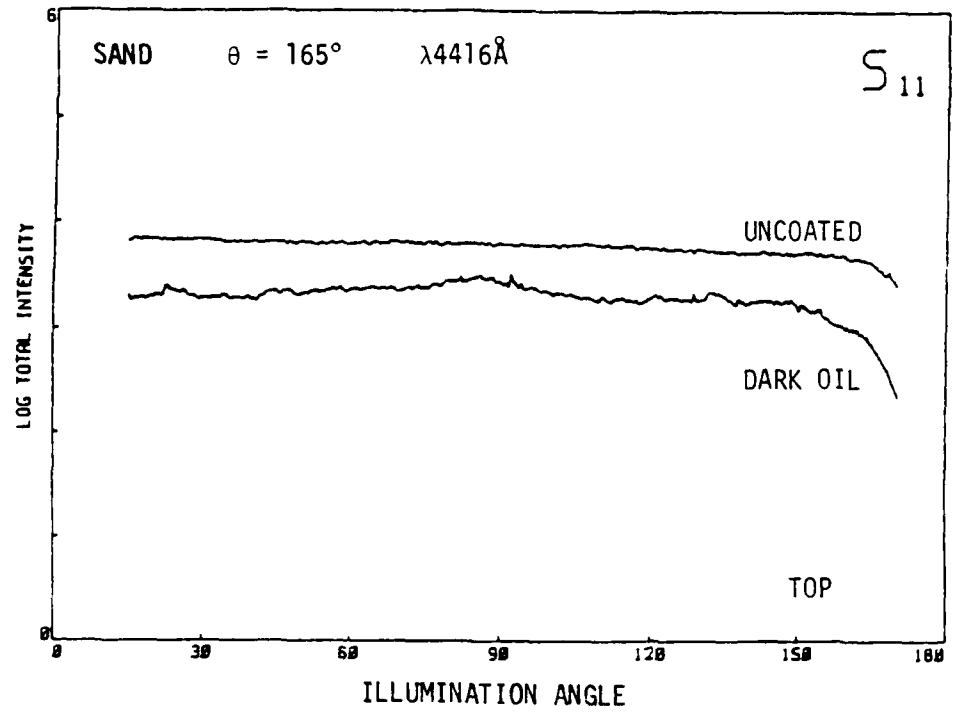

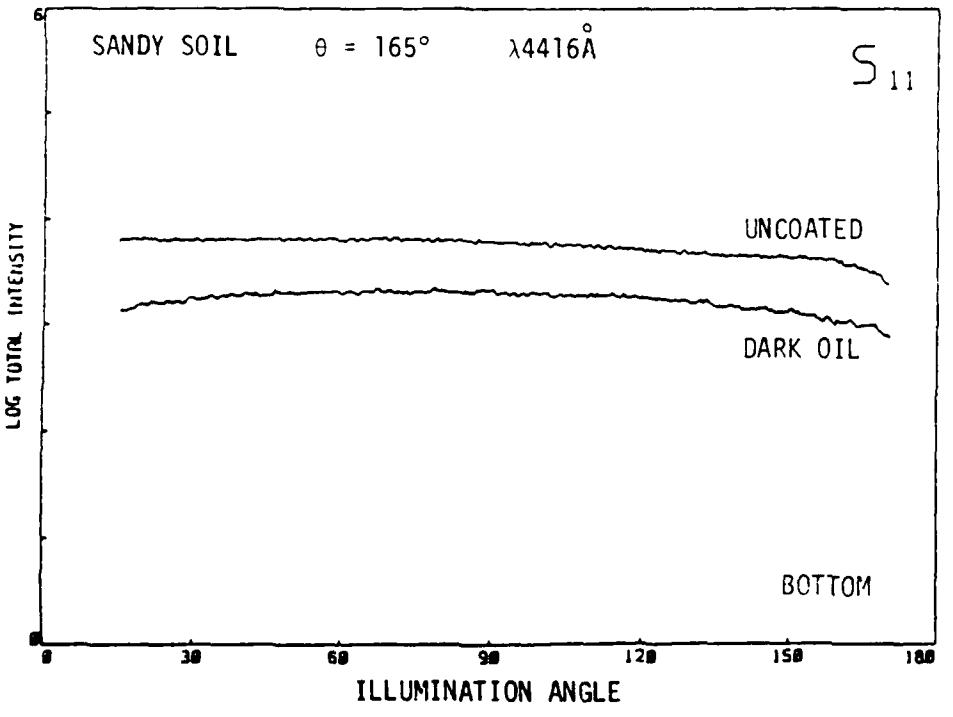

FIGURE 84. The backscatter matrix element S_{11} for uncoated and dark oil coated surfaces. Sand (TOP); Sandy soil (BOTTOM).

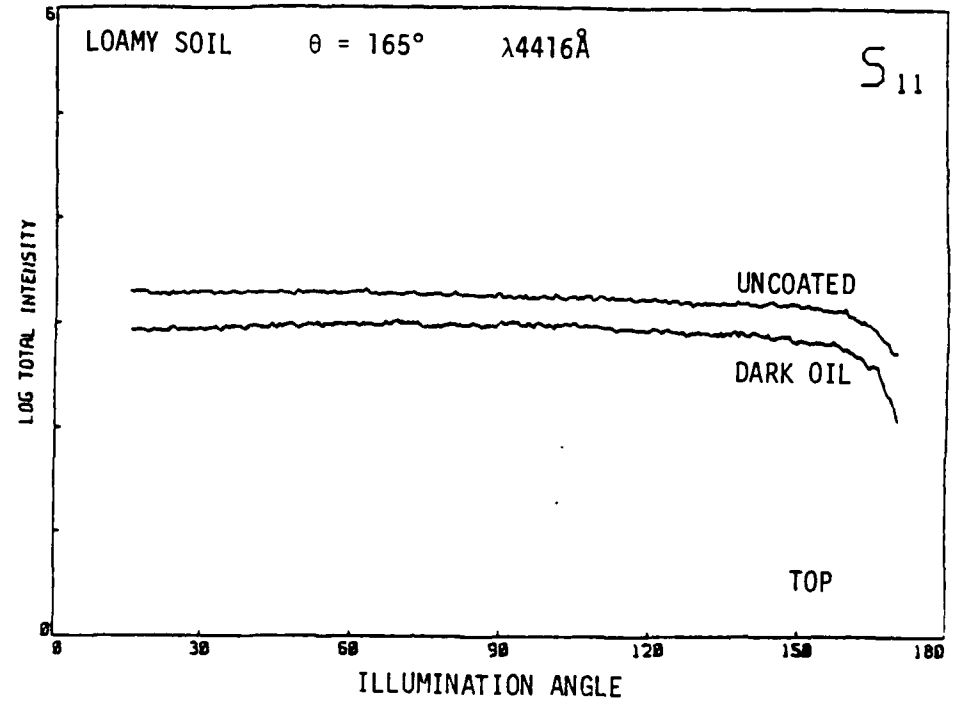

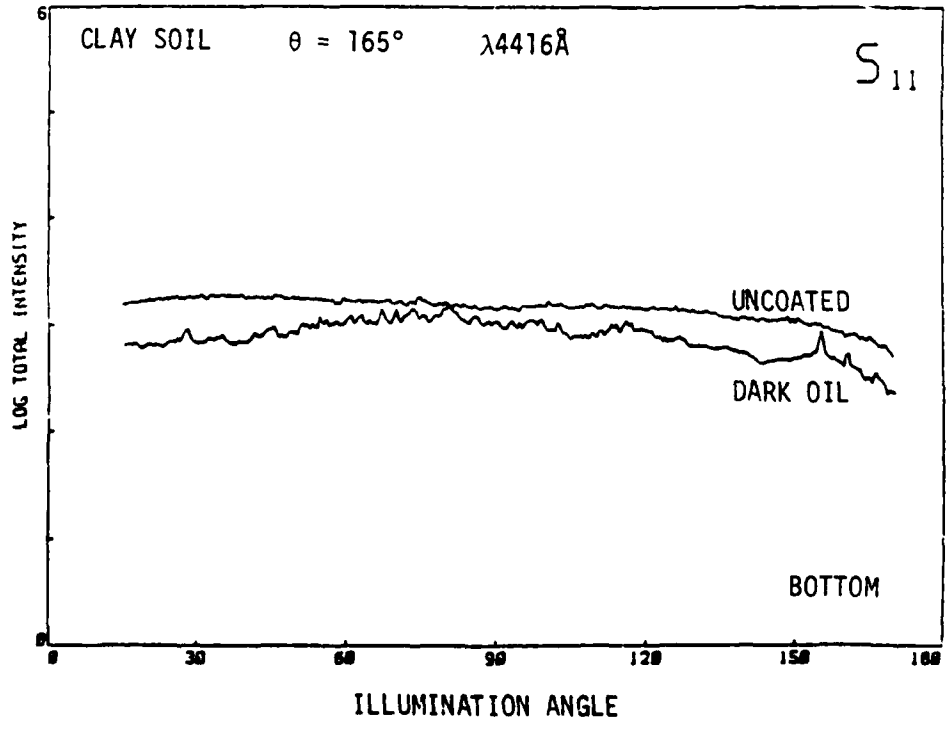

FIGURE 85. The backscatter matrix element S_{11} for uncoated and dark oil coated surfaces. Loamy soil (TOP); Clay soil (BOTTOM).

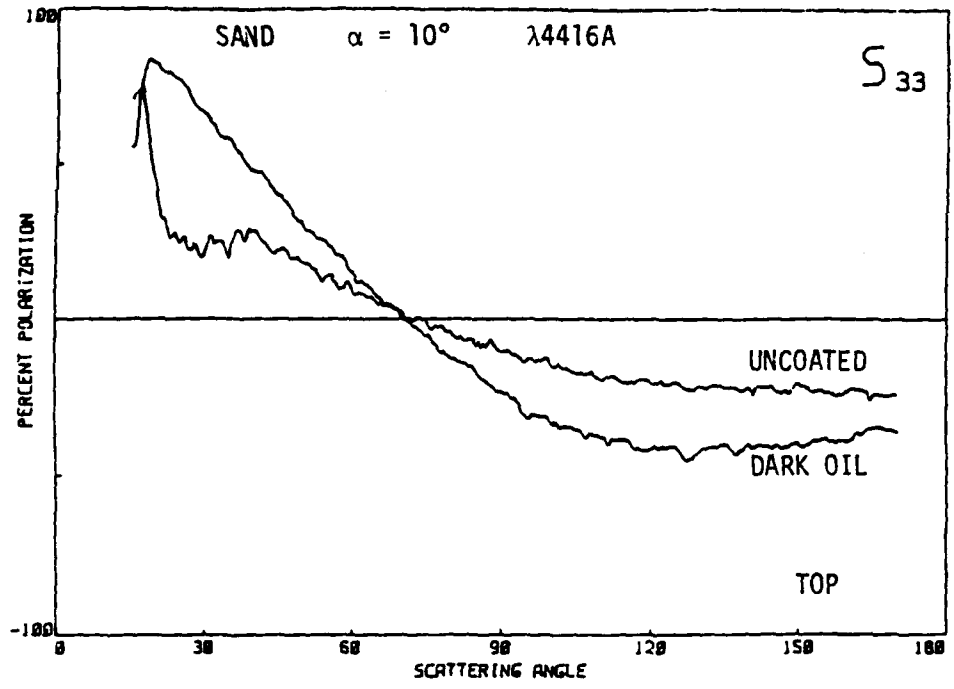

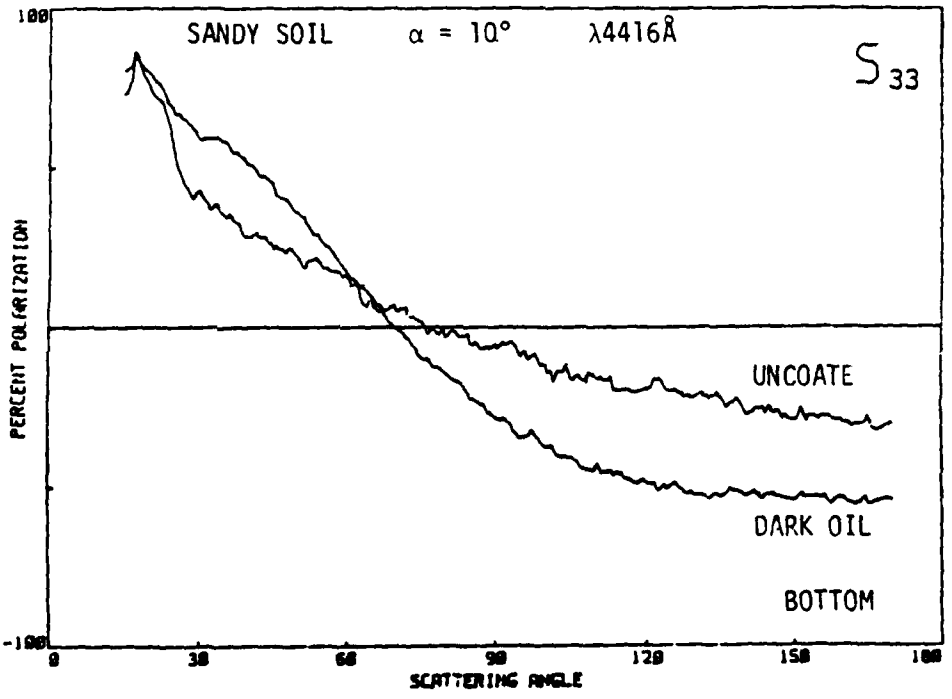

FIGURE 86. Matrix element S_{33} for uncoated and dark oil coated surfaces. Sand (TOP); Sandy soil (BOTTOM).

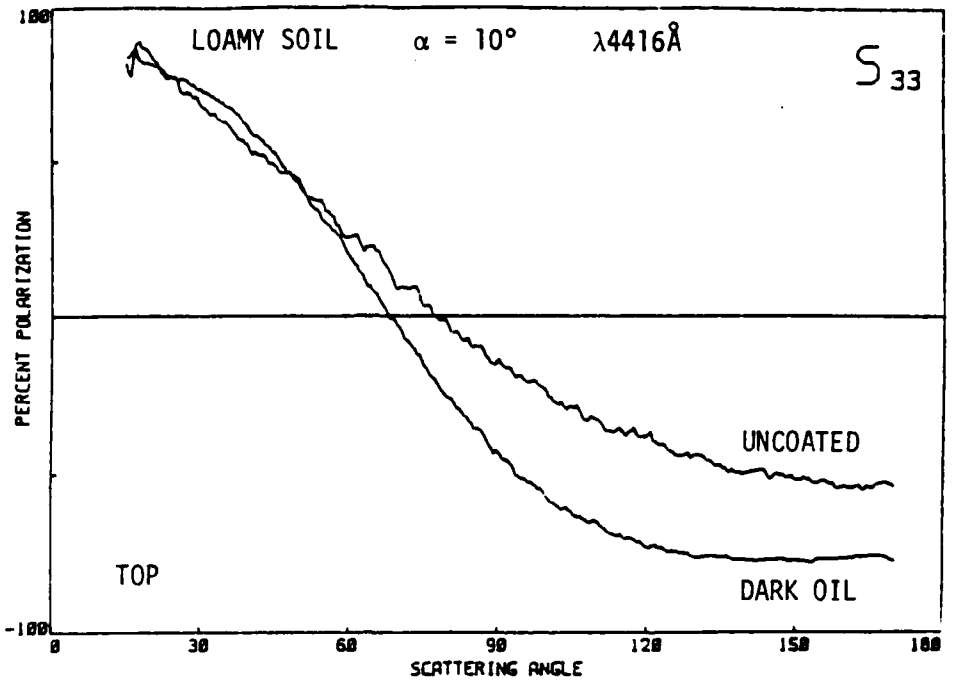

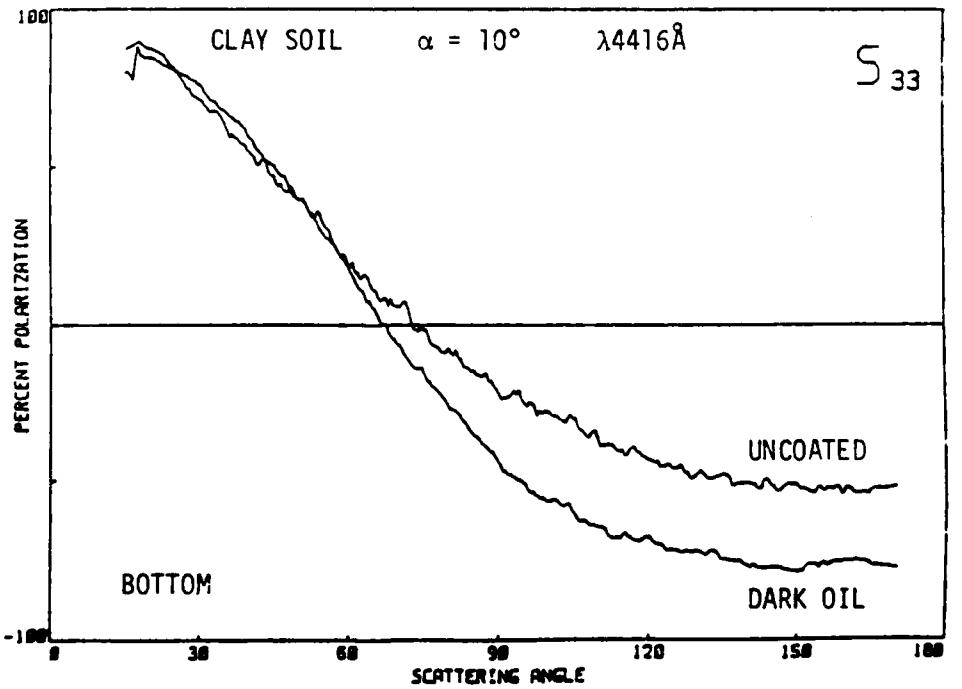

FIGURE 87. Matrix element S_{33} for uncoated and dark oil coated surfaces. Loamy soil (TOP); Clay soil (BOTTOM).

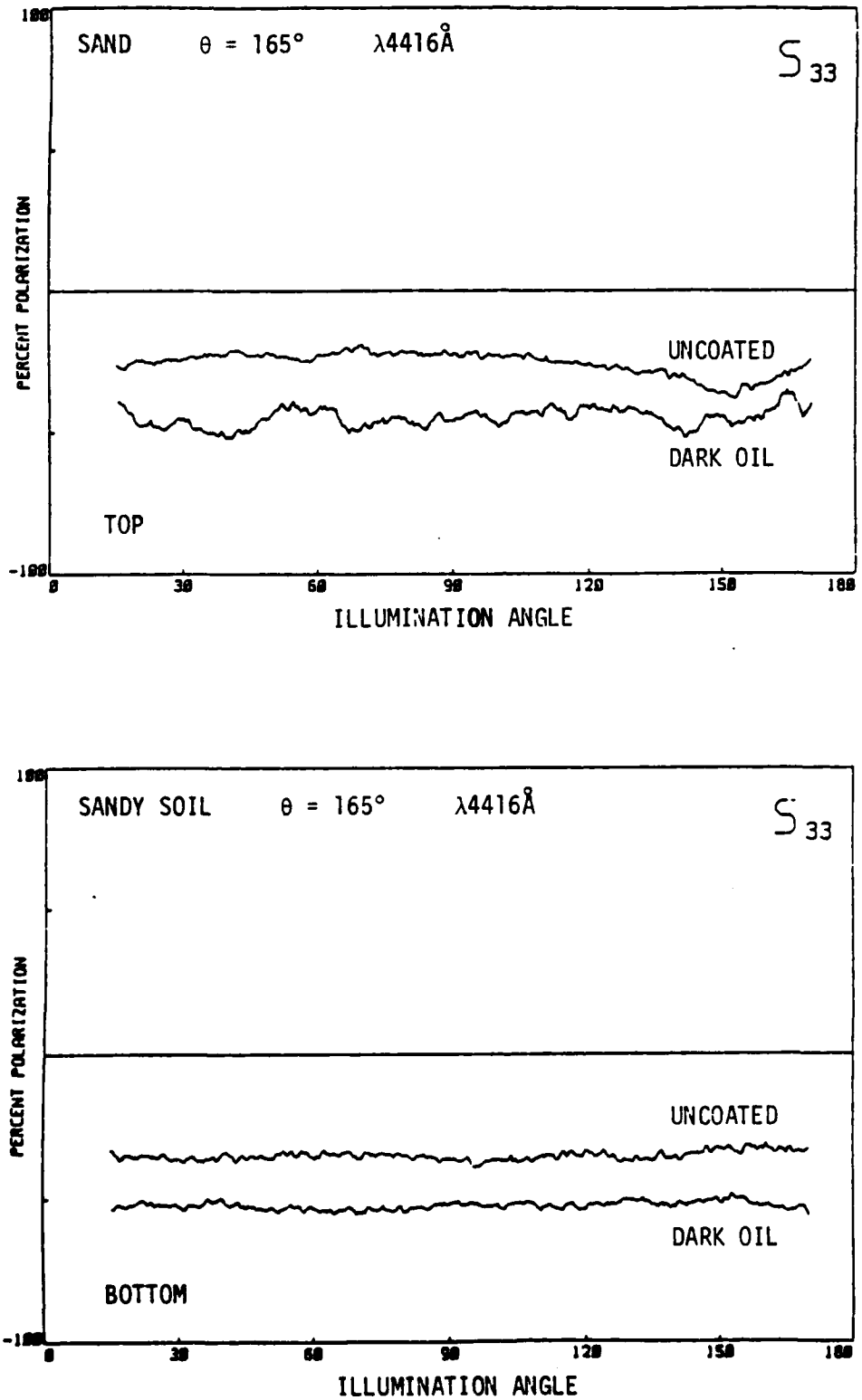

FIGURE 88. The backscatter matrix element S_{33} for uncoated and dark oil coated surfaces. Sand (TOP); Sandy soil (BOTTOM).

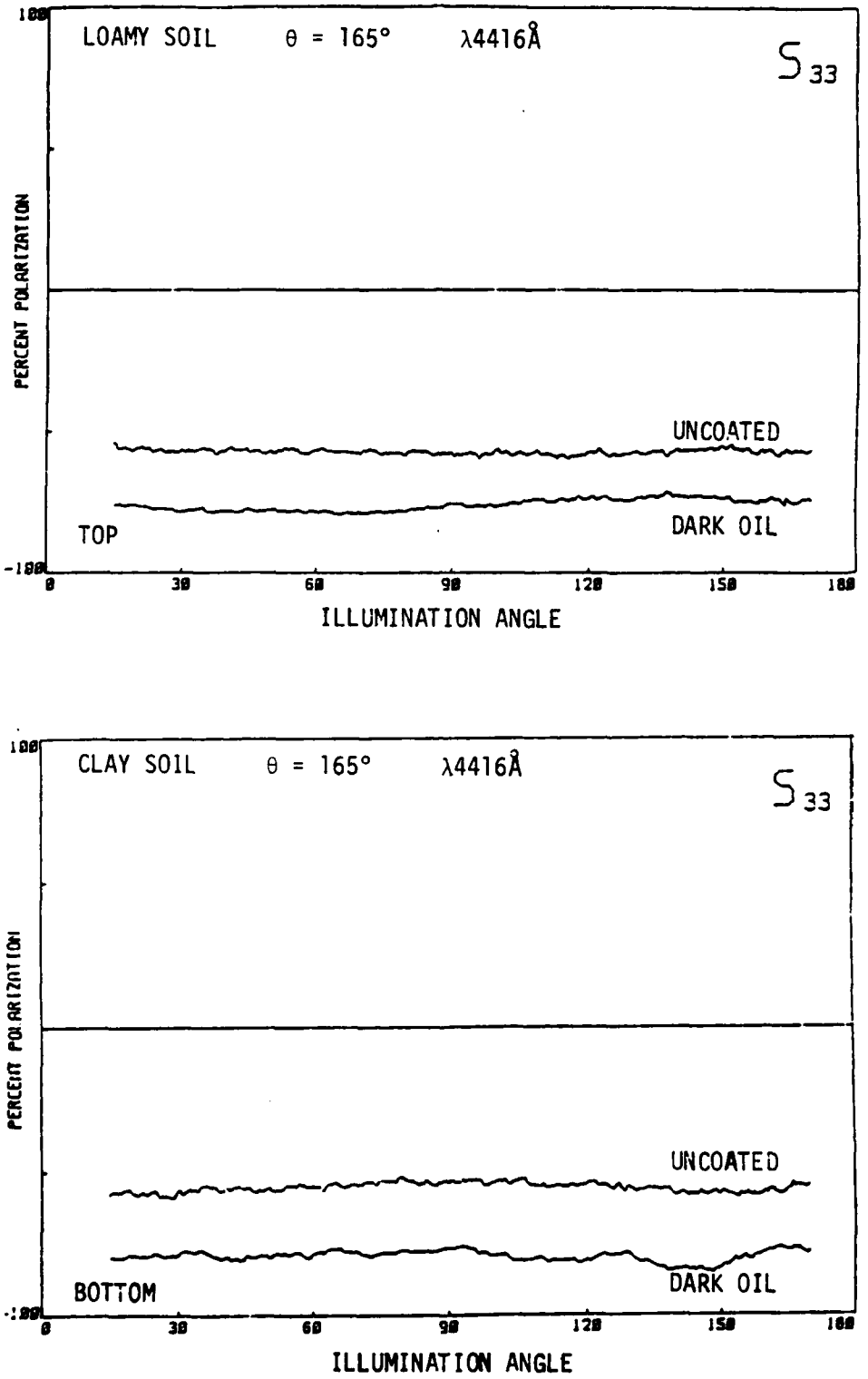

FIGURE 89. The backscatter matrix element S_{33} for uncoated and dark oil coated surfaces. Loamy soil (TOP); Clay soil (BOTTOM).

20. CONCLUSIONS

A picture is worth a thousand words. The previous 19 sections present over 80 figures of matrix elements and backscatter data for various soils coated to different thicknesses with different liquids. The surfaces were illuminated at various angles with two different laser wavelengths. The goal was to measure the Mueller light scattering matrices for four different soil surfaces to see what they looked like and to see how they responded to changes in surface character. We investigated the scattering signal reproducibility for different but identically prepared soil surfaces, the matrix element response to changing illumination angles, and their sensitivity to changes in surface character.

This data set is is quite different from the theoretically solvable matrix elements that characterize perfect spheres and fibers. Anyone who has experimentally measured the matrix elements of these systems as a function of radii, refractive index, absorption, and illumination wavelength is quite familiar with the main features of each matrix element curve and how they change as any one of the parameters are changed.

The matrix elements for rough surfaces are a different story however. The information available about sphere and fiber scattering and perfect surface scattering cannot be extrapolated to predict how a perfect fiber on a perfect surface scatters. As surfaces become more optically complex and geometrically irregular, we lose access to exact theories to predict scattering. When this happens, experimental measurements are necessary. At the beginning of this study, very little was known about the matrix element curves for surfaces or how sensitive they were to changes in surface properties. At first there were several surprises -- one being the almost total insensitivity of S_{34} to any surface property. As the experiments progressed, patterns and systematics appeared until the "big picture" emerged and no more surprises occurred.

This experimental data set, measured for the four, rough soil surfaces, involves a wide range of experimental parameters (illumination and scattering angles, roughness liquid type, layer thickness, and wavelength). With care it can be used to interpolate and extrapolate to predict what will occur for other parameters. From the vast amount of information contained in these data sets, one can get a general impression about how rough surfaces scatter. The main conclusions drawn from this study are listed below.

1. The scattering information for rough surfaces is contained mainly in matrix elements S_{11}, S_{12}, S_{33} and S_{34}.

2. S_{11} responds to virtually every change in surface parameter. However, since it is an unnormalized total intensity signal, the reference signal (starting point) is unknown. The signal will depend on laser power.

3. The matrix element S_{33} is the most sensitive polarization probe for changes of surface structure. Not only are S_{33} curves different for different soils (surfaces), they are also sensitive to small differences in soil structure such as compaction.

4. The polarization matrix element S_{12} is a very weak probe. This matrix element is essentially zero for all surfaces studied and its response to surface change is low.

5. The polarization matrix element S_{34} is practically useless. It is essentially zero for all surfaces studied. Recall that the S_{34} was the most sensitive probe for biomaterial. The opposite is the case for surfaces.

6. Coating any one of the four surfaces with dark oil (or black paint) affects all four matrix elements $S_{ij}(\theta)$. The response of the S_{ij} to increasing surface absorption is as follows:

   a) S_{11} decreases for all α and θ

   b) S_{12} changes significantly from near zero percent polarization at all (θ) to polarization values as large as 50%.

   c) S_{33} increases in the forward scatter and decreases in the backscatter. The "uncoated and dark-coated" curves cross near 70°.

   d) S_{34} increases only slightly from zero percent to about 10%. This is a much smaller change than occurs in S_{12}.

7. Coating any one of the four surfaces with dark oil (or with black paint) affects only matrix elements S_{11} and S_{33} in the backscatter (θ = 165°, $\theta < \alpha < 180°$). Matrix elements S_{12} and S_{34} cannot discriminate between light and dark (absorbing) oil coatings in the backscatter.

8. The time dependence of matrix elements $S_{ij}(\theta)$ or backscatter signals $S_{ij}(\alpha)$ after surface coating is not sufficient to determine the kind of liquid (light or dark) that is coating the surface. Very little long-term time dependence (t > 1 hour) was observed for any soil. The short-term time dependence (t < 10 sec), while dramatic, was essentially nonreproducible and too fast to be used as a probe for liquid characterization.

9. The percent polarization fluctuations for separate but identically prepared soil surfaces are large enough to be of concern. They are nearly the same for all matrix elements and soil surfaces. S_{11} fluctuations were the largest. The total scattered intensity S_{11} could vary as much as 97% over different areas of the same surface or from different but identically prepared surfaces. Fluctuations in the polarization matrix elements S_{12}, S_{33}, and S_{34} were smaller (~26%) but still large enough to mask out the subtle changes caused by liquid coatings. The fluctuation size was independent of surface illumination angle.

10. The minimum detectable thickness of a light or dark oil coating on these rough surfaces was about 25 microns. This means that an uncoated surface scanned through α or θ would need an oil coating >25 microns to create a light scattering signal that was significantly different from the one for the uncoated surface. A coating less than 5 microns is needed to change the light scattering signal from a fixed spot on the rough surface.

Blank

LITERATURE CITED

1. Iafelice, V. J. The Polarized Light Scattering Matrix Elements for Select Perfect and Perturbed Surfaces. M.S. Thesis (University of Arizona 1985).

2. Bell, B. W. Single Fiber Light Scattering Matrix: An Experimental Determination. M.S. Thesis (University of Arizona 1981).

3. Bohren, C., and Huffman, D. Absorption and Scattering of Light by Small Particles. John Wiley and Sons, Inc., New York, NY. 1983.

4. Jenkins, F., and White, H. Fundamentals of Optics. 4th Edition. McGraw-Hill Book Company, New York, NY 1957.

5. Post, D. F., Barbarick, K. A., and Ahlrichs, J. L. Collecting and Preparing Micro, Miniature, and Macro Soil Profiles. J. Agronomic Education 5, 9-16 (1976).